INVESTIGATION OF CONCENTRATION PROFILES IN CARBON NANOTUBE PRODUCTION REACTOR

A THESIS SUBMITTED TO
THE GRADUATE SCHOOL OF NATURAL AND APPLIED SCIENCES
OF
MIDDLE EAST TECHNICAL UNIVERSITY

BY

MUSTAFA YALIN

IN PARTIAL FULFILLMENT OF THE REQUIREMENTS
FOR
THE DEGREE OF MASTER OF SCIENCE
IN
CHEMICAL ENGINEERING

SEPTEMBER 2009

Approval of the thesis:

INVESTIGATION OF CONCENTRATION PROFILES IN CARBON NANOTUBE PRODUCTION REACTOR

submitted by **MUSTAFA YALIN** in partial fulfillment of the requirements for the degree of **Master of Science in Chemical Engineering Department, Middle East Technical University** by,

Prof. Dr. Canan Özgen
Dean, Graduate School of **Natural and Applied Sciences**

Prof. Dr. Gürkan Karakaş
Head of Department, **Chemical Engineering**

Prof. Dr. H. Önder Özbelge
Supervisor, **Chemical Engineering Department, METU**

Examining Committee Members:

Prof. Dr. Gürkan Karakaş
Chemical Engineering, METU

Prof. Dr. H. Önder Özbelge
Chemical Engineering, METU

Assoc. Prof. Dr. Burhanettin Çiçek
Chemical Engineering, Ankara University

Assoc. Prof. Dr. Yusuf Uludağ
Chemical Engineering, METU

Dr. Serkan Kıncal
Chemical Engineering, METU

Date:

I hereby declare that all information in this document has been obtained and presented in accordance with academic rules and ethical conduct. I also declare that, as required by these rules and conduct, I have fully cited and referenced all material and results that are not original to this work.

Name, Last Name: MUSTAFA YALIN

Signature :

ABSTRACT

INVESTIGATION OF CONCENTRATION PROFILES IN CARBON NANOTUBE PRODUCTION REACTOR

Yalın, Mustafa
M.S., Department of Chemical Engineering
Supervisor : Prof. Dr. H. Önder Özbelge

September 2009, 112 pages

Carbon nanotubes have received considerable attention since their discovery due to their novel properties. They have potential application areas in physics, chemistry and biology. Arc discharge, laser furnace, chemical vapor deposition and floating catalyst methods are the most commonly used methods to produce carbon nanotubes. Although carbon nanotubes have superior properties compared to other materials, they could not be used widely. The main reasons of this are that continuous and large scale production of carbon nanotubes could not be achieved and impurities have to be removed. To solve these problems more information about formation of carbon nanotubes has to be known. In this study concentration profiles of reactant and byproducts in a cylindrical reactor are investigated during carbon nanotube production.

A special probe to collect gas samples along the reactor and samples loops to store the gas samples were designed and constructed. Gas samples were analyzed one by one in GC/MS. Experiments were done with and without catalyst at same experimental conditions. Thus, effects of catalyst on concentration profiles of chemicals were analyzed. To produce carbon nanotubes more acetylene was used compared to amount of acetylene used in pyrolysis. Increasing reaction temperature from 800°C to 875°C caused decomposing more acetylene and producing more carbon nanotubes.

It is believed that data accumulation on the reactions involved in the gas phase will lead to large scale production and lower product costs with a large catalyst surface to be produced in the reactor.

Keywords: Carbon Nanotube, Chemical Vapor Deposition, Gas Phase Analysis

ÖZ

KARBON NANOTÜP ÜRETİM REAKTÖRÜNDE KONSANTRASYON PROFİLLERİNİN İNCELENMESİ

Yalın, Mustafa
Yüksek Lisans, Kimya Mühendisliği Bölümü
Tez Yöneticisi : Prof. Dr. H. Önder Özbelge

Eylül 2009, 112 sayfa

Üstün özelliklerinden dolayı karbon nanotüpler keşiflerinden itibaren ilgi çekmektedirler. Fizik, kimya ve biyoloji gibi konularda kullanım alanlarına sahiptirler. Ark boşaltımı lazer fırını kimyasal buhar çökeltimi ve akışkan katalizör yöntemi karbon nanotüp üretimi için en çok kullanılan yöntemlerdir. Karbon nanotüpler diğer malzemelere göre üstün özelliklere sahip olmalarına rağmen yaygın olarak kullanılamamaktadır. Bunun başlıca sebepleri karbon nanotüplerin sürekli ve büyük ölçekli üretiminin gerçekleştirilememesi ve safsızlıkların giderilmesinin gerekmesidir. Bu sorunları çözmek için karbon nanotüplerin oluşumu ile ilgili daha fazla bilgiye ihtiyaç vardır. Bu çalışmada karbon nanotüp oluşurken reaktantın ve yan ürünlerin konsantrasyon profilleri silindirik reaktör içerisinde incelendi.

Reaktör boyunca gaz örneklerini toplamak için özel bir probe ve gaz örneklerini saklamak için örnek loopları tasarlandı ve yaptırıldı. Gaz örnekleri sırayla GC/MS'de analizlendi. Aynı deney şartlarında deneyler katalizli ve katalizsiz olarak tekrarlandı. Bu sayede kataliz varlığının incelen kimyasalların konsantrasyon profillerine etkisi incelendi. Karbon nanotüp oluşumu için asetilen pirolizine oranla daha fazla asetilen harcandı. Reaksiyon sıcaklığının 800°C'den 875°C'ye çıkarılması asetilenin daha fazla parçalanmasına ve daha fazla karbon nanotüp üretilmesine neden oldu.

Gaz fazında gerçekleşen reaksiyonlar ile ilgili bilgi toplamanın reaktör içerisinde geniş yüzey alanına sahip katalizör ile büyük ölçekli üretime ve daha az ürün maliyetine neden olacağına inanılmaktadır.

Anahtar Kelimeler: Karbon Nanotüp, Kimyasal Buhar Çökeltme, Gas Fazı Analizi

To my mother, my father and my sister

ACKNOWLEDGMENTS

I would like to express my deepest appreciation to my supervisor Prof. Dr. Hilmi Önder Özbelge for his guidance and interest throughout this study. I would also like to thank Assoc. Prof. Dr. Burhanettin Çiçek for his ideas and suggestions.

I would also want to thank the technicians of Chemical Engineering Department for their help in the preparation of my experimental setup.

I gratefully acknowledge Furkan Soysal and İbrahim Mutlay for their friendship and collaboration.

I would also thank my friends Hasan Zerze, Dominic Deo Androga, Deniz Barer and Bahram Lotfi Sadigh for their help and moral support.

I wish to thank The Scientific and Technological Research Council of Turkey (TÜBİTAK) for supporting me with scholarship throughout my study.

Most importantly I would like to provide my deepest and endless thanks to my family since they always support me in everything during my entire life.

TABLE OF CONTENTS

CHAPTERS

APPENDICES

LIST OF TABLES

TABLES

LIST OF FIGURES

FIGURES

CHAPTER 1

INTRODUCTION

Nowadays, nanotechnology is one of the most popular research topics, and carbon nanotubes (CNTs) are popular research subject in nanotechnology. Since their discovery in 1991 a lot of research has been done related with production methods, properties and application areas of CNTs. The field of CNTs is undergoing an explosive growth due to both the intrinsic interests in these molecular structures and their superior properties suitable for applications in novel nanometer scale electronic and mechanical devices, catalysts, and energy storage [1]. Theoretical studies of CNTs have revealed that they will have unusual mechanical, electrical, and magnetic properties of fundamental scientific interest and possibility of technological importance [2]. Already, theoretical studies of the individual hollow concentric graphitic nanotubes predict that these nanometer-scale diameter nanotubes will exhibit conducting properties ranging from metals to moderate bandgap semiconductors, depending on their radii and helical structure [2]. Other theoretical studies have focused on structural properties and have suggested that these nanotubes could have high strengths and rigidity resulting from their graphitic and tubular structure [2]. In near future carbon nanotubes will find wide spread applications in many areas especially in physics and biology. However, many challenges remain in the production of CNT. First, an efficient growth approach to structurally perfect nanotubes at large scales is still lacking [3]. Second, growing defect free nanotubes with macroscopic lengths has been difficult [3]. Third, chirality of single wall CNTs can not be controlled with an existing production methods [3]. To cope with these challenges experimental data is needed to understand the mechanisms, and to find out the effect of various parameters in the processes involved.

Commonly used methods to produce CNTs are arc-discharge, laser ablation and chemical vapor deposition (CVD) methods. However, these methods are not suitable for continuous production of CNTs. In arc-discharge method, reaction stops when anode graphite rod is used up. In laser ablation method, carbon source has to be renewed since it vaporizes during the reaction. In CVD method, preparation of substrates has to be repeated since CNTs only grow on these substrates. Hence, only batch production of CNTs can be achieved with these methods. Floating catalyst method is suitable for continuous production of CNTs. In this method, both carbon source and catalyst source are sent to reactor in the gas phase. Iron containing organometals used as a catalyst source are dissolved in organic solvent. This solution is continuously injected to the reactor during the reaction. Hence, CNTs can grow everywhere inside the reactor. There is no need for time consuming catalyst preparation. Moreover, reaction temperature of floating catalyst method is lower than that of arc-discharge and laser ablation. Temperature, pressure, inert gas flow rate, concentration and flow rate of organic solution are the main experimental parameters of floating catalyst method. However, optimization of these parameters for production of CNTs has not been done yet.

There are two main reasons why applications of CNTs are not so common. These are related with production and impurities. Large scale and continuous production method for CNTs has not been developed yet. At the present time CNTs are produced with using batch production methods. Hence, price of the CNTs is high. Other problem is that produced CNTs contain a lot of impurities that are need to be removed. Metals used as a catalyst and carbon materials like amorphous carbon are main impurities. To remove these impurities various separation methods have to be applied after production.

For continuous and large scale production of CNTs the most promising method is floating catalyst method. In last few years more and more researchers started to use this method. However, main reason of problem related with production is that formation of CNTs is still not known. Obtaining experimental data about formation mechanism of CNTs will help to find better catalyst and more suitable experimental conditions for high yield CNT production.

In this thesis work as an effort to contribute to the better understanding of CNT production a new experimental set up was introduced for continuous data acquisition and data was obtained for concentration profiles in the reactor without catalysis and with solid phase catalysis for CNT production by CVD.

CHAPTER 2

LITERATURE SURVEY

2.1 CARBON NANOTUBES

Carbon nanotubes (CNTs) were discovered in 1991 by Sumio Iijima [4]. Multi wall carbon nanotubes (MWCNTs) were found in the samples of arc discharge experiment [4]. Very small diameter carbon filaments were prepared in the 1970's and 1980's through the synthesis of vapor grown carbon fibers by the decomposition of hydrocarbons at high temperatures in the presence of transition metal catalyst particles of less than 10 nm diameter [5]. However, no detailed systematic studies were reported until Iijima's discovery [5]. CNTs are allotrope of carbon like diamond, graphite and fullerene [6]. Nanotubes are composed of graphite plates that have sp^2 bonds [7]. These plates are bended and have cylindrical shapes [7]. Diameters of CNTs are in few nanometers whereas their length is up to few microns. Electron microscope image of nanotubes that Iijima discovered are given in Figure 2.1. In Figure 2.1-b there is a nanotube that is composed of two graphite plates. Inner and outer diameters of these plates are 4.8 nm and 5.5 nm, respectively [4]. Inner and outer graphite plates are separated by a distance of 0.34 nm [4]. Iijima observed smallest nanotube diameter as 2.2 nm [4].

2.1.1 Types of Carbon Nanotubes

CNTs are divided into two groups according to the number of bended plates; single wall carbon nanotube (SWCNT) and multi wall carbon nanotube (MWCNT). If there is one bended plate, it is called as SWCNT. If there are two or more than two graphite layers, it is called as MWCNT. Nanotubes that Iijima discovered in 1991 are MWCNTs. Iijima's nanotubes

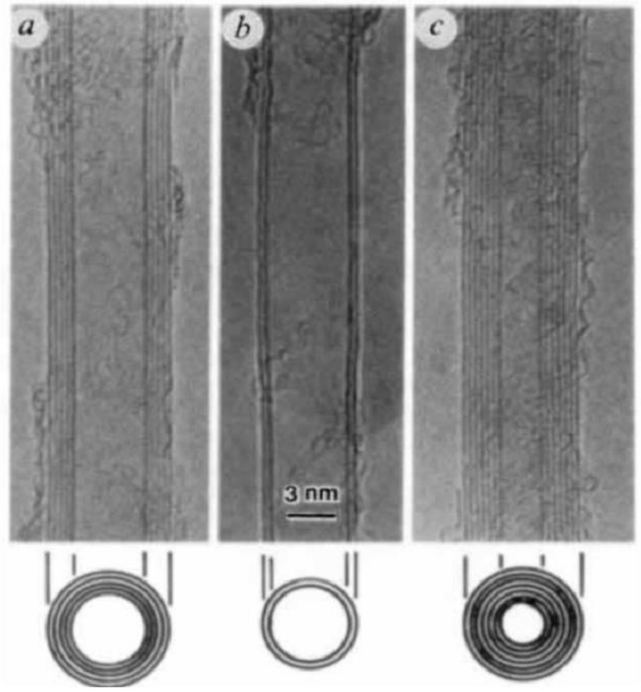

Figure 2.1: Electron Microscope Image of Iijima's Nanotubes [4]

have 2 to 50 sheets and diameters changed from 4 to 30 nm [4]. Bethune et al. at IBM Research Division and Iijima et al. at NEC Corporation independently discovered SWCNTs in 1993 [7, 8]. Both research groups covaporized carbon and a transition metal catalyst and produced SWCNTs approximately 1 nm in diameter and up to several microns long [9]. Iijima et al. produced SWCNTs by vaporizing graphite and Fe in an Ar/CH_4 atmosphere [9]. The tubes were found in the deposited soot [9]. Bethune et al. vaporized Co and graphite under helium buffer gas and found SWCNTs in both the soot and in web-like material attached to the chamber walls [9]. In Figure 2.2 TEM and computer generated images of both single and multi wall carbon nanotubes are given.

CNTs are also categorized according to how the two dimensional graphite layers roll up [10]. There are three types; zig-zag, arm-chair and chiral. The circumference of any CNT is expressed in terms of the chiral vector which connects two crystallographically equivalent sites on two dimensional graphite layer [11]. Chiral vector is defined as $C_h = n.a_1 + m.a_2$ and in this equation, a_1, a_2 are unit vectors in the two dimensional hexagonal lattice, and n and m are integers [10]. The angle between C_h and a_1 is called as chiral angle (θ) [10]. In Figure

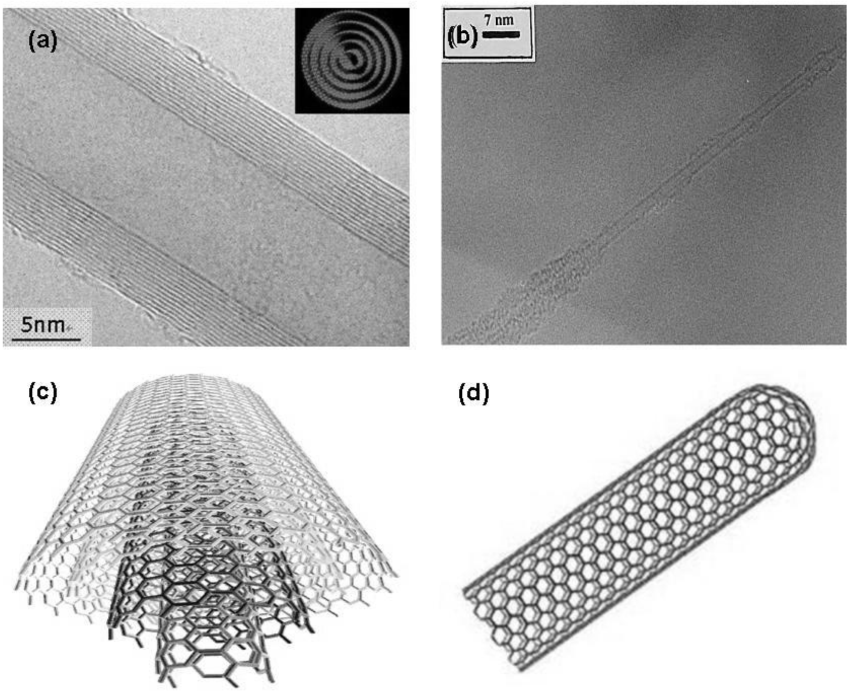

Figure 2.2: TEM and Computer Generated Images of Single and Multi Wall Carbon Nanotubes

2.3 schematic representation of chiral vector and angle is given. When n = m and chiral angle is 30°, CNT is called as arm-chair [10]. When n or m is zero and chiral angle is 0°, CNT is called as zig-zag [10]. When chiral angle is between 0° and 30°, CNT is called as chiral [10]. In figure 2.4 samples are given for armchair, zig-zag and chiral nanotubes.

2.1.2 Properties of Carbon Nanotubes

CNTs are one of the strongest materials known because of their tensile strength and elastic modulus [13]. Tensile strength of SWCNTs is 45 GPa; in contrast, most strong steel has maximum 2 MPa tensile strength [14]. According to test done in 2000, it was observed that MWCNT had 63 GPa tensile strength [13].

Young's modulus of MWCNTs changes between 1-1.2 TPa and that of SWCNTs is around 1 TPa [15]. Young's modulus of the MWCNTs decreases as the disorder within the walls increases [16].

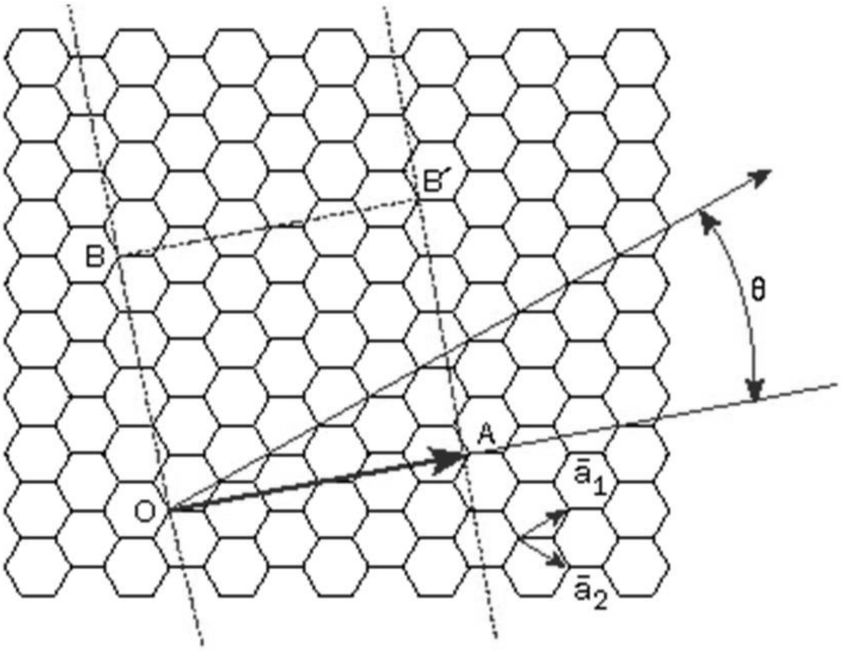

Figure 2.3: Schematic Representation of Chiral Vector and Angle [10]

Resistivity of single and multi walled carbon nanotubes is 10-6 Ωm and maximum current density of them changes between 10^7-10^9 A/cm^2 whereas copper wires burn at 10^6 A/cm^2 [14, 15].

At room temperature, SWCNTs have 1750-5800 W/mK thermal conductivity [15]. Thermal conductivity of MWCNT is greater than 3000 W/mK [15]. To show their superior thermal conductivities, they can be compared with diamond which is known as having the highest thermal conductivity of any known solid at room temperature [13]. Thermal conductivity of pure diamond is only 3320 W/mK [14].

Electrical behavior of CNTs may be the most important property. SWCNTs can be either a metal or a semiconductor without adding any material [16]. Depending on the specification nanotube may be a true one dimensional metal or a semiconductor with a gab [16]. Chiral vector determines the electrical behavior of SWCNTs [16]. For a given (n, m) nanotube, if n+m=3q (where q is an integer), then the nanotube is metallic, otherwise the nanotube is a semiconductor [10]. Bandgap of metallic SWCNTs is 0 eV whereas that of semiconductor SWCNTs changes between 0.4-0.7 eV [15]. Conduction occurs through the outermost shell

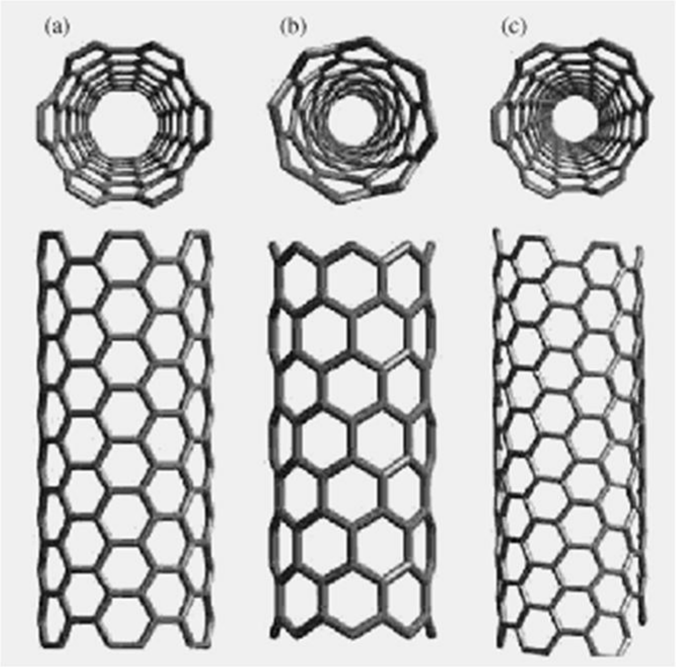

Figure 2.4: Classification of carbon nanotubes: (a) armchair (b) zig-zag (c) chiral [12]

for MWCNTs [15]. As the diameter of outer nanotube increases, the gap approaches 0 eV and the nanotube is essentially nonsemiconducting [15].

The ends or caps of the CNTs are more metallic than the cylinders, due to the concentration of pentagonal defects [17]. These defects also enhance the reactivity of tube ends, giving the possibility of opening the tubes, functionalizing the tube ends and filling the tubes with foreign substances [17].

2.1.3 Application Areas of Carbon Nanotubes

High surface area and atomic structure make CNTs promising candidates for nanoscale sensing materials [18]. In fact, the electronic properties of CNTs, especially semiconducting CNTs, are very sensitive to the chemical environments [18]. The presence of electron-donor or electron-acceptor gas molecules can either donate or remove electrons from CNTs by changing their overall electrical conductivity [18]. Charge transfer between CNTs and adsorbed molecules produces a chemical gating effect that can be used for molecular sensing

[18]. CNT sensors offer potential and significant advantages over traditional sensor materials (mainly semiconducting metal oxides) in terms of sensitivity, operation at room temperature, small sizes for device miniaturization, massive sensor arrays [18].

CNTs also have significant potential as the central elements of nano-electronic devices including field effect transistors, single-electron transistors and rectifying diodes [3]. Electron field emitters based on CNTs are currently investigated as the next generation cold cathode materials, particularly for flat-panel field-emission displays and the back light units of liquid crystal displays [19]. In order to function as good field emitters, CNTs should have good crystallinity, a clean surface, and good electrical contact with the substrate [19]. Considerable effort has been made to develop various methods for fabricating CNT field emitters [19].

CNTs are one of the strongest materials. Hence, composite materials with improved mechanical properties can be produced using CNTs. CNTs have already been used for reinforcement of nanostructural composite materials, polymers and concrete [20]. High strength light materials and strong fibers can be produced [1].

Since CNTs can be both conductor and semiconductor, they can be used in electrical areas. Magnetic and optic nanodevices, memory elements, capacitors, transistors, diodes, logic circuits and electronic keys can be produced from CNTs [14]. CNTs have already been used as electromechanical actuators [3].

Individual CNTs have been used for field emission sources, tips for scanning probe microscopy and nano-tweezers [3]. Since CNTs have very large surface area, nano scale super capacitors can be produced [14]. Artificial muscle production becomes possible using these capacitors [14]. Tips for Atomic Force Microscope (AFM) using CNTs have been developed [17]. CNTs may also be used for taking samples from cells or for injecting of molecules to cells [20].

CNTs can be used for lithium and hydrogen storage [21, 17]. Main problem of using hydrogen as a fuel is to store hydrogen safely and efficiently [21]. CNTs can absorbs hydrogen molecules into their inner surfaces [20]. Thus, they can be used as hydrogen storage materials for future fuel cells.

MWCNTs can be used as efficient supports in heterogenous catalysis and as microelectrodes in electrochemical reactions [17]. In addition, CNTs can be used in production of advanced solar cells since they have very large surface area and very high thermal conductivity and also they are physically and chemically stable [20].

At room temperature, electrical resistances of semiconducting CNTs are highly influenced by gases in medium [20]. Thus, chemical sensors using CNTs have been developed [20].

Another interesting application that has been considered for CNT is their use as membrane filters [22]. Several groups have published papers in recent years suggesting that membranes made from aligned CNT arrays (both SWCNTs and MWCNTs) could be used for selective transport of species [22]. Activated and porous carbons have been traditionally used as filters (e.g., water purification) but the advantage of CNT is that the pore sizes are very uniform and small, so that separation of really small molecules becomes possible [22]. Although the pore size is small, the flow rate is not reduced due to the unique nature of the flow of solvents through the CNT cavities [22]. Another advantage could be that the CNT surfaces may be chemically modified to develop nanotube-based membranes for filtration, molecular as well as gas separation, these are still far from commercial products and their development could take more than a decade [22].

2.2 PRODUCTION METHODS OF CARBON NANOTUBES

Many methods have been developed to produce carbon nanotubes. The most widely used methods are arc discharge method, laser furnace method, chemical vapor deposition method and floating catalyst method.

2.2.1 Arc discharge method

CNTs are first produced with arc-discharge method [4]. In this method, DC arc is applied between two graphite rods in an oxygen free medium [23]. Because of applied arc high temperature occurs [23]. At high temperatures, graphite rod at anode evaporates [23]. Evaporated carbon mixture condenses at cold reactor walls and on cathode [23]. Produced CNTs are inside this condensed soot [23]. In arc discharge reactor, both SWCNTs and MWCNTs can be produced. When pure graphite rods are used, MWCNTs are obtained [23]. When metal catalysts are added to graphite rods, SWCNTs are obtained [23].

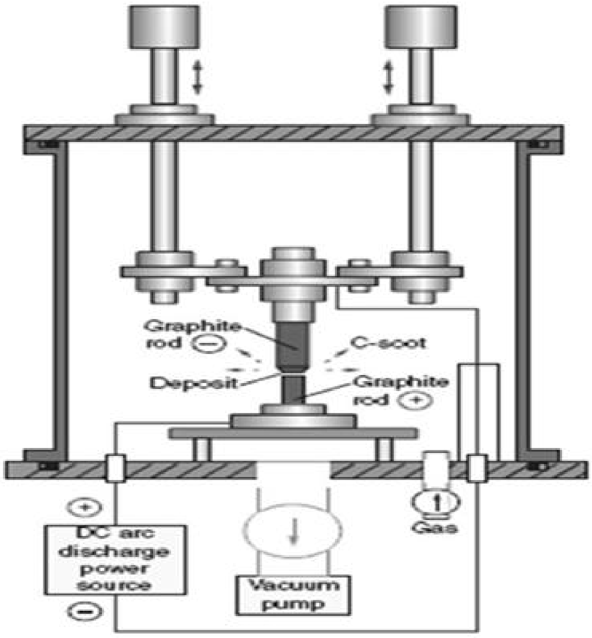

Figure 2.5: Schematic Representation of Arc-Discharge Method [23]

Pure graphite rods are used to produce MWCNT by using arc discharge method. Helium, argon and methane gases can be used in reactor. Ando et al. studied the effects of helium, argon and methane [23]. They found that methane is the most suitable gas because CNTs with high crystallinity can be obtained and low byproducts are produced in methane gas medium [23]. Moreover, pure H_2 gas is used for medium gas [23]. With H_2 gas, produced CNTs had excellent crystal structure and inner diameter as thin as 0.3 nm [23]. The reason may be that hydrogen arc has high temperature and high activity [23].

To produce SWCNTs by arc discharge method, metal catalyst should be added to graphite rod at anode [23]. Two metals groups are used as catalyst. One is transition metals, such as Fe, Co, Ni and Cu and other is lanthanides, such as Gd, Nd, La and Y [2]. When transition metals are used as catalyst, high yield is obtained [2]. Moreover, produced CNTs have length-to-diameter ratio as high as several thousand [2]. In contrast, shorter are obtained when lanthanides are used as catalyst [2]. However, the purity of the arc discharge fabricated MWCNTs is much better than SWCNTs, since magnetic materials are not used in their production [16].

While producing CNTs with arc discharge methods, gas pressure, flow rate of gas and metal concentrations can be changed in wide ranges [2]. Although they do not affect the characteristics of CNTs, such as diameter, they change the yield [2]. However, some elements such as sulfur, bismuth and lead improve yield and properties of CNTs despite the fact that they cannot act as catalyst when they are used alone [2].

2.2.2 Laser furnace method

In 1996, Smalley and co-workers produced high yield (>70) of SWCNTs by laser ablation of graphite rods with small amounts of Ni and Co at 1200°C [24]. In laser furnace method, a carbon source is decomposed by laser and CNTs are produced. It is seen that, in figure 2.6, there is a furnace, inside furnace graphite is placed. During experiment, laser beam is focused on graphite rod. Graphite rod vaporizes and vaporized particles are carried by inert gas [23]. They condense at water-cooled trap [23]. Produced CNTs are taken from there [23]. The vaporization surface is kept as fresh as by changing the focus point or moving the target [23]. The aim of this is to vaporize graphite rod more uniformly [25]. The average CNT diameter and size distribution can be changed by adjusting the growth temperature, the catalyst composition and other process parameters [25].

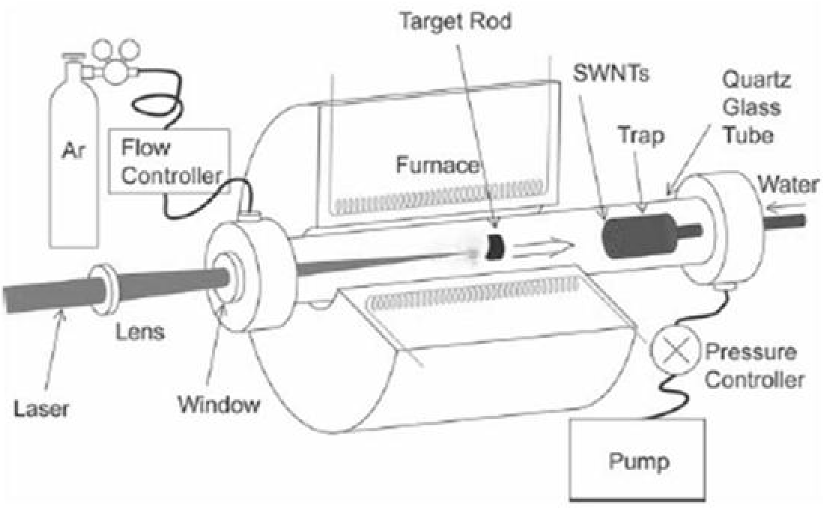

Figure 2.6: Schematic Representation of Laser Furnace Method [23]

If a pure graphite target is used, MWCNTs are produced like in the arc discharge method [26]. However, if the target is composed e.g. of 1.2 atom % Co/Ni with equal amounts of Co and Ni added to the graphite then SWCNTs are synthesized [26]. The produced material consists of ropes of SWCNTs with a diameter between 10 and 20 nm and up to 100 μm or more in length [26]. The average CNT diameter and diameter distribution can be adapted by varying the synthesis temperature and the composition of the catalyst [26].

2.2.3 Chemical Vapor Deposition Method

Although arc discharge and laser furnace methods seem to have superior properties, they have an important drawback that is only graphite rod can be used for CNTs synthesis and they are extremely difficult to control in terms of process parameters [27]. Hence, CNTs that are produced with arc discharge and laser furnace contain significant fractions of unwanted material [27]. For these reasons, chemical vapor deposition method (CVD) is used to produce CNTs. CVD method has been extensively investigated as a powerful method for large-scale production of both SWCNTs and MWCNTs [28]. Moreover, this method is more controllable and cost efficient as compared with those of arc discharge and laser ablation methods [28]. People who first applied CVD method to produce CNTs are Endo et al. and Yacamán et al. [23]. Schematic representation of CVD method is given in Figure 2.7.

In this method, carbon source decomposes at high temperatures and forms CNTs on catalyst. There is a furnace and inside furnace there is a quartz tube. Before the experiment catalyst particles are put in quartz tube. Transition metals, such as Fe, Co, Ni, are the most commonly used catalyst [23]. The reason of using these metals is related with phase diagrams of metals and carbon. At high temperatures, carbon has finite solubility in these metals [11]. Carrier gas containing carbon source passes through tube [23]. At high temperatures carbon source decomposes [23]. Decomposed carbon species are dissolved in the metal particles [23]. After reaching supersaturation, CNTs are produced on the surfaces of catalyst particles [23]. Hydrocarbons which are carbon source, catalyst and growth temperature affect CNT production in CVD method [11].

Preparation of catalyst in chemical vapor deposition method is very important. Diameter of catalysts particles and uniform distribution are closely related with quality and quantity of

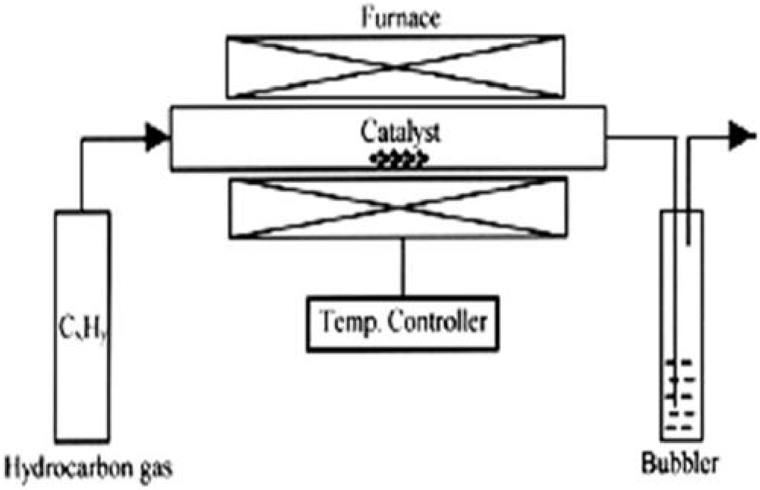

Figure 2.7: Schematic Representation of Chemical Vapor Deposition Method [23]

products. To prepare catalyst different methods can be used such as e-beam evaporation and sol-gel.

Cui et al. prepared the catalyst by e-beam evaporation [29]. They deposited the multilayered catalyst structures on 1 cm^2 silicon substrates [29]. First they deposited aluminum, then iron and finally molybdenum [29]. 500 sccm argon, 100 sccm hydrogen and 2 sccm acetylene were fed to the reactor in order to produce CNTs [29]. They investigated the effects of growth temperature [29]. It was changed from 500°C to 1100°C [29]. At 500°C no CNTs were observed [29]. When growth temperature was increased to 600°C, MWCNTs were observed [29]. Produced CNTs at that temperature were highly defective [29]. With further temperature increase to 700°C, the length of produced MWCNTs increased [29]. Moreover, diameters of CNTs and number of graphite layers decreased [29]. Although the length of CNTs decreased at 800°C, SWCNTs were observed [29]. More CNT bundles were observed at 900°C [29]. When growth temperature was increased to 1000°C, carbon fibers with larger diameters were found among smaller CNTs [29]. At 1100°C, only carbon fibers were produced [29].

Mauron et al. synthesized oriented carbon nanotube films with catalyst prepared by spin-coating [30]. They used iron (III) nitrate ethanol solution at different concentrations [30]. Concentration of solution affects the thickness of deposited film [30]. The coated substrate was heated to the desired temperatures at 10^{-6} mbar [30]. After that pressure was increased to 500 mbar with 98 sccm flow of nitrogen [30]. Iron oxide clusters were formed by heating the iron (III) nitrate-coated substrate [30]. Then, they sent 2 sccm acetylene with 98 sccm nitrogen for 30 minutes to produce carbon nanotubes [30]. They used four different iron (III) nitrate solutions (7.5, 15, 30 and 60 mmol/l) at three different reaction temperatures (650, 700 and 750°C) [30]. They could not produce carbon nanotubes at high iron (III) nitrate concentration since catalyst particles did not form at high concentration [30]. They obtained the highest carbon nanotube densities with the lowest iron (III) nitrate concentration at high temperatures [30].

Terrado et al. prepared their caltayst by spray-coating method [31]. They deposited two different types of iron solutions on substrates [31]. They also used two different substrates; quartz and alumina [31]. One solution was prepared by dissolving iron (III) nitrate in ethanol [31]. Then, prepared solution was sprayed onto substrate with an air pressure of 1 bar [31]. Other solution was prepared by sol-gel method [31]. 1.5 M iron (III) nitrate aqueous solution (15 ml) was mixed with 10 ml tetraethylorthosilicate (TEOS) and 15 ml ethanol [31]. After solution was sprayed onto substrate, it was dried overnight at 80°C [31]. Then, pretreatments were done to both catalysts to obtain Fe-catalyst nanoparticles [31]. After pretreatment, catalysts were etched with 100 sccm ammonia flow for 5 minutes at CNT growth temperature [31]. They passed 20 sccm acetylene at atmospheric pressure for 15 minutes in order to produce CNTs [31]. Three different growth temperatures (800, 850 and 900°C) were used for first catalyst [31]. For catalyst prepared by sol-gel method experiment was done only at 900°C [31]. According to scanning electron microscope (SEM) and transmission electron microscope (TEM) images, they were able to produce MWCNTs [31]. They observed that the diameter of CNTs increased with CNT growth temperature [31]. Average diameter of CNTs increased from 55 nm to 100 nm as temperature increased from 800°C to 900°C [31]. Average diameter of CNTs was 95 nm for catalyst prepared by sol-gel method on quartz substrate [31]. Average diameter decreased to 75 nm with catalyst on alumina substrate [31].

Nath et al. prepared the substrate by a sol-gel process [32]. They mixed 2 ml of tetraethylorthosilicate with 2 ml absolute ethanol and 9 ml of 1.5 M aqueous solution of iron (III) nitrate [32]. They stirred solution for 20 minutes. After adding few drops of concentrated hydrogen fluoride solution, they stirred for another 20 minutes [32]. The aim of adding hydrogen fluoride is to achieve slow gelation [32]. The resulting gel was deposited on glass substrates and dried in an oven at 60°C for 12 hours [32]. It was then calcined at 450°C for 1 hour under vacuum and reduced in hydrogen at 500°C for 2 hours [32]. Carbon nanotubes were produced under flow of 15 sccm acetylene and 85 sccm argon at 700°C for 1 hour [32]. SEM image of the iron-silica catalyst surface subjected to calcination and reduction showed a uniform distribution of iron-silica nanoparticles on the surface [32]. According to TEM images diameters of the most of the particles were in the range of 5-20 nm [32]. SEM images of the produced carbon nanotubes showed the bundles of aligned carbon nanotubes growing out perpendicularly from the catalyst surface [32]. The carbon nanotube diameters were in the range of 15-150 nm [32].

Pan et al. also prepared the substrates by a sol-gel process [33]. They mixed 10 ml tetraethylorthosilicate with 1.5 M iron (III) nitrate aqueous solution (15 ml) and ethyl alcohol (10 ml) by magnetic stirring for 20 minutes [33]. After adding 0.4 ml concentrated hydrogen fluoride, they stirred for another 20 minutes [33]. The mixture was then dropped onto a quartz plate to form a film of 30-50 μm thick [33]. After gelation, the film was dried overnight at 80°C [33]. The substrates were calcined at 450°C for 10 hours under vacuum [33]. After that they were reduced at 500°C for 5 hours in a flow of 9 % H_2/N_2 under 180 Torr [33]. To produce carbon nanotubes 9 % acetylene in nitrogen at 600°C was send for 1-48 hours under 180 Torr [33]. The lengths of the produced carbon nanotube arrays reached about 2 mm after 48 hours of growth [33]. They concluded that the lengths of the carbon nanotube arrays increased with growth time [33]. Outer diameter of the carbon nanotubes were uniform and between 20-40 nm [33]. According to high-magnification SEM images most of the carbon nanotubes in the arrays were highly aligned [33]. They noted that no traces of polyhedral particles or other graphitic nanostructures were detected in both the bottom part and central part of the array [33]. This indicated that the produced carbon nanotubes had very high purity and thus had very high quality [33].

2.2.4 Floating Catalyst Method

Although arc discharge, laser furnace and CVD methods can be used to produce CNTs, they are not suitable for continuous production. Some modifications are done on CVD method for continuous production, and floating catalyst method is developed. Floating catalyst method does not require a support for the catalyst; the catalyst and the carbon source are directly reacted in the gas phase where the carbon source decomposes to form the CNTs [34]. When studies about floating catalyst method are examined, there are 3 main experiment systems.

2.2.4.1 Classic Floating Catalyst Method

In this method, there are two furnaces and a quartz tube which passes through furnaces [35]. Schematic representation of system is given in Figure 2.8. Metal catalysts which are generally in the form of organometallic compounds are placed into first furnace. During experiment, catalyst is sublimed in the first furnace [36]. Carrier gas and carbon source brings sublimed catalyst to second furnace [37]. In the second furnace, organometals are decomposed at high temperature and metal particles are formed [38]. CNTs are formed on these metal particles [38].

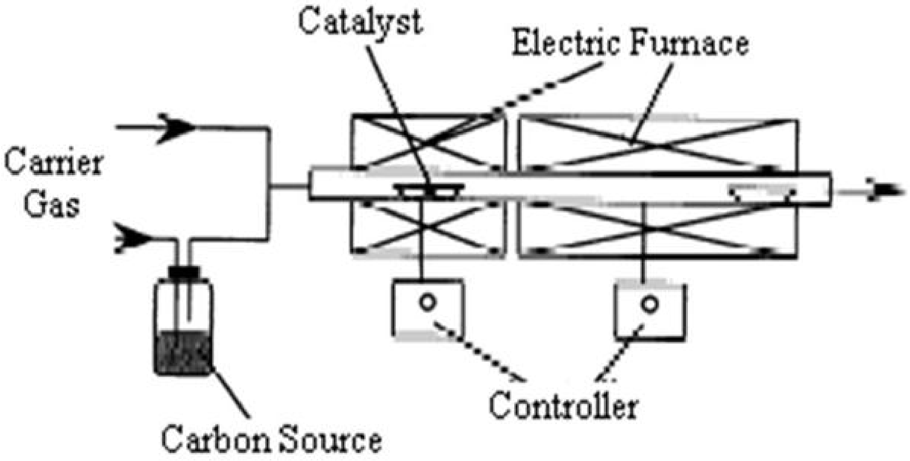

Figure 2.8: Schematic Representation of Classic Floating Catalyst Method [35]

Ci et al. produced SWCNTs in 2001 using classic floating catalyst method [36]. They used argon gas as a carrier gas, acetylene as a carbon source and ferrocene as a catalyst [36]. According to Ci et al, when the acetylene partial pressure was higher than 12 Torr, SWCNT could not be obtained [36]. Product mass was grown with the acetylene partial pressure increased when the acetylene partial pressure was below 5 Torr [36]. However, SWCNT production began to decrease when the acetylene partial pressure was above 5 Torr [36]. Above 5 Torr, more thermal decomposed carbon was produced [36]. This made the catalyst particles inactive [36]. They also observed that production rate increases with increasing temperature and amount of sublimed ferrocene [36].

2.2.4.2 Catalyst-Carbon Source Mixture Method

In this method, there are two furnaces and a quartz tube which passes through furnaces [39]. Schematic representation of system is given in Figure 2.9. Organometallic compounds are dissolved in carbon source [40]. Then, this solution is placed in first furnace [40]. In the first furnace, solution is vaporized and carrier gas brings vaporized solution to second furnace [41]. In the second furnace, organometals are decomposed at high temperature [40]. Because of high temperature carbon source is also decomposed and formed carbon particles are produced CNTs on metal particles [40].

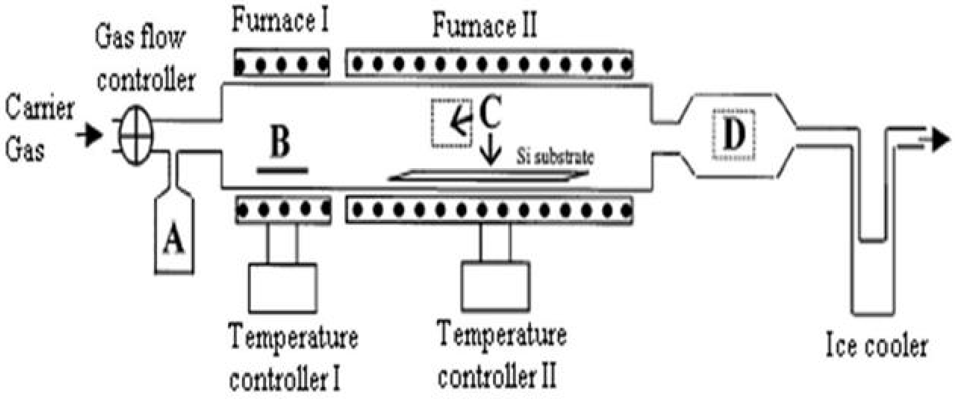

Figure 2.9: Schematic Representation of Catalyst-Carbon Source Method [39]

The reaction temperature determines the diameter of CNTs and controls their yield [40]. It is suggested that larger diameter CNTs originate from large-sized catalytic particles [40]. At high temperature catalyst source forms larger amounts of particles with larger diameter [40]. However, small diameter particles are produced at lower reaction temperature [40].

Hou et al. synthesized CNTs using catalyst-carbon source mixture method [39]. They used two different carrier gas in their experiments [39]. In the first experiment, they used hydrogen as a carrier gas, anthracene as a carbon source and ferrocene as a catalyst [39]. In the second experiment, argon gas was used as a carrier gas and 9,10-dibromoanthracene was used as a carbon source [39]. Ferrocene was also used as a catalyst in the second experiment [39].

Table 2.1: The Synthesis Conditions and Properties of Products of H. Hou et al [39]

Sample	Carrier Gas	Temperature (°C)	Ferrocene/ Anthracene	Yield (mg)	Properties of Products	Outer Diameter (nm)
A	H_2	580-700	1/1	452	MWCNT	30-60
B	H_2	580-700	1/2	294	MWCNT	10-30
C	H_2	580-700	1/2.5	205	MWCNT	5-25
D	H_2	580-700	1/7	63	Nanospheres	100-200
E	H_2	580-700	1/0	761	Nanospheres	50-150
F	Ar	900-1000	1/0	658	Nanospheres	100-200
G	Ar	1000-1100	1/1	50-110	SWCNT+ MWCNT	8.8-1.5 + 20-50

According to Table 2.1, MWCNTs were produced for case A, B and C. In addition, both SWCNTs and MWCNTs were produced for case G. It is observed that diameter of CNTs decreases with the increase of anthracene content in mixture.

2.2.4.3 Injection Method

In this method, there are two furnaces and a quartz tube which passes through furnaces [42]. Schematic representation of system is given in Figure 2.10. Organometallic compounds are dissolved in carbon source [42]. This solution is given to first furnace by syringe [43]. Solution is passed through capillary tube and injected into furnace [43]. It is immediately vaporized [43]. Carrier gas brings it to second furnace [43]. At high temperature, carbon source and organometals are pyrolysis and CNTs are formed on metal particles [42].

Andrews et al. synthesized CNTs using injection method [42]. They used argon-hydrogen mixture as a carrier gas, xylene as a carbon source and ferrocene as a catalyst [42]. Ap-

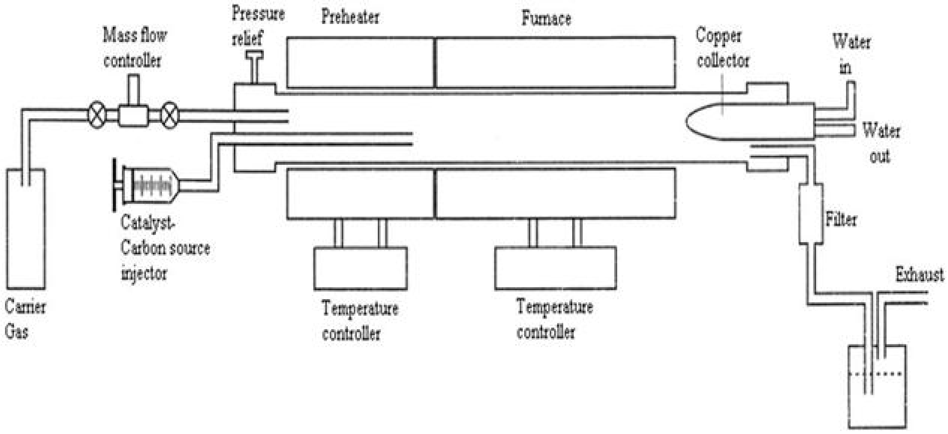

Figure 2.10: Schematic Representation of Injection Method [42]

proximately 6.5 mol % of ferrocene was dissolved in xylene and was fed continuously into preheater [42]. The reason of using xylene is that boiling point point of xylene, 140°C, is below the decomposition temperature of ferrocene, 190°C [42].

Liu et al. used floating catalyst method to produce MWCNTs [44]. They used ferrocene as a catalyst source and toluene as a carbon source [44]. All reactions were carried out at atmospheric pressure under 5 % H_2 in Argon (v/v) [44]. A solution of ferrocene in toluene (0-15 wt%) was placed in a 10 ml syringe [44]. They found that the thickness of the carbon film decreases with distance from the injection point [44]. They used 4 different growth temperatures (700, 800, 900 and 1000°C) [44]. As growth temperature increased up to 900°C they observed that CNT yield increased [44]. After 900°C, CNT yield started to decrease [44]. The carbon yield increased with ferrocene content up to a 10 wt% mixture, and then decreased with a 15 wt% mixture [44]. Also they observed that the thickness of the aligned CNT film deposited on the quartz plate increased with the ferrocene content [44]. They tried different solution injection speeds (0.1, 0.2, 0.5, 1.0, 2.7 ml/min) [44]. Carbon yield decreased with an increase of injection speed [44]. They found that a high carrier gas flow rate favored a high yield of the CNTs [44].

Bai et al. used floating catalyst method to produce aligned CNTs [45]. They used ferrocene as a catalyst source and xylene as a carbon source [45]. They produced CNTs between 720 and 820°C [45]. Up to 780°C, growth rate increases with increasing growth temperature

[45]. After 780°C, growth rate decreases sharply [45]. The ratio of G band to D band intensities increases and then decreases with increasing temperature, indicating that the graphite structure of the CNTs depends on the pyrolysis temperature [45]. They used different ferrocene concentration (0-0.08 g/ml) to see the effects of catalyst concentration [45]. Growth rate increases rapidly with increasing ferrocene concentration and it reaches its maximum at ferrocene concentration of 0.01 g/ml [45]. After this concentration, growth rate starts to decrease [45]. At lower ferrocene concentrations, the reason of lower growth rate is that there are insufficient Fe clusters to catalyze the growth of the aligned CNTs [45]. At high ferrocene concentration larger Fe clusters occurs [45]. Since these larger Fe clusters have low catalytic activity, growth rate decreases at high ferrocene concentrations [45]. Aligned CNTs synthesized at lower ferrocene concentrations have smaller diameters compared to CNTs synthesized at higher concentrations [45]. They changed preheating temperature from 180°C to 340°C [45]. They observed that growth rate increases with increasing preheating temperature [45]. At the higher preheating temperature range, the ferrocene and xylene form fine uniform droplets in the preheating zone, which are uniformly heated so that they decompose into Fe/C clusters that enhance the growth of aligned CNTs with smaller diameters [45].

Singh et al. used ferrocene as a catalyst source and toluene as a carbon source [46]. The growth temperature was varied between 550 and 940°C [46]. According to their results, the diameter of the CNTs increased with increasing temperature [46]. They also observed that CNT diameters and total carbon yield decrease with decreasing ferrocene concentration as a result of the formation of smaller iron clusters [46].

Mohlola et al. used $[CpFe(CO)_2]_2$ or $CpFe(CO_2)Me$ as a catalyst source, toluene as a carbon source [34]. The injection rate (0.2-0.8 ml/min) was observed to have no effect on the morphology and size of the CNTs formed, but did affect the amount of carbonaceous material formed at the lower injection rate (0.2 ml/min), generating more carbonaceous material [34]. $CpFe(CO_2)Me$ catalyzed reactions were studied at 800-1000°C [34]. When a lower temperature (800°C) was used the $CpFe(CO_2)Me$ catalyst formed more CNTs than amorphous carbon and carbon fibers, than at higher temperature (1000°) [34]. The outer diameter of the nanotubes generally increased with the reaction temperature [34]. They observed that a low catalyst concentration of catalyst in toluene (5 wt%) yielded more CNTs relative to a high catalyst concentration (10 wt%) [34].

Bhowmick et al. used ferrocene as a catalyst source and ethanol as a carbon source [47]. They used alcohol precursor instead of traditional hydrocarbon sources since using alcohol precursor's results in a better yield of the SWCNT [47]. Decomposed OH radicals react with solid carbon and this reduces the formation of soot and hence restricts the generation of amorphous carbon in the SWCNT product [47]. They varied ferrocene concentration (0.25, 0.5 and 1.0 wt%) [47]. They observed that higher metal concentrations produce larger quantities of larger diameter CNTs [47]. Also the average catalyst particle size for the 1.0 wt% sample was found to be larger than that for the 0.25 wt% sample [47]. They found that the percentage of the SWCNT decreases linearly with increasing ferrocene concentration in the sample [47]. As the temperature was increased, there was a definite increase in the range of the SWCNT diameters produced [47]. The quality of the SWCNT produced increases as a function of the growth temperature, evidenced by the increase in the intensity ratio of the G to D band for the higher temperature samples [47]. Average diameter of the CNTs decreased as temperature increased [47].

Sinnott et al. used two different Fe:C atomic ratios to investigate the effect of catalyst particle size on CNT diameters [48]. Ferrocene was dissolved in xylene at 0.75 and 0.075 at% Fe:C atomic ratios [48]. Then this solution was fed to the furnace under argon and 10% hydrogen flow [48]. Their results were given in Table 2.2.

Table 2.2: Average CNT and Fe Particle Diameters at Different Fe/C Ratio [48]

Fe/C (at%)	Average CNT inner D (nm)	Average CNT outer D (nm)	Average Fe particle D (nm)
0.75	5.8	33.6	35.3
0.075	4.3	28.3	28.2

According to their results CNTs have average diameter of about 33 nm at the higher ratio [48]. CNTs have smaller average diameter of about 28 nm at the lower ratio and narrower diameter distribution [48]. The generation of smaller iron clusters is the reason of obtaining the smaller average CNT diameter at the lower Fe:C ratio [48]. Iron atoms can not agglomerate into large clusters at a lower iron concentration in the vapor phase [48]. Thus, formation of smaller iron clusters is more favorable [48].

2.3 GAS PHASE ANALYSIS RESEARCHES DURING PRODUCTION OF CARBON NANOTUBES

These studies are mainly performed to investigate kinetics of CNT formation at floating catalyst system. Mainly the gas phase analysis of reaction medium was made.

Endo et al. analyzed hydrocarbon concentrations in the tail gas during CNT production [49]. They used xylene as a carbon source [49]. Ferrocene, their catalyst source, was first deposited on the furnace walls [49]. Then, xylene was fed to the furnace under argon and hydrogen flow [49]. Analysis of the tail gas from their reactor showed the presence of toluene, benzene and methane as key reaction byproducts [49]. Trace amounts of some C_2 hydrocarbons were also detected [49]. They studied two gas-phase reactions and four surface reactions [49]. The rate constants obtained by Benson and Shaw were used for gas-phase reactions [49]. The rate constants of surface reactions were determined based on their tail gas analysis [49]. They calculated axial concentration distributions of xylene, toluene, benzene and methane along z axis and their results is given in Figure 2.11 [49]. From Figure 2.11, it is seen that xylene starts to decompose at the entrance of furnace [49]. Its concentration decreases along the z axis [49]. Toluene and methane concentrations rapidly increase between z=0.6 and z=0.7 m [49]. After z=0.7 m the toluene concentration slowly increases whereas the methane concentration slowly decreases [49]. Moreover, after this point, benzene starts to form and its concentration increases along the z axis [49].

Kuwana et al. analyzed hydrocarbon concentrations at different reaction times during CNT production [50]. They employed a two-step method [50]. Ferrocene, their catalyst source, was deposited on the furnace wall [50]. After iron nano particles were formed, xylene, their carbon source, was fed to the reactor under argon and hydrogen flow [50]. At different reaction times, the exhaust gas was analyzed with mass spectrometer and concentrations of hydrocarbons were measured [50]. Concentrations of hydrocarbons are given in Table 2.3. They observed that xylene concentration at the exhaust gas increases as times goes on [50]. This means that xylene consumption inside the reactor continuously decreases.

Wasel et al. analyzed gas samples taken from reaction medium [51]. They used floating catalyst method to produce CNTs [51]. They used xylene as a carbon source and ferrocene as

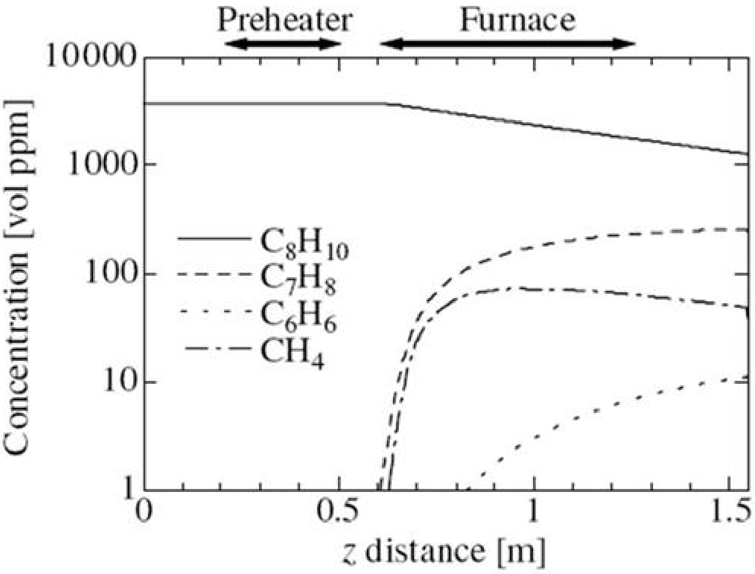

Figure 2.11: Axial Concentration Distributions of Xylene, Toluene, Benzene, and Methane along the z axis [49]

a catalyst source [51]. They used total 1500 cm^3/min of Ar and 10% H_2 as carrier gas [51]. They took gas samples from reaction medium and analyzed them with gas chromatography [51]. At 700, 800, 1000 and 1200°C pyrolysis of xylene was investigated [51]. At 700 and 800°C experiments were repeated using xylene and ferrocene [51]. They were able to detect concentrations of methane, total C_2 species (C_2H_x) and argon plus hydrogen [51]. Argon and hydrogen could not be separated in their gas chromatogram [51]. They observed that both methane and total C_2 species concentrations increased by 5-10% both at 700 and 800°C with the presence of ferrocene [51]. This result may suggest that methyl radicals are produced via a C-C bond split during catalytic decomposition of xylene on the surface of iron particles [51].

How CNTs are formed has carried on its mystery since their discovery in 1991. Though some studies were done to find formation mechanism of CNTs, most of them depend on computational fluid dynamics (CFD) modeling. In literature few researchers studied gas phase analysis during CNT formation. However, in these studies, few chemicals can be analyzed. To understand formation mechanism of CNTs gas phase analyses should be done more detailed manner and considering more chemicals. New CFD models can be suggested according to the

Table 2.3: Measured Exhaust Gas Concentrations at Different Reaction Times [50]

Time (min)	Xylene (ppm)	Toluene (ppm)	Benzene (ppm)	Methane (ppm)
5	135	12	1	5
15	182	17	0	11
30	379	73	2	21
60	657	99	2	23
90	1240	161	4	42
120	1234	172	4	38

results of detailed gas phase analyses. Thus, new CFD models will become one step closer to reality.

In this study change of gas phase composition along the reactor was studied experimentally at different space times in the presence and absence of solid catalyst, under CNTs production conditions.

CHAPTER 3

EXPERIMENTAL

3.1 EXPERIMENTAL SETUP

Experimental system that is used to produce carbon nanotubes with chemical vapor deposition method is formed in Department of Chemical Engineering in Ankara University. Schematic representation of the set up is given in Figure 3.1.

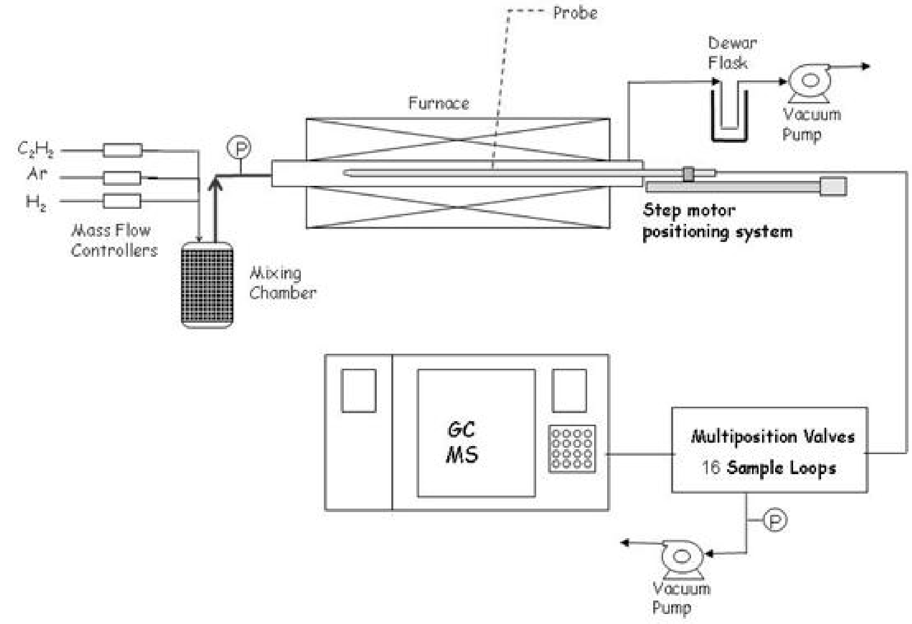

Figure 3.1: Schematic Representation of Experimental System

In experiments three gases are used. These are argon as a carrier gas, acetylene as a hydrocarbon source and hydrogen as a reducing agent. Flow rates of argon, acetylene and hydrogen that are used in the experiments are adjusted with electronic flow meters (Alicat Scientific). After flow meters, gases enter mixing chamber. The aim of using mixing chamber is to ensure that gases are well mixed and to prevent differences in gas pressure to cause any problems.

Gases leaving mixing chamber enter quartz tube with a 40 mm outer diameter. Quartz tube is put inside the furnace (Protherm). Temperature of the furnace is controlled by control unit. Temperature profiles of the furnace were obtained at different set points. Detailed work about temperature profile of the furnace is given in appendices A.

Pressure inside quartz tube is adjusted with vacuum pump and pressure regulator that are at the end of line. Pressures of loops are adjusted with another vacuum pump and regulation valve.

Gases leaving quartz tube pass through dewar flask. Harmful gases condense there and rest are exhausted.

While reaction takes place inside quartz tube, samples were taken from reaction medium, and analyzed in gas chromatography and mass spectrometry (GC/MS).

To take samples a steel probe was used. Length of the probe is 110 cm. Probe is composed of 3 concentric pipes. In Figure 3.2 schematic representation of steel probe is given. Outer diameters of these 3 pipes are 16, 10 and 6 mm, respectively. Inner pipe is used to take samples. Cooling liquid that cools probe passes through the annular space. Different fluids were tried to cool probe. Cooling studies of probe are given in appendices B. Leakproof stainless steel connection element is designed and made to connect quartz tube and probe to each other.

Step motor system is used to move probe inside the furnace. Aluminum and stainless steel components are designed and made to attach probe to step motor.

To obtain concentration profile along the furnace samples should be taken from gas phase and analyzed. After analysis at one point is completed, probe is moved to new point and same procedure has to be repeated. For each point it is necessary to wait approximately 45 minutes for completing analysis. In this case, system has to be kept at same conditions for 12 hours to obtain concentration profile of 16 cm with a 1 cm interval. However, it is not possible to keep system at same conditions for such a long time since catalyst particles start to deactivate

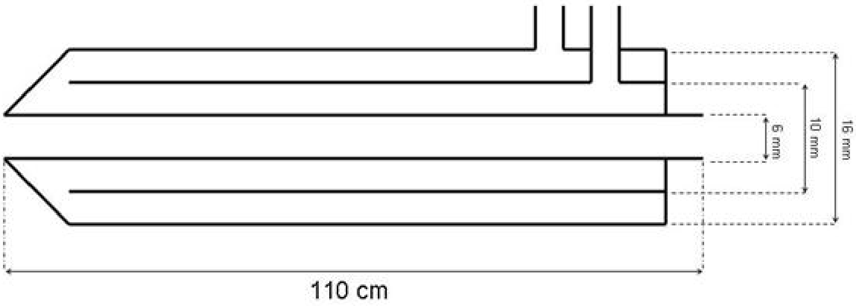

Figure 3.2: Schematic Representation of Steel Probe

after a certain time. Since it is not possible to analyze all the samples taken simultaneously during the experiment, samples taken from reaction medium are stored in 16 loops as shown in Figure 3.3. Each loop has a volume of 0.5 ml. Vacuum pump is connected to suction line to take samples inside the loops. Regulation valve and pressure sensor are also connected to suction line. Hence, loops can be filled with samples of desired pressure. Experiments were done with sample loops to check whether they were suitable for our researches. Studies done with sample loops are given in appendices C.

Loops are placed into storage box whose temperature can be controlled so that condensation of samples inside loops can be prevented.

Since volumes of loops are known and their temperature and pressure can be controlled, same amount of samples can be taken to loops in each experiments.

After all the loops are filled with gas samples, position of 6 port valve is changed. Samples in loops are sent to be analyzed in GC/MS with new position of 6 port valve. In Figure 3.3 schematic representation of 6 port valve is given.

Three different columns are used in GC to separate components in samples, which are HP1, PLOTQ and Molecular Sieve. HP1 is a 60 m length column with 0.250 mm inner diameter [52]. Inside of the column is covered with dimethylpolysiloxane [52]. It is used to separate heavy hydrocarbons in our system. PLOTQ is a bonded polystyrene-divinylbenzene based column [52]. Length and inner diameter of the column are 30 m and 0.53 mm, respectively [52]. It is an excellent column for C1 to C3 isomers, CO_2, methane, air/CO [52]. It can separate ethane, ethylene and acetylene [52]. Molecular Sieve is a PLOT column for the analysis of permanent gases [52]. It has a length of 30 m and inner diameter of 0.53 mm [52]. It separates H_2, Ar, N_2, O_2 and CO [52]. Three columns are used to separate and analyze wide range of chemicals. Two valves are placed into GC. With these valves samples entering columns are analyzed either with thermal conductivity detector (TCD) or MS. TCD detector detect the ability of conduction of gas [53]. When the component was changed, the conductivity changed by different gas component [53]. In Figure 3.4 paths of samples according to positions of valves are given.

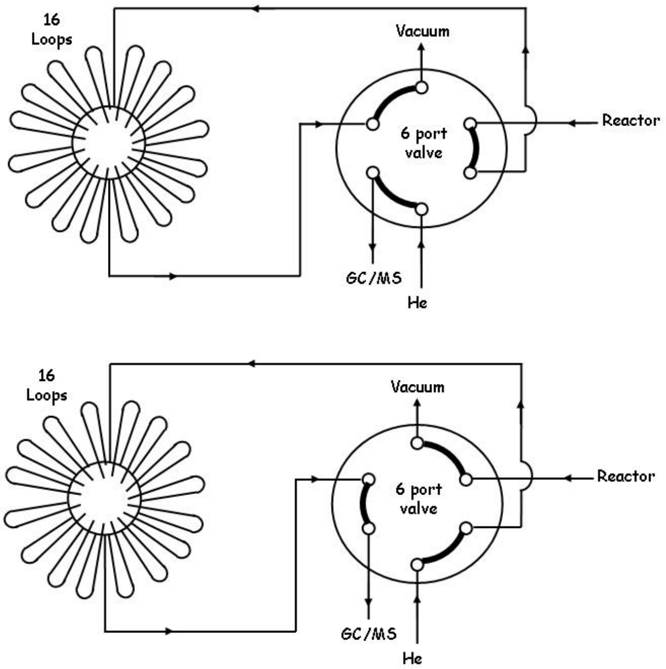

Figure 3.3: Schematic Representation of 6 Port Valve

3.2 EXPERIMENTAL METHOD

3.2.1 Catalyst Preparation

For catalyst preparation method and procedure, catalyst preparation method and procedure in Soysal's thesis [55] were chosen. Catalysts used in carbon nanotube production were prepared

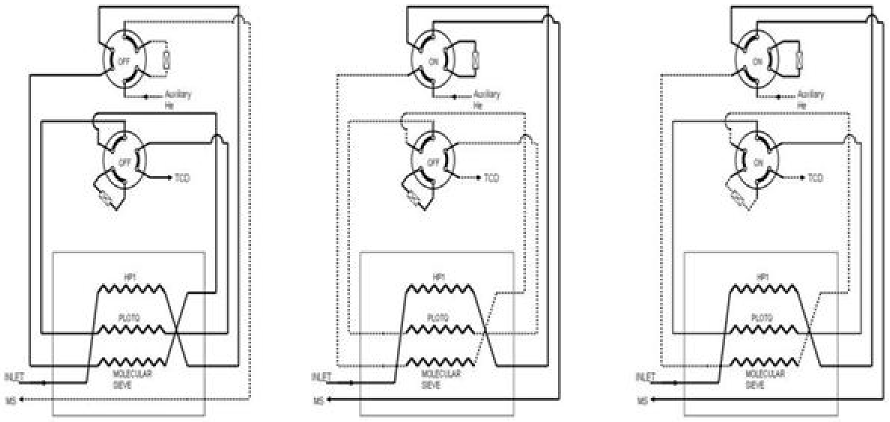

Figure 3.4: Paths of Samples According to Positions of Valves

by sol-gel method. 1.4 g iron (III) nitrate nonahydrate ($Fe(NO_3)_3 \cdot 9H_2O$) was mixed with 1540 μl tetraethylorthosilicate (TEOS), 1540 μl ethyl alcohol and 1750 μl water. The solution prepared was well-mixed, and deposited onto quartz tube with 34 mm outer diameter, where the solution was dried at room temperature for 5 hours. Then quartz tube was put inside another quartz tube with 40 mm outer diameter. 40 mm quartz tube was put inside furnace. Calcination was done under vacuum at 450°C for 12 hours. After calcination reduction was done at 300 Torr and 500°C. It took 2 hours under 1 l/min argon and 0.1 l/min hydrogen flow.

3.2.2 CNT Production and Gas Phase Analysis

Experimental conditions were decided according to the results of the previous experiments. The CNT formation reaction was not very significant below 850°C. H_2 / C_2H_2 feed ratio was found such that at that ratio iron catalyst could be kept at its reduced state.

Two types of experiments were done with and without catalyst. In case of catalyst gas samples during acetylene pyrolysis with catalyst were taken. In case of no catalyst catalyst preparation was not done and experiments were done without catalyst. Gas samples during acetylene pyrolysis without catalyst were taken.

After reduction furnace was heated under argon flow. After temperature of the furnace reached to the set point, acetylene and hydrogen were fed to the system. 5 minutes was allowed to reach steady state. After that it was started to take gas samples into loops. After taking sample at one point was completed, loop was changed and probe was moved to new point with step motor.

When filling loops was completed, flows of acetylene and hydrogen were shut and furnace was allowed to cool under argon flow.

After filling process, position of 6 port valve was switched. Gas samples inside loops were analyzed in GC/MS one by one. After all loops were analyzed, they were purged and after that they were cleaned by passing argon.

Furnace was cooled down with argon flow. The reason of cooling under argon flow was that exposure to air at elevated temperatures can cause damage to carbon nanotubes [54]. After furnace was cooled down, samples inside quartz tube were collected.

To prepare quartz tube for the next experiment, it should be first cleaned. To do so, furnace was heated to 600°C. Air was send inside quartz tube with using compressor so that carbon residues remaining in quartz tube can burn.

3.3 CHARACTERIZATION TECHNIQUE

Scanning electron microscopy is a widely used characterization technique for researchers interested with nanotechnology. It can be used to prove the existence of CNTs on the product. To prove CNTs produced with catalyst QUANTA 400F Field Emission SEM equipment in METU Central Laboratory was used. SEM images of collected products after experiments were taken under low vacuum and without coating.

CHAPTER 4

RESULTS AND DISCUSSIONS

Five different sets of experiments were performed to analyze the effects of catalysts on carbon nanotube production. The first two were without catalyst. In the first set acetylene pyrolysis was carried on at 800°C and 400 Torr. Then, acetylene pyrolysis was repeated with addition of hydrogen at the same conditions. Thirdly, same experiments were repeated with catalysts. Finally, last two experiments were repeated at 875°C.

4.1 ACETYLENE PYROLYSIS EXPERIMENT

1.5 l/min argon and 0.225 l/min acetylene were fed to the reactor. Set point of the furnace and pressure inside reactor were 800°C and 400 Torr, respectively. Samples were taken with probe starting from entrance of the furnace with 2 cm interval. Reactor was scanned up to 28 cm behind the entrance of the furnace. In last 30 cm of the furnace formation of polyaromatic hydrocarbons (PAHs) whose molecular weights are greater than biphenyl was increased. When taking gas samples was tried in last 30 cm, pressures of loops could not be adjusted and probe started to plug due to those PAHs. To prevent plugging of the probe taking gas samples was done at first 30 cm of the furnace. Loops were filled at approximately 210 Torr. Temperatures of the loops were kept constant at 150°C.

Then, samples inside the loops were analyzed at GC/MS one by one. Argon and acetylene were analyzed at TCD, benzene and hydrocarbons with molecular weights greater than benzene were analyzed at MS. Sample chromatogram and spectrum were given in appendix D.

In literature it was proposed that large number of reactions were involved in acetylene pyrolysis. Details of those reactions can be found in references [49, 51, 56, 57, 58, 59, 60, 61].

Benzene, toluene, styrene, indene, naphthalene, 1-methyl naphthalene, acenaphthalene and biphenyl were observed as products of acetylene pyrolysis. Areas of these chemicals were measured from obtained spectrums and chromatograms for each point where samples were taken. Moles of chemicals whose calibrations were completed were calculated from areas. Details of calibrations are given in appendix E. Space times were also calculated. Space times calculations are given in appendix F.

4.2 ACETYLENE PYROLYSIS WITH ADDITION OF HYDROGEN

After acetylene pyrolysis experiment was completed, these experiments were repeated with addition of hydrogen. So that effect of hydrogen on acetylene pyrolysis was investigated. 1.5 l/min argon, 0.225 l/min acetylene and 0.300 l/min hydrogen were fed to the reactor. Set point of the furnace and pressure inside reactor were 800°C and 400 Torr, respectively. Samples were taken with probe starting from entrance of the furnace with 2 cm intervals. Reactor was again scanned up to 28 cm behind the entrance of the furnace. Loops were filled at approximately 210 Torr. Temperatures of the loops were kept constant at 150°C.

Then, samples inside the loops were analyzed at GC/MS one by one. Argon and acetylene were analyzed at TCD, benzene and hydrocarbons with molecular weights greater than benzene were analyzed at MS. This experiment was repeated once more at same conditions for reproducibility. After completing 800°C experiments, experiment was repeated once more at 875°C.

Areas of these chemicals were measured from obtained spectrums and chromatograms for each point where samples were taken. Moles of chemicals whose calibrations were completed were calculated from areas.

4.3 CARBON NANOTUBE PRODUCTION EXPERIMENTS

Difference in concentration profiles of chemicals were investigated at same conditions with addition of solid catalyst. 1.5 l/min argon, 0.225 l/min acetylene and 0.300 l/min hydrogen were fed to the reactor. All the experimental methods and the parameters were identical with the previous two cases.

Experiment were repeated once more at the same conditions for reproducibility. After completing 800°C experiments, experiments were repeated two times at 875°C. Moreover, one more experiment was done at 800°C to check the activity of catalyst with time. Details of experiment were given in appendix G. According to results of experiment amounts of acetylene, benzene and toluene were not change with time. This concluded that activity of catalyst remained constant for at least 75 minutes time interval.

4.4 SEM RESULTS

Summary of experiments for carbon nanotube production are given in Table 4.1. Products of experiments with catalyst, Exp 4, Exp 5, Exp 7 and Exp 8, were send to SEM analysis.

Table 4.1: Summary of Experimental Parameters in Carbon Nanotube Production Experiments

Exp #	Temperature, °C	Pressure, Torr	Ar Flow Rate, l/min	C_2H_2 Flow Rate, l/min	H_2 Flow Rate, l/min	Catalyst
1	800	400	1.5	0.225	-	NO
2	800	400	1.5	0.225	0.3	NO
3	800	400	1.5	0.225	0.3	NO
4	800	400	1.5	0.225	0.3	YES
5	800	400	1.5	0.225	0.3	YES
6	875	400	1.5	0.225	0.3	NO
7	875	400	1.5	0.225	0.3	YES
8	875	400	1.5	0.225	0.3	YES

According to SEM results CNTs production was achieved in experiments with catalyst. SEM images of four experiments done at 800°C and 875°C are given in Figures 4.1, 4.2, 4.3 and 4.4. Experiments 4 and 5 done at 800°C had lower CNTs than experiments done 875°C. Increasing temperature increased the amount of produced CNTs.

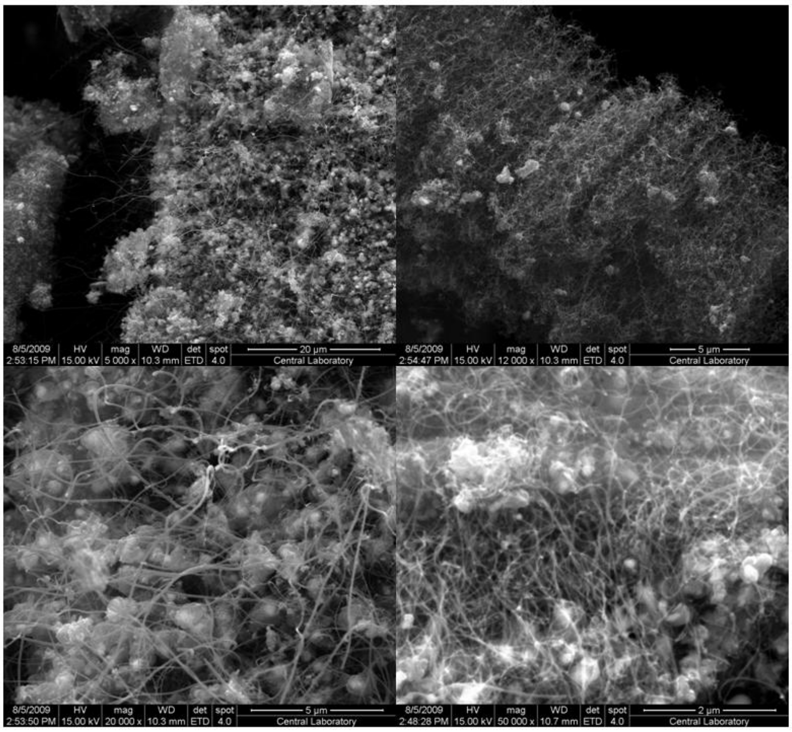

Figure 4.1: SEM Images of Experiment 4

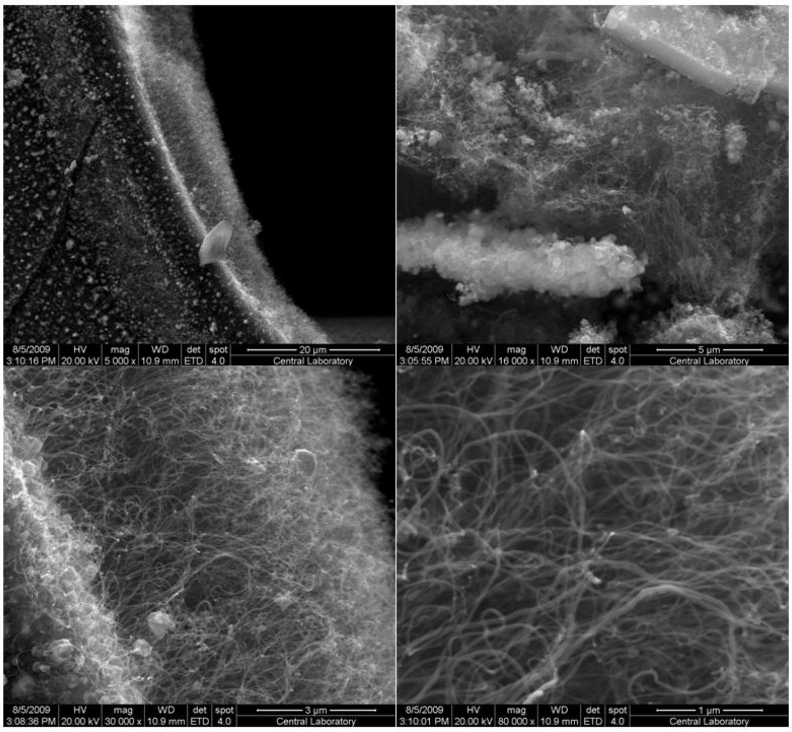

Figure 4.2: SEM Images of Experiment 5

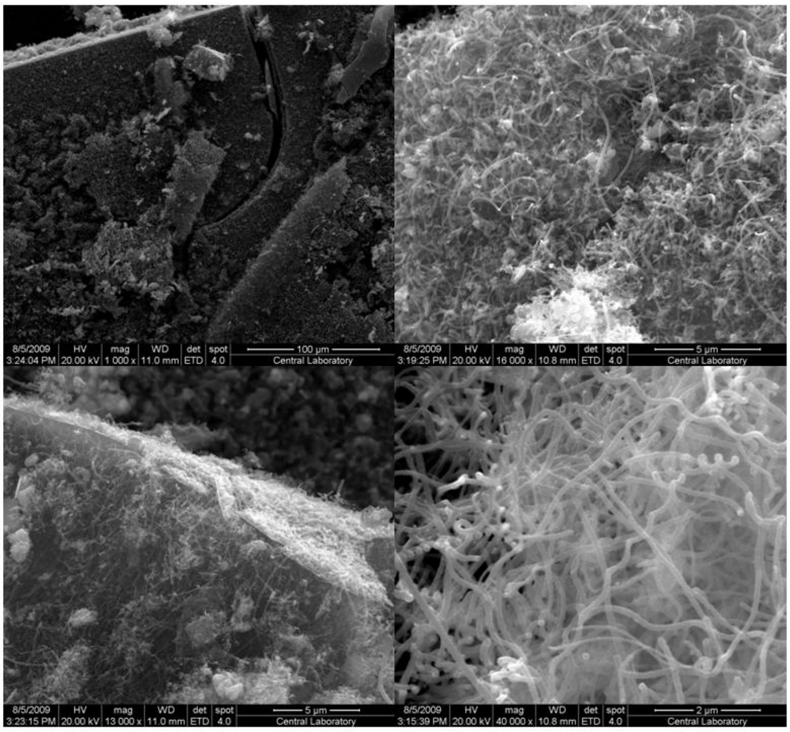

Figure 4.3: SEM Images of Experiment 7

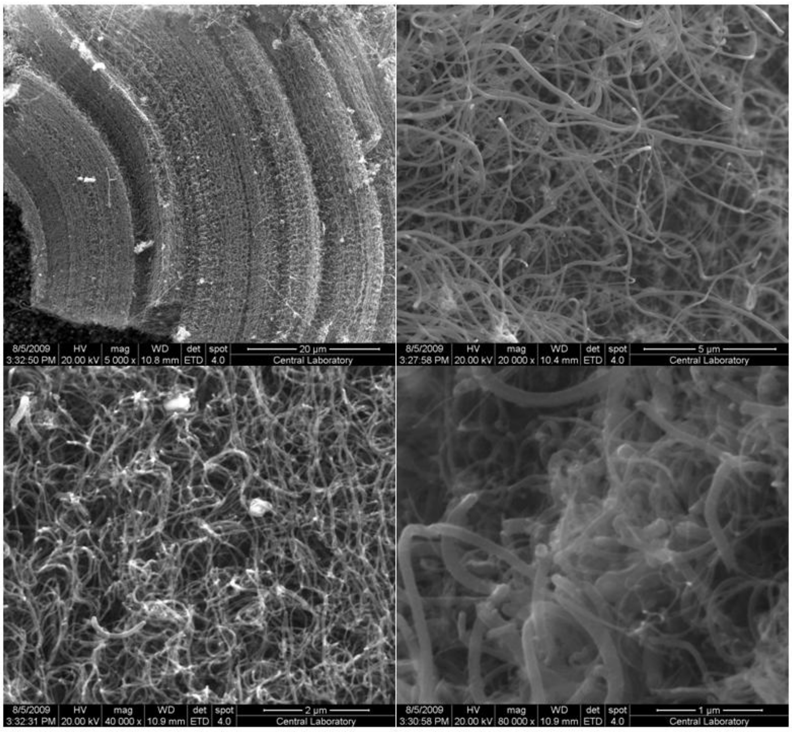

Figure 4.4: SEM Images of Experiment 8

4.5 COMPARISON OF 800°C EXPERIMENTS

Furnace temperature data were collected from furnace temperature controller for all experiments. Before moving probe to next point furnace temperature was noted. Temperature controller measured furnace temperature from midpoint. Furnace temperature data for experiments 1, 2, 3, 4 and 5 are plotted in Figure 4.5. In experiment 1 temperatures read from furnace temperature controller were less than set point while probe was moving in first 14 cm. When probe came in front of the furnace, 60 cm of probe was exposed to hot surface of furnace. Furnace tried to heat steel probe however heating power of the furnace was not sufficient. So furnace could not be heated up to desired temperature. Since only first 30 cm of the furnace was used for analysis, outside of last 30 cm of quartz tube inside the furnace was covered with glasswool. Thus part of the probe staying in that region was not exposed to hot surface. Other experiments were done with that protection. As it was seen from Figure 4.5, temperature remained at set point. Since temperature in experiment 1 was lower than temperatures in other experiment, results of experiment 1 were excluded from comparisons.

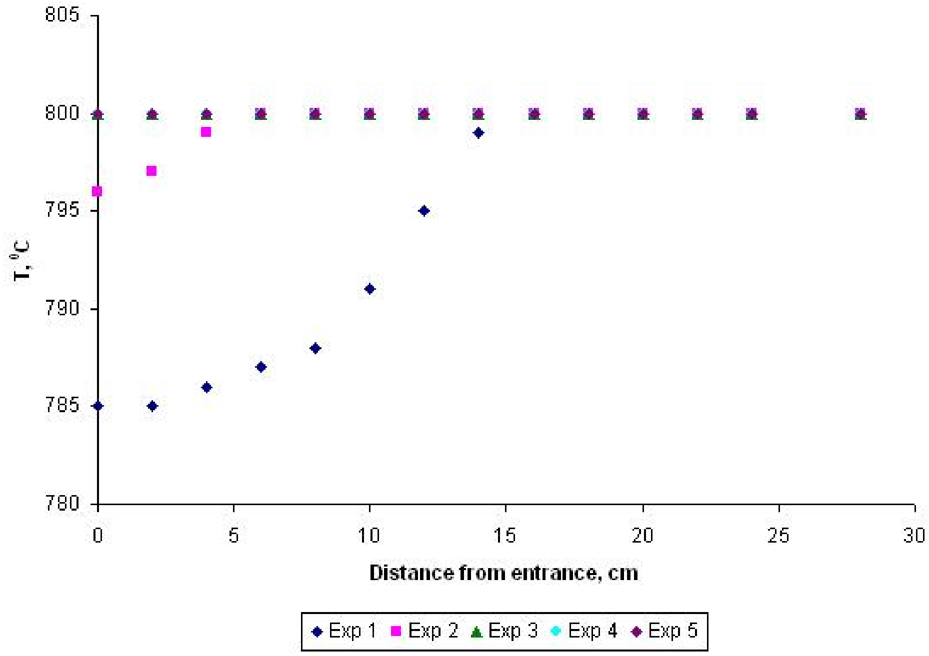

Figure 4.5: Furnace Temperature Along the Reactor for 800°C Experiments

Mole percentages of argon for the two sets of experiments are plotted in Figure 4.6. Calculations of mole percentages of argon are given in appendix F. Average of experiments done without catalyst were taken and plotted in Figure 4.6. Average of experiments done with catalyst were also taken. Since absence and presence of catalyst did not affect amount of argon, mole percentages of argon should be same. There were differences in mole percentages of argon with and without catalyst however those differences were in the range of experimental errors.

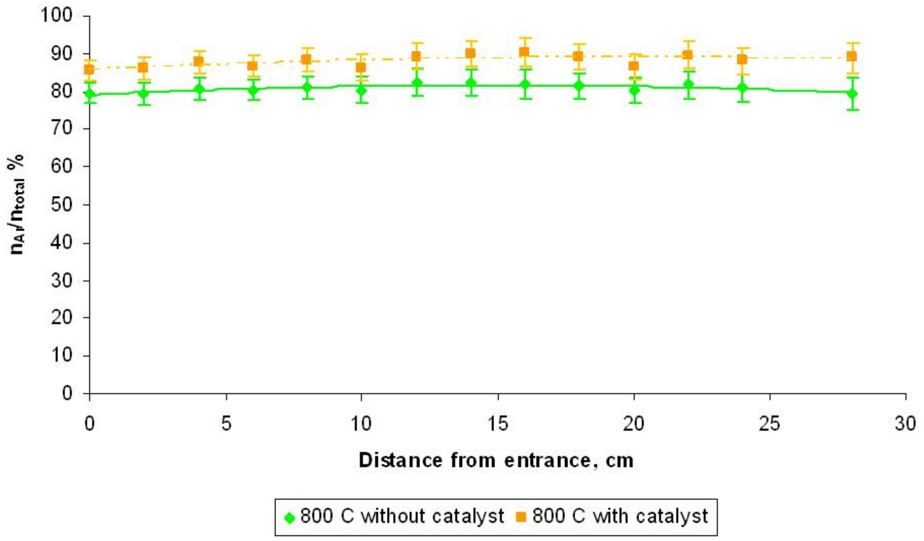

Figure 4.6: Mole Percentages of Argon Along the Reactor for 800°C Experiments

To compare concentrations of chemicals with each other list of concentrations of chemicals at one point for one of the experiment is given in table 4.2.

Mole percentages of acetylene for two sets of experiments are plotted in Figure 4.7. Amounts of acetylene with and without catalyst were close to each other. Amounts of acetylene with catalyst were slightly less in the scanned region. However, those differences were in the range of experimental error. Hence, it is concluded that no significant difference in concentration of acetylene was observed since amount of produced CNTs was low at 800°C.

Table 4.2: Comparison of Order of Magnitudes of the Concentrations for 800°C Experiment without catalyst at x=14 cm

Chemical	n_i/n_{total} %	Chemical	n_i/n_{total} %
Argon	82.24	Indene	$6.11 x 10^{-4}$
Acetylene	9.01	Naphthalene	$2.14 x 10^{-3}$
Benzene	$5.65 x 10^{-3}$	1-Methyl Naphthalane	$3.62 x 10^{-4}$
Toluene	$0.61 x 10^{-3}$	Acenaphthalene	$12.53 x 10^{-4}$
Styrene	$6.36 x 10^{-4}$	Biphenyl	$5.09 x 10^{-4}$

Mole percentages of produced benzene for two sets of experiments are given in Figure 4.8. Mole percentages of benzene were close to each other. Since temperature was not sufficient to produce large amounts of CNTs with catalyst, no significant difference was observed between mole percentages of benzene.

Mole percentages of produced toluene are plotted in Figure 4.9. Amounts of toluene in experiment with catalyst were higher than amounts of toluene in experiment without catalyst. Addition of catalyst caused to an increase in toluene concentration.

Mole percentages of styrene with and without catalyst are plotted in Figure 4.10. More styrene was produced in experiment with catalyst compared to experiment without catalyst. Addition of catalyst caused to an increase in styrene concentration. The reason for producing more styrene with catalyst was either styrene was produced while CNTs were formed or a byproduct of CNTs formation was converted to styrene.

Mole Percentages of indene for two sets of experiments are plotted in Figure 4.11. Similar to toluene and styrene more indene was obtained with catalyst experiment. Addition of catalyst caused to an increase in indene concentration.

Mole percentages of naphthalene are plotted in Figure 4.12. Concentrations of naphthalene were higher in catalyst experiment between x=10 cm and x=24 cm. Addition of catalyst caused to an increase in naphthalene concentration.

Mole percentages of 1-methyl naphthalene are plotted in Figure 4.13. Amounts of 1-methyl naphthalene in experiment with catalyst were higher than amounts of 1-methyl naphthalene

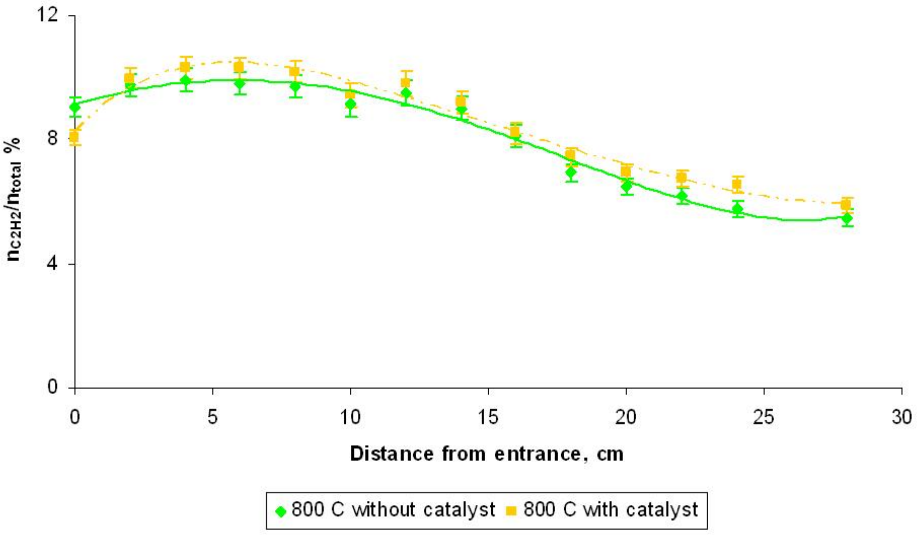

Figure 4.7: Mole Percentages of Acetylene Along the Reactor for 800°C Experiments

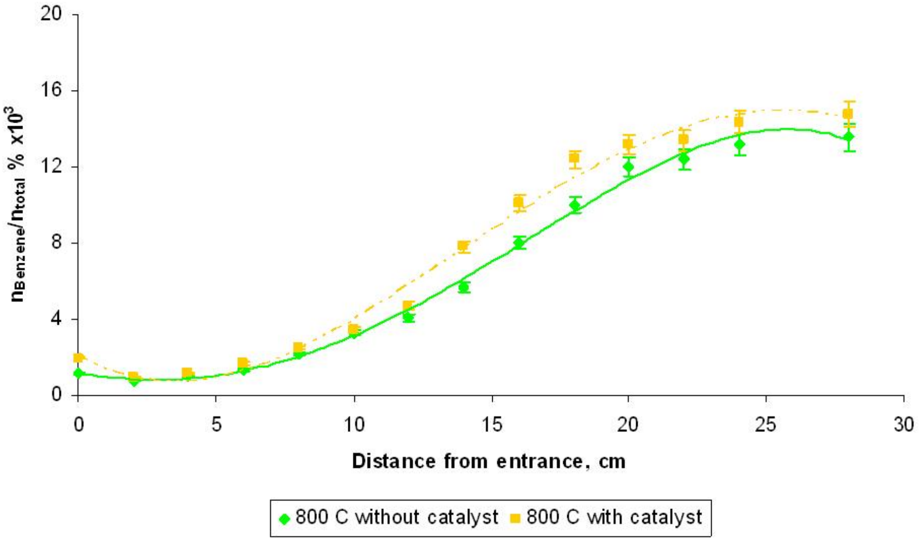

Figure 4.8: Mole Percentages of Benzene Along the Reactor for 800°C Experiments

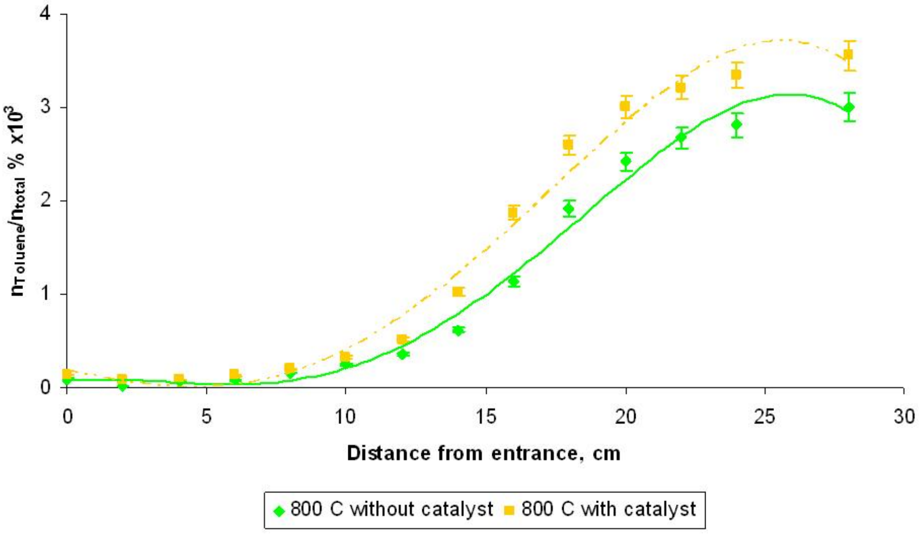

Figure 4.9: Mole Percentages of Toluene Along the Reactor for 800°C Experiments

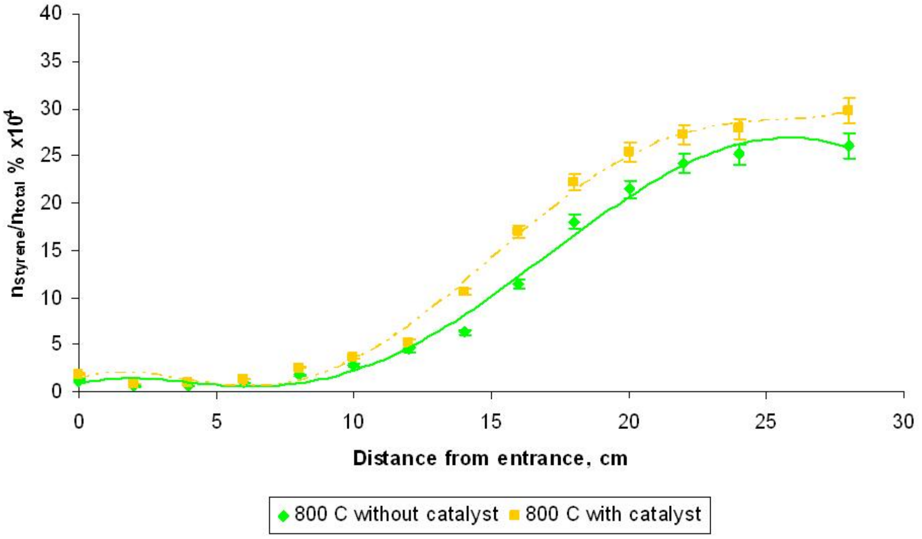

Figure 4.10: Mole Percentages of Styrene Along the Reactor for 800°C Experiments

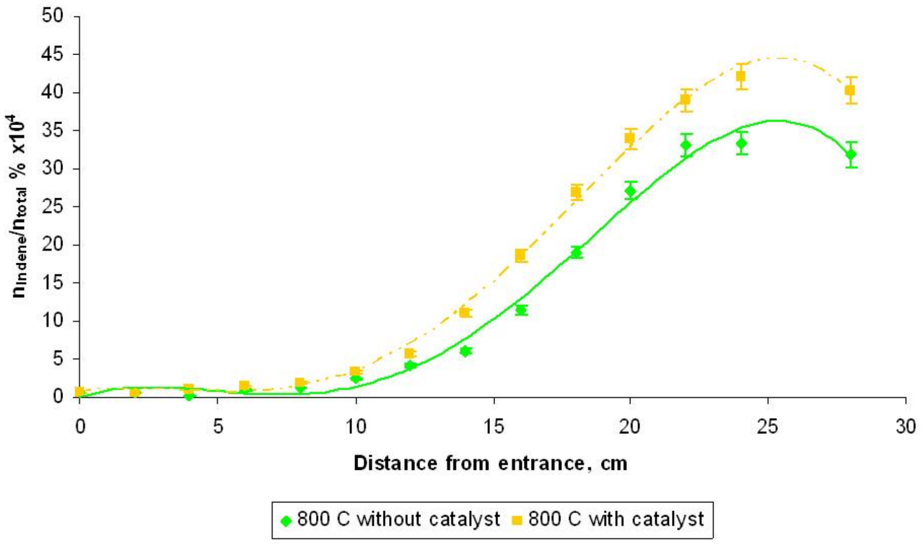

Figure 4.11: Mole Percentages of Indene Along the Reactor for 800°C Experiments

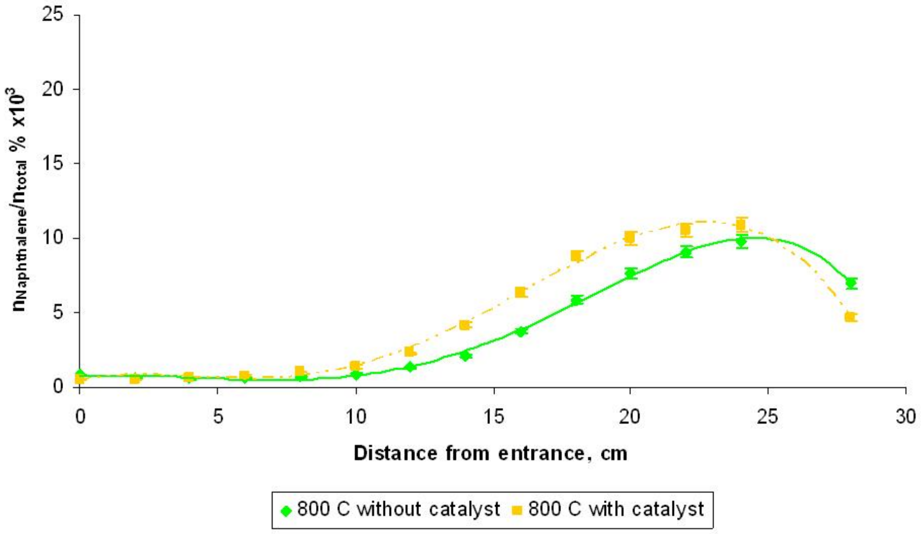

Figure 4.12: Mole Percentages of Naphthalene Along the Reactor for 800°C Experiments

in experiment without catalyst. Differences in concentrations were out of the range of experimental error.

Mole percentages of acenaphthalene are plotted in Figure 4.14. Concentrations of acenaphthalene were higher in experiment with catalyst in the first 18 cm. After that point concentrations of acenaphthalene were lower in experiment with catalyst.

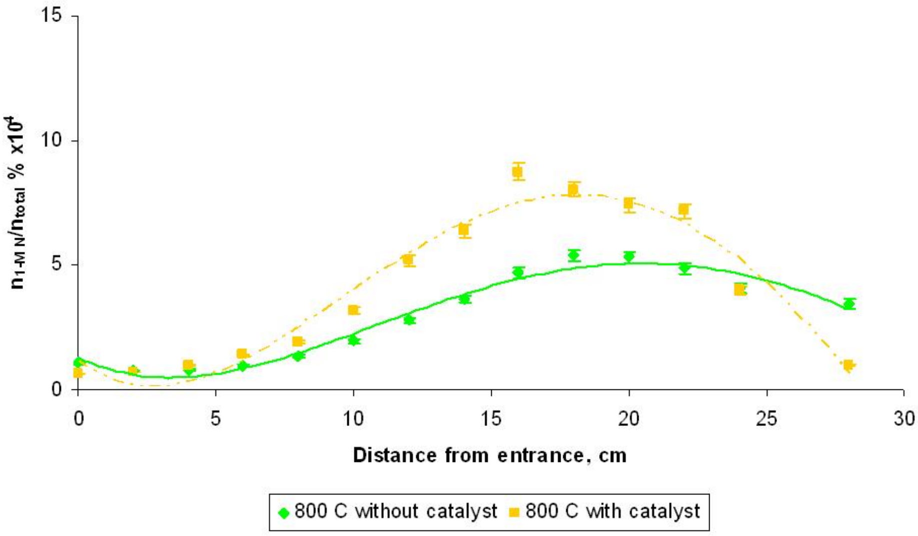

Figure 4.13: Mole Percentages of 1-Methyl Naphthalene Along the Reactor for 800°C Experiments

Mole percentages of biphenyl given in Figure 4.15. More biphenyl was produced in experiment with catalyst compared to experiment without catalyst.

4.6 COMPARISON OF 875°C EXPERIMENTS

Furnace temperature data for experiments 6, 7 and 8 are plotted in Figure 4.16. In all three experiments temperatures read from furnace temperature controller were less than set point while probe was moving in first 20 cm.

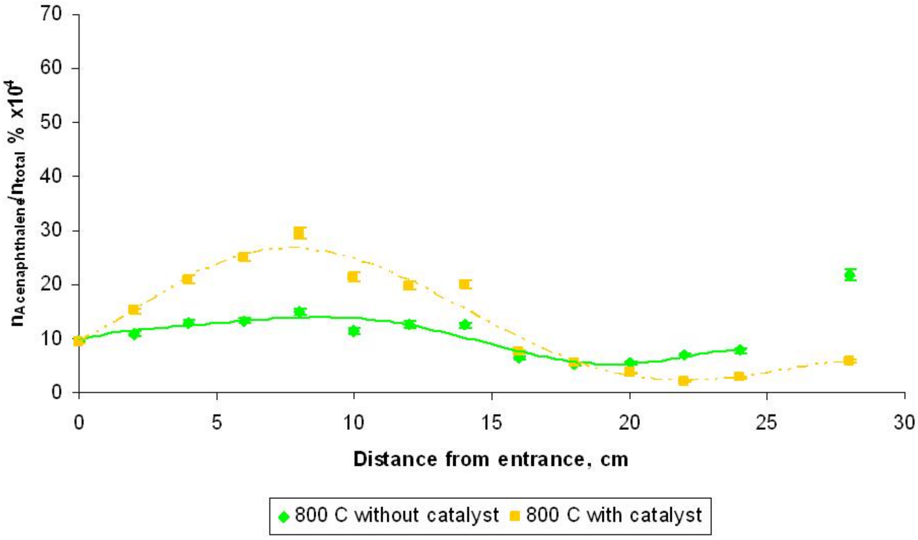

Figure 4.14: Mole Percentages of Acenaphthalene Along the Reactor for 800°C Experiments

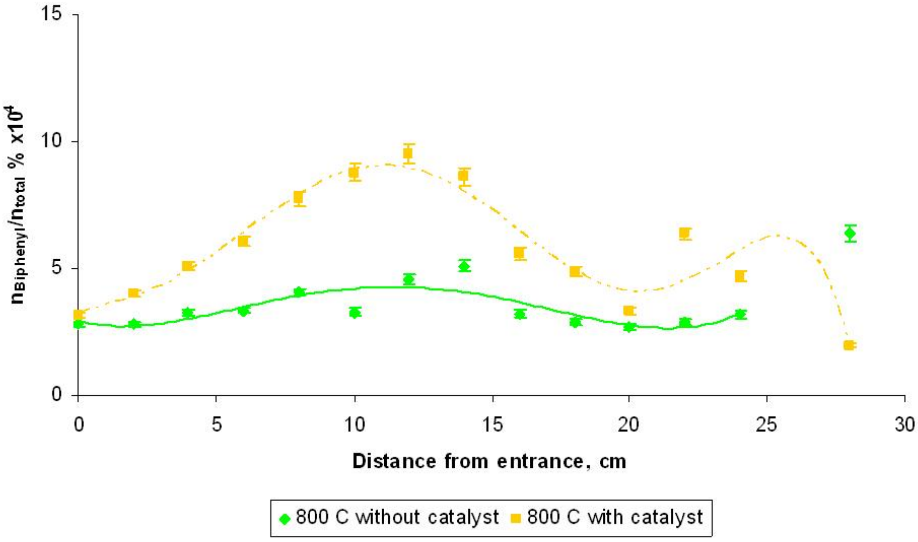

Figure 4.15: Mole Percentages of Biphenyl Along the Reactor for 800°C Experiments

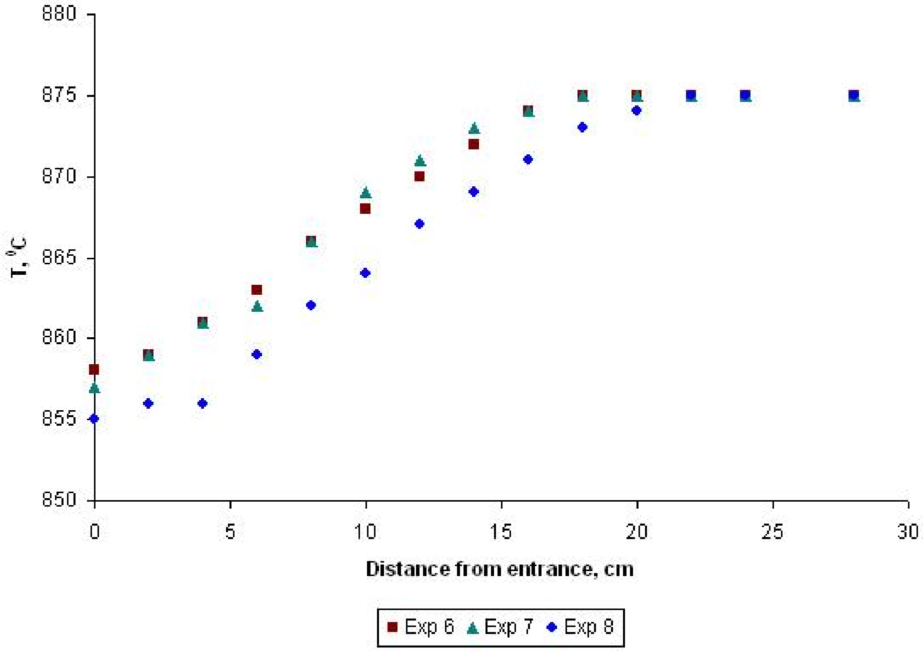

Figure 4.16: Furnace Temperature Along the Reactor for 875°C Experiments

Mole percentages of argon for two sets of experiments are plotted in Figure 4.17. Average of experiments done with catalyst were taken and plotted in Figure 4.17. Mole percentages of argon in experiments with and without catalyst were almost same as it was expected.

Mole percentages of acetylene for two sets of experiments are plotted in Figure 4.18. Amounts of acetylene in experiment with catalyst were lower than amounts of acetylene in experiment without catalyst. Differences in concentrations were out of the range of experimental error. Decomposing more acetylene in experiment with catalyst compared to experiment without catalyst was proved that more acetylene was used while CNTs were formed compared to pyrolysis of acetylene.

Mole percentages of produced benzene and toluene are plotted in Figures 4.19 and 4.20. Concentrations of benzene were higher in catalyst experiment between x=6 cm and x=20 cm. Concentrations of toluene were higher in catalyst experiment between x=6 cm and x=16 cm. After that point concentrations of toluene with and without catalyst were almost same. Addition of catalyst caused to an increase in benzene and toluene concentrations. The reason

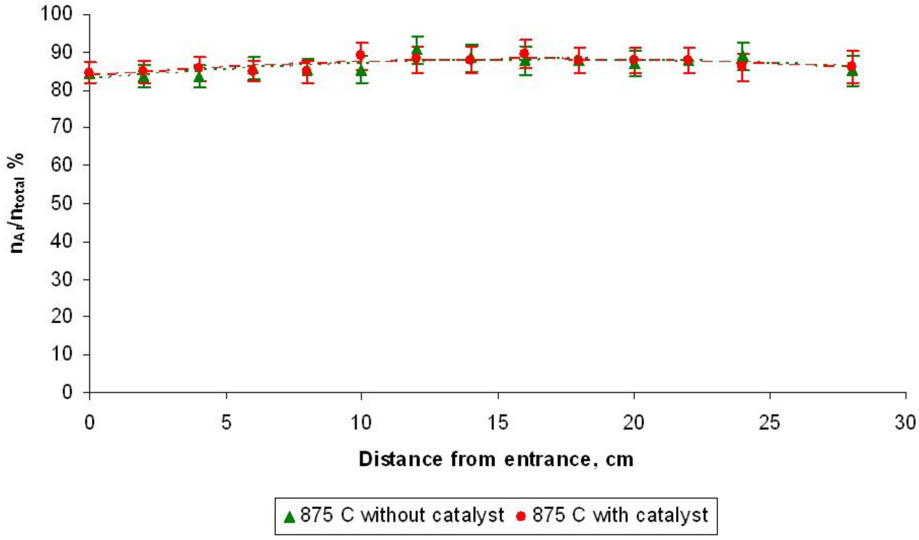

Figure 4.17: Mole Percentages of Argon Along the Reactor for 875°C Experiments

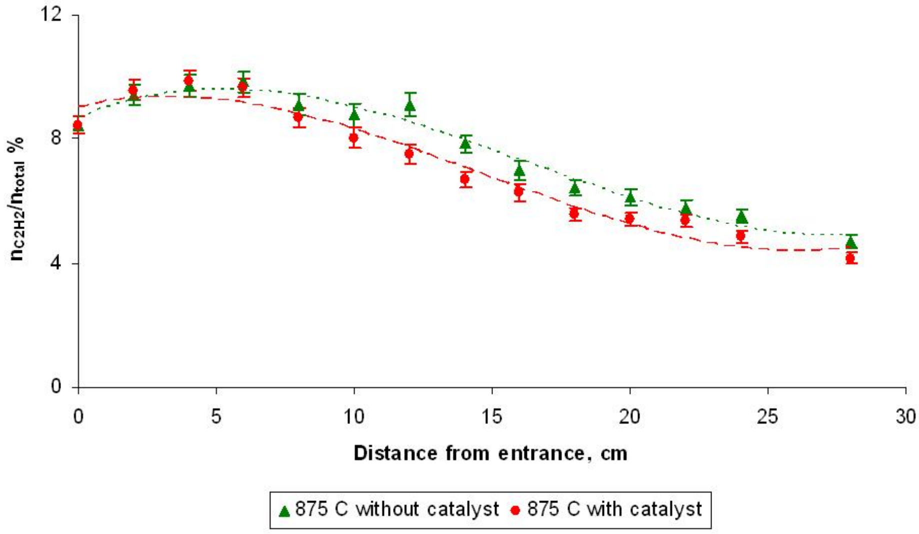

Figure 4.18: Mole Percentages of Acetylene Along the Reactor for 875°C Experiments

of observing more benzene and toluene with catalyst may be that more benzene and toluene were produced while CNTs formed.

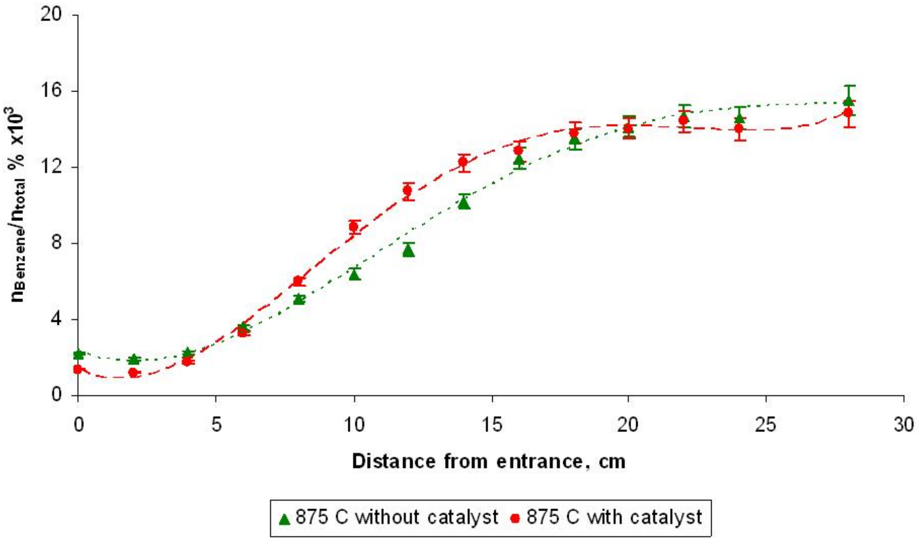

Figure 4.19: Mole Percentages of Benzene Along the Reactor for 875°C Experiments

Mole percentages of styrene are plotted in Figure 4.21. Similar to benzene and toluene more styrene was obtained with catalyst experiment between x=6 cm and x=16 cm. Addition of catalyst caused to an increase in styrene concentration.

Mole percentages of indene for two sets of experiments are plotted in Figure 4.22. Amounts of indenein experiment with catalyst were higher between x=6 cm and x=12 cm. However, after that point amounts of indene in experiment without catalyst were higher.

Mole percentages of naphthalene are plotted in Figure 4.23. Concentrations of naphthalene with and without catalyst increased up to x=20 cm. After that concentrations of naphthalene decreased. Concentrations of naphthalene were higher in experiment with catalyst at the first 20 cm. At the first 20 cm differences in experiments with and without catalyst were out of the range of experimental error. Addition of catalyst caused to an increase in naphthalene

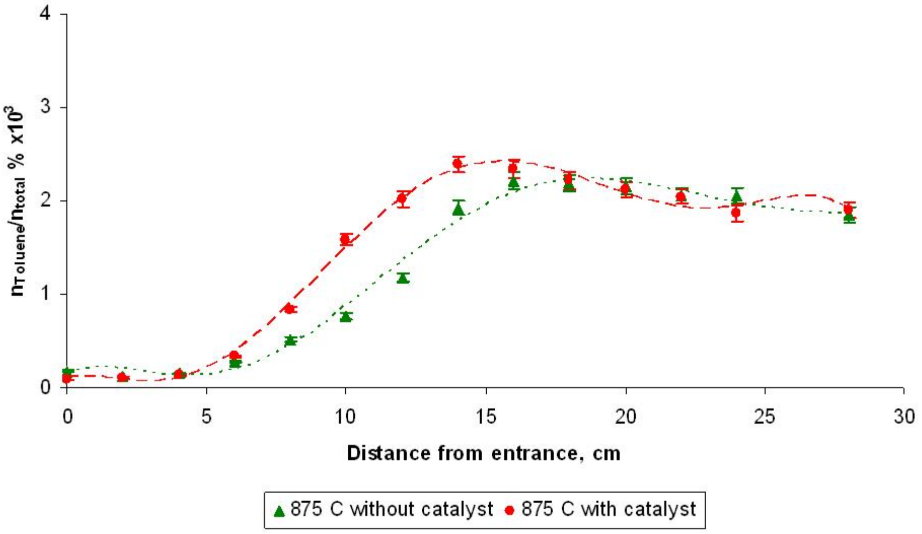

Figure 4.20: Mole Percentages of Toluene Along the Reactor for 875°C Experiments

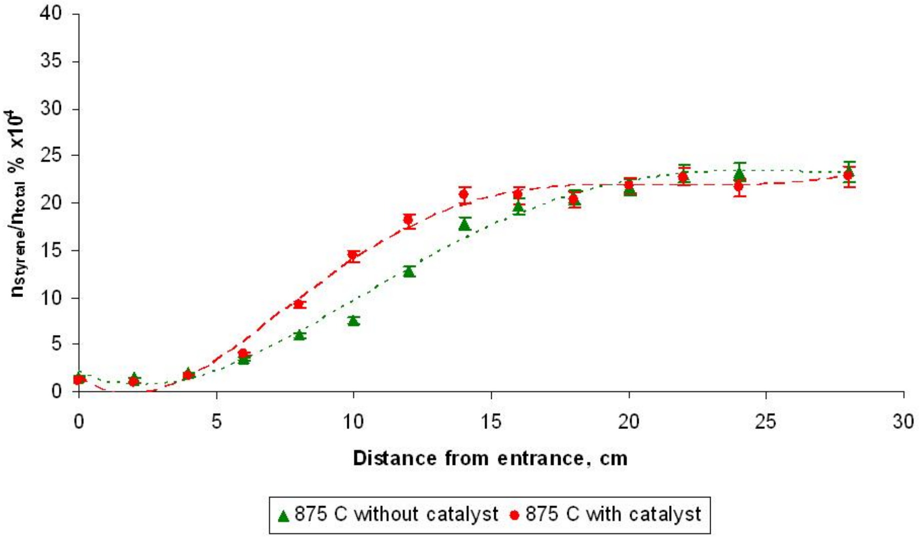

Figure 4.21: Mole Percentages of Styrene Along the Reactor for 875°C Experiments

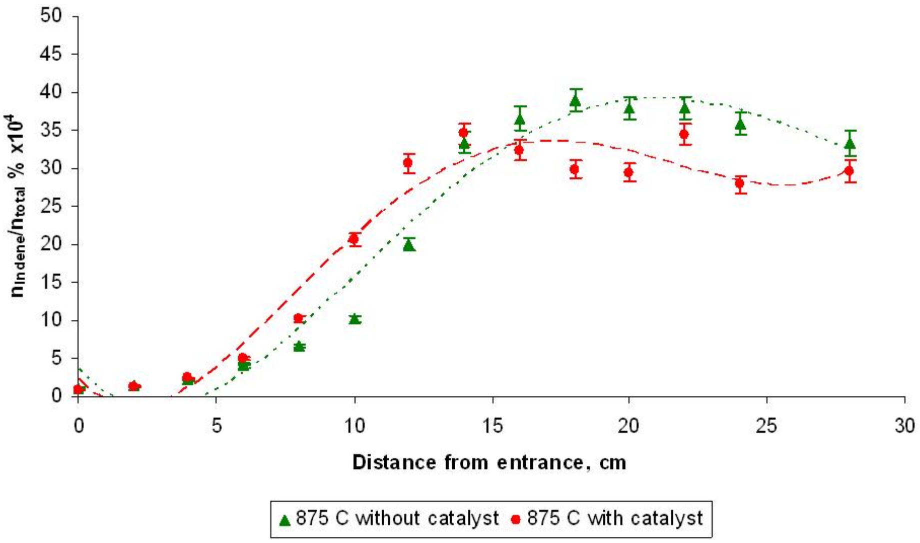

Figure 4.22: Mole Percentages of Indene Along the Reactor for 875°C Experiments

concentration.

Mole percentages of 1-methyl naphthalene are plotted in Figure 4.24. 1-methyl naphthalene in catalyst experiment produced early and started to decrease after x=20 cm. Concentrations of 1-methyl naphthalene in catalyst experiment were higher at the first 10 cm. After that point concentrations of 1-methyl naphthalene in experiment without catalyst were higher. Moreover, maximum amount of 1-methyl naphthalene in experiment without catalyst was higher.

Mole percentages of acenaphthalene and biphenyl are plotted in Figures 4.25 and 4.26. In experiment without catalyst, biphenyl produced and decomposed later compared to catalyst experiment. Moreover, maximum amount of biphenyl was higher than maximum amount of biphenyl in catalyst experiment.

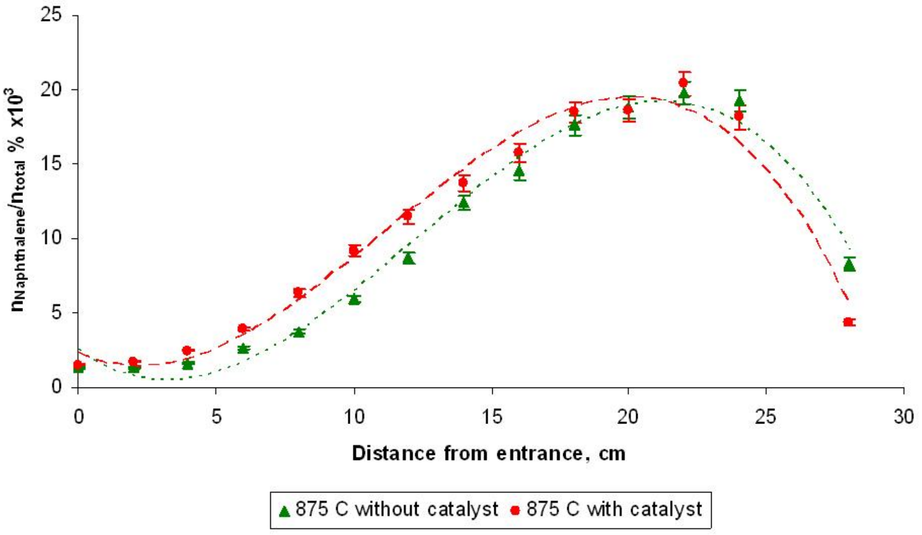

Figure 4.23: Mole Percentages of Naphthalene Along the Reactor for 875°C Experiments

4.7 COMPARISON OF 800°C AND 875°C EXPERIMENTS

Mole percentages of argon for 800°C and 875°C experiments are given in Figure 4.27. Although there were differences in mole percentages of argon, those differences were in the range of experimental error. Mole percentages of argon in all experiments were close to each other.

Mole percentages of acetylene for all experiments are given in Figure 4.28. More acetylene was decomposed as temperature increased with and without catalyst.

Mole percentages of produced benzene and toluene for all experiments are given in Figures 4.29 and 4.30. As it was seen in Figure 4.29, more benzene was obtained with an increase of temperature. Concentrations of toluene started to increase at x=6 cm for higher temperature experiments. For lower temperature experiments concentrations of toluene started to increase beyond x=6 cm and with a lower slope. Concentrations of toluene at higher temperatures decreased earlier than lower temperatures. Moreover, maximum amount of toluene was higher

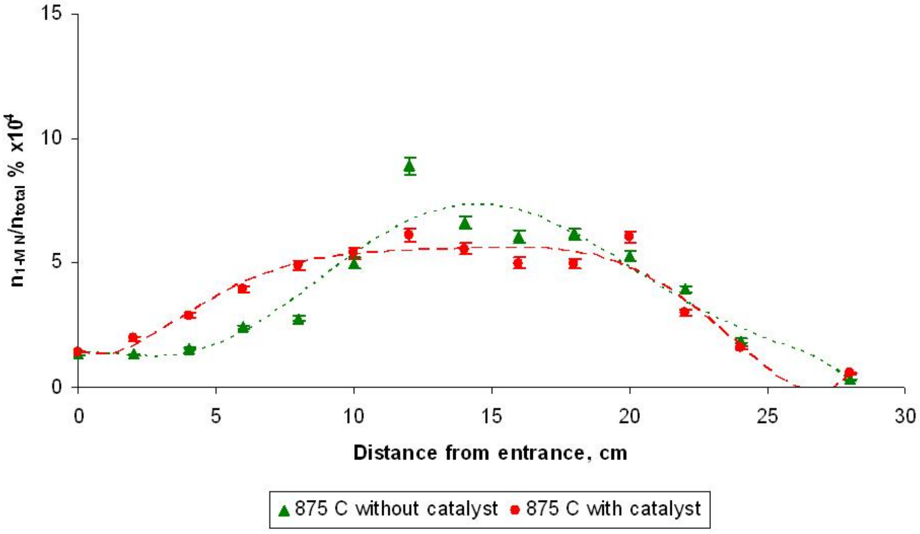

Figure 4.24: Mole Percentages of 1-Methyl Naphthalene Along the Reactor for 875°C Experiments

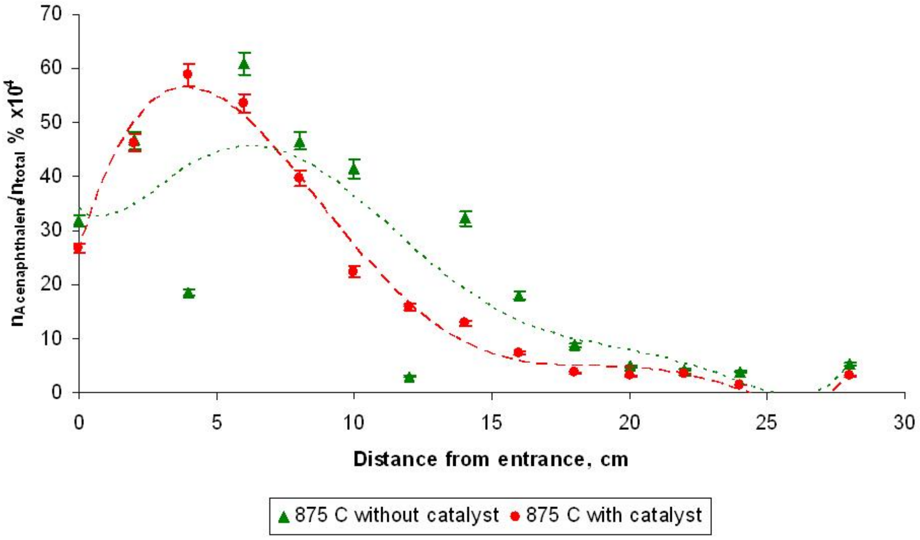

Figure 4.25: Mole Percentages of Acenaphthalene Along the Reactor for 875°C Experiments

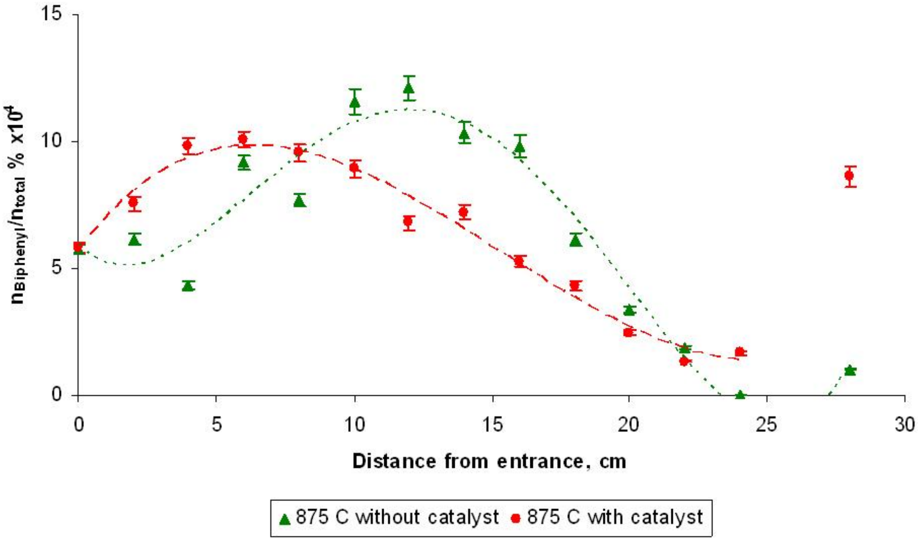

Figure 4.26: Mole Percentages of Biphenyl Along the Reactor for 875°C Experiments

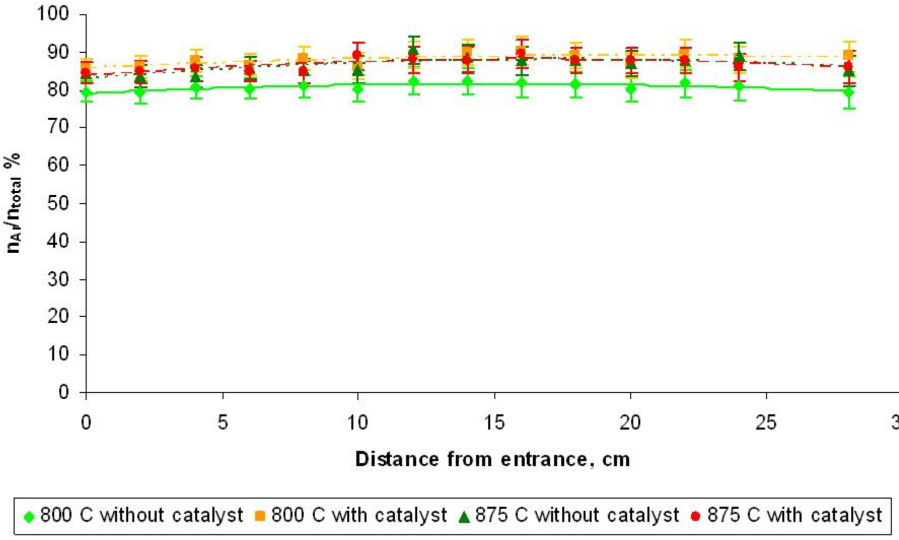

Figure 4.27: Mole Percentages of Argon Along the Reactor for All Experiments

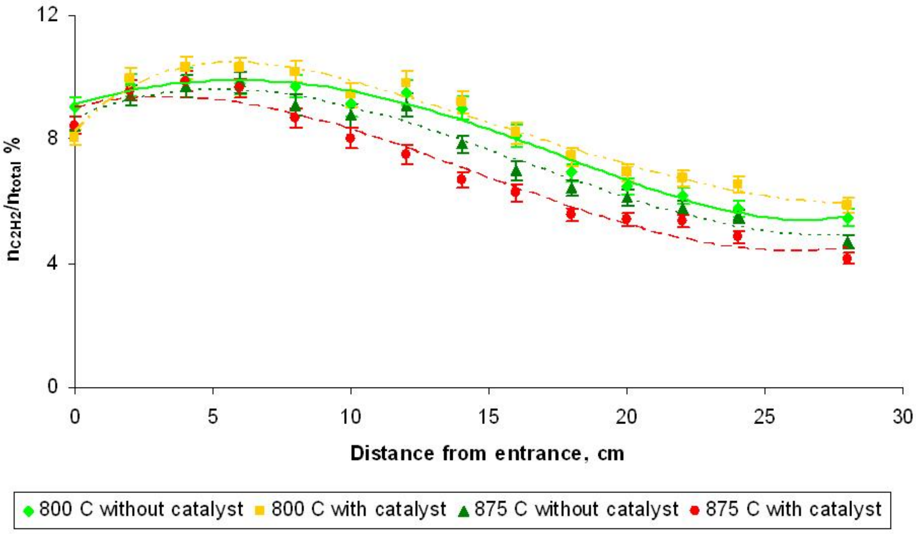

Figure 4.28: Mole Percentages of Acetylene Along the Reactor for All Experiments

at lower temperature experiments.

Mole percentages of styrene and indene for 800°C and 875°C experiments are given in Figures 4.31 and 4.32. In 875°C experiments with and without catalyst, styrene and indene produced early. Increasing experiment temperature caused early formation of styrene and indene.

Mole percentages of naphthalene for all experiments are given in Figure 4.33. When temperature increased, more naphthalene was produced for experiments both with and without catalyst.

Mole percentages of 1-methyl naphthalene, acenaphthalene and biphenyl are plotted in Figures 4.34, 4.35 and 4.36. Increasing reaction temperature led to produce more acenaphthalene and biphenyl.

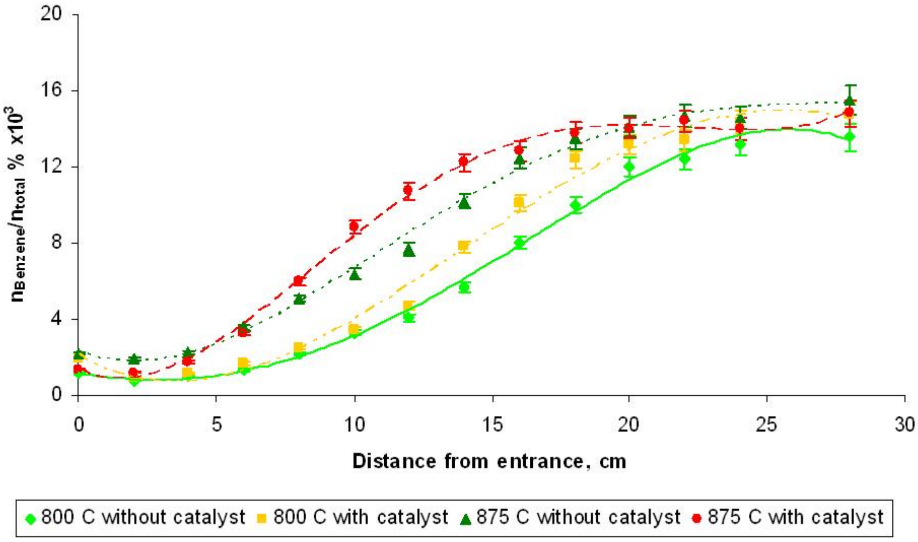

Figure 4.29: Mole Percentages of Benzene Along the Reactor for All Experiments

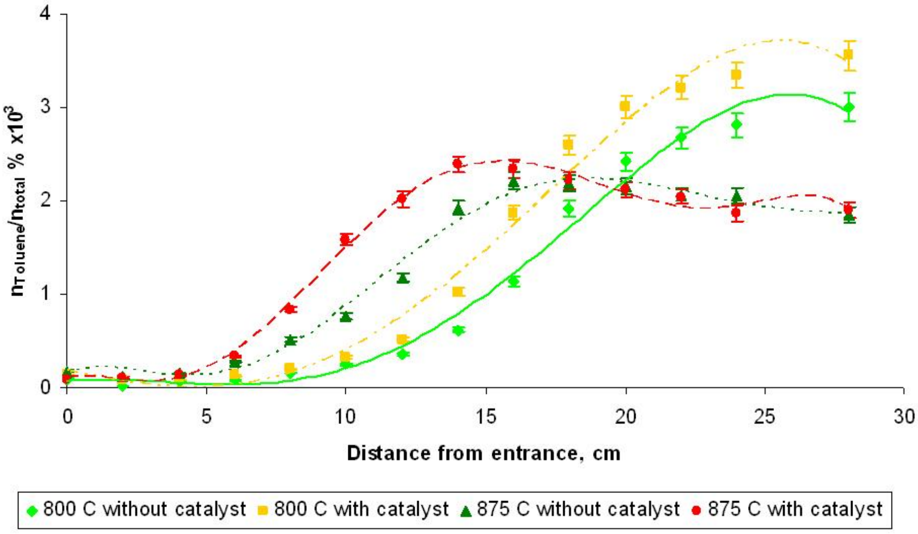

Figure 4.30: Mole Percentages of Toluene Along the Reactor for All Experiments

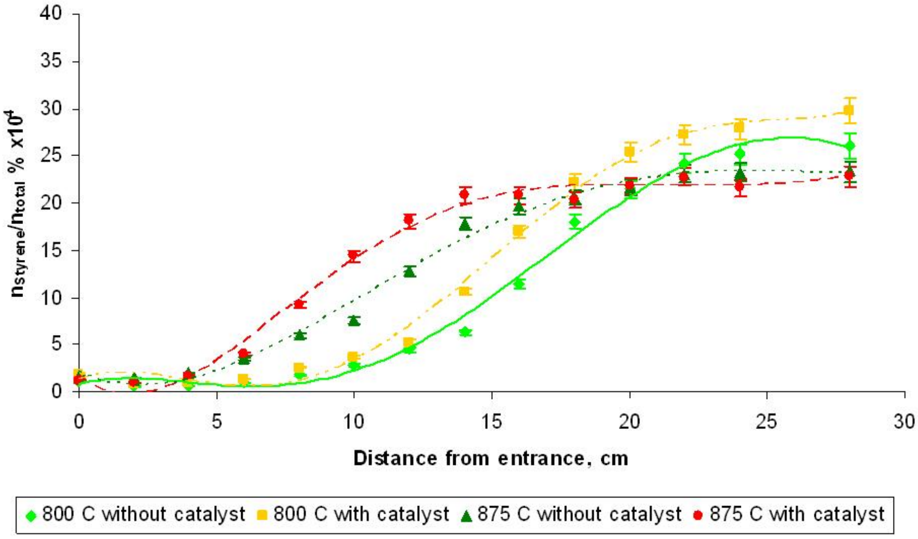

Figure 4.31: Mole Percentages of Styrene Along the Reactor for All Experiments

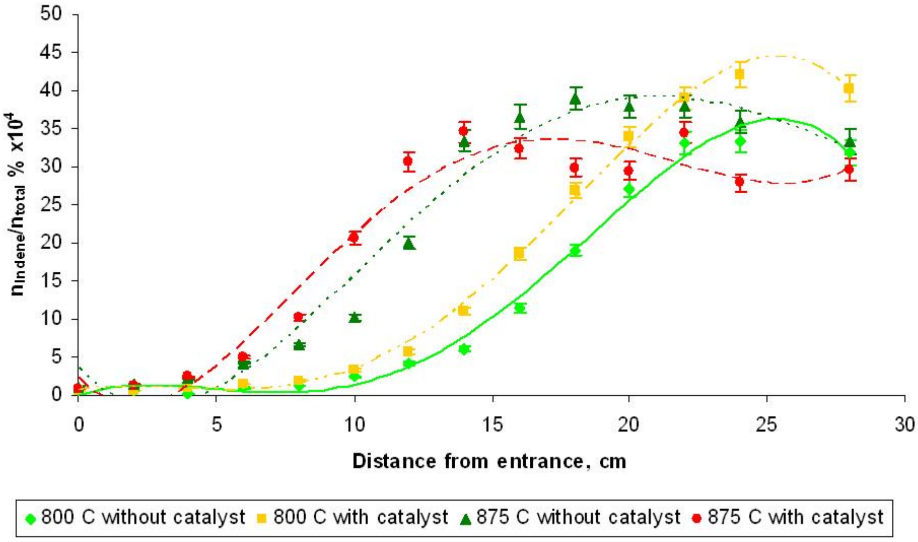

Figure 4.32: Mole Percentages of Indene Along the Reactor for All Experiments

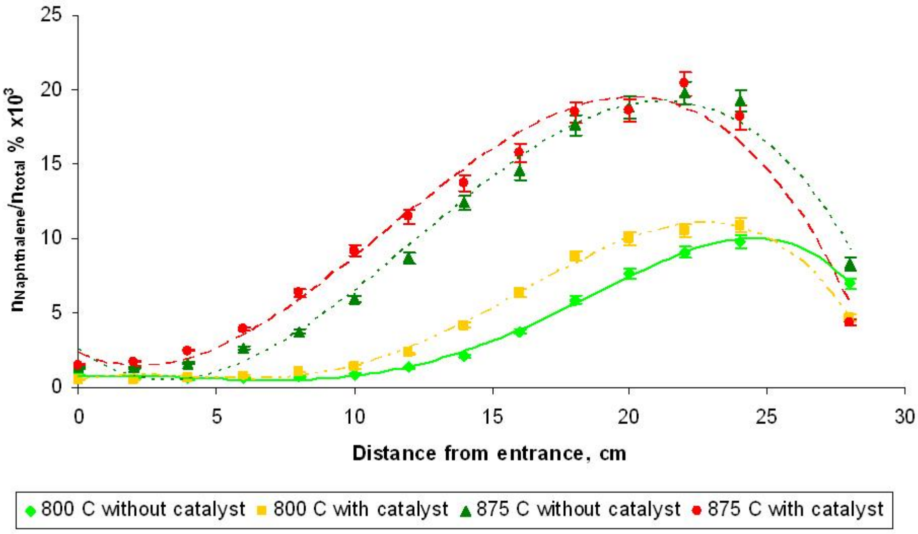

Figure 4.33: Mole Percentages of Naphthalene Along the Reactor for All Experiments

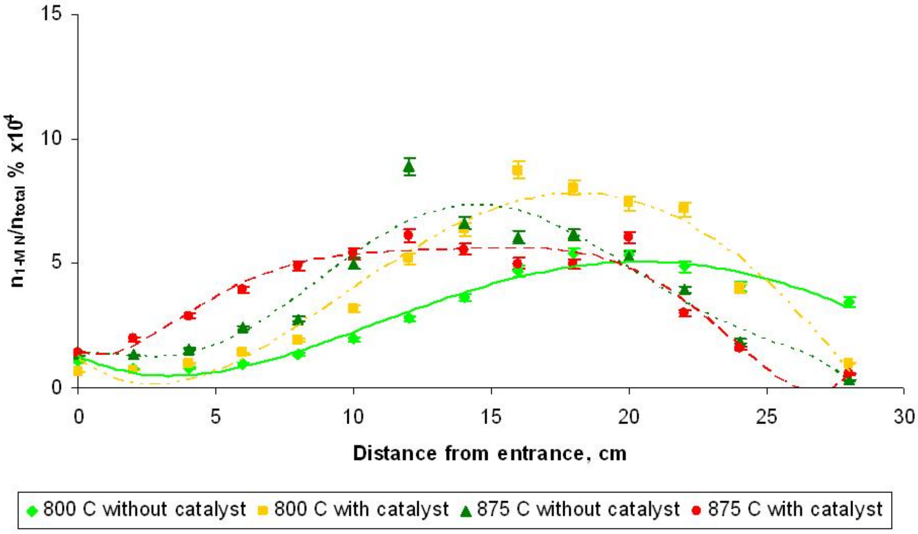

Figure 4.34: Mole Percentages of 1-Methyl Naphthalene Along the Reactor for All Experiments

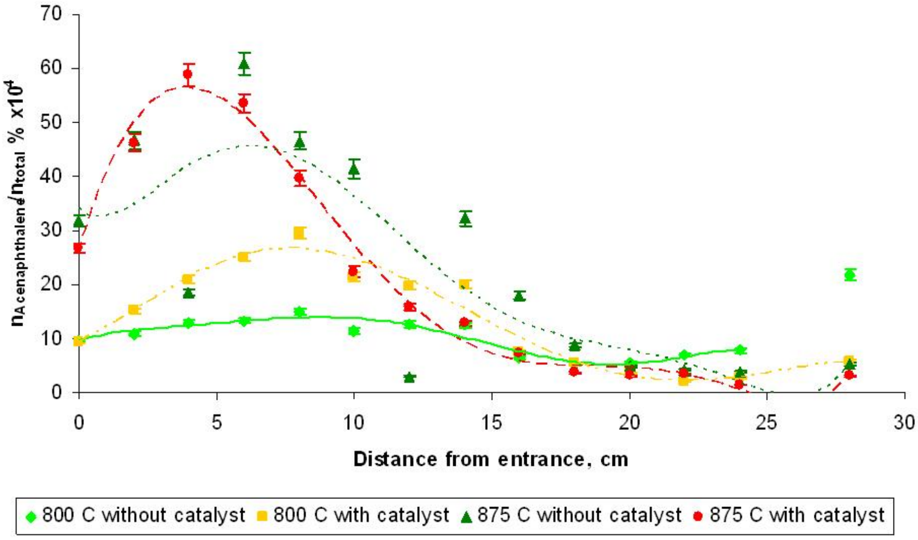

Figure 4.35: Mole Percentages of Acenaphthalene Along the Reactor for All Experiments

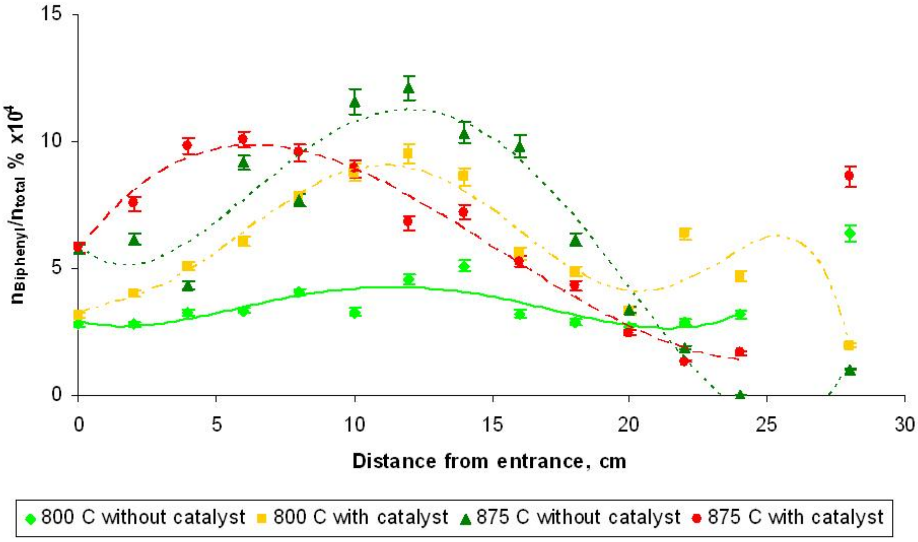

Figure 4.36: Mole Percentages of Biphenyl Along the Reactor for All Experiments

CHAPTER 5

CONCLUSIONS AND RECOMMENDATIONS

5.1 CONCLUSIONS

We designed and constructed gas sampling probe and sample loops such that the reaction can be frozen at the sampling point and the gas samples would keep their composition during their stay in the loops.

It was possible to collect gas samples in the CVD reactor and analyze them in GC/MS.

Production of CNTs at 800°C and 875°C with catalyst was achieved when probe was also inside reactor.

It was observed that increasing reaction temperature caused formation of more CNTs.

It was observed that catalyst prepared by sol gel method stayed active for 75 minutes.

Increasing reaction temperature caused decomposition of more acetylene with and without catalyst.

It was observed that more acetylene was used to produce CNTs compare to pyrolysis of acetylene.

It was observed that either toluene, styrene and naphthalene was produced while CNTs were produced or a byproduct as a result of CNTs formation was converted to them.

Increasing reaction temperature caused formation of more benzene, naphthalene, acenaphthalene and biphenyl.

Increasing reaction temperature caused early formation of toluene, styrene and indene.

Increasing reaction temperature caused a decrease in maximum amount of toluene.

It was observed that chemicals were not adsorbed in samples loops with time.

5.2 RECOMMENDATIONS

Chemicals such as methane, propene, diacetylene and vinylacetylene should be supplied so that their peaks on chromatograms that were already obtained will be quantified. Thus, the faith of those chemicals along the reactor can be understood.

To analyze the change in hydrogen concentration all experiments should be repeated using Molecular Sieve column.

When prepared catalyst solution was deposited onto quartz tube, it migrated to the bottom of quartz tube. CNT production reaction only took place in that narrow region. Hence, not much difference between experiments with and without catalyst was observed. Covering all surface of quartz tube with catalyst solution will increase amount of region that CNT production reaction takes place. In future experiments doing experiments that way will help to observe effects of catalyst better.

In future experiments limited region in axial direction of furnace should be covered with catalyst instead of covering all the furnace surface. So that effects of catalyst on concentration profiles can be understood.

When probe was inside the furnace, furnace could not reach high temperatures, such as 900°C. The design of the probe and the reactor should be changed to allow higher temperatures in the reactor.

Possibilities of different interesting catalyst effects may be observed using Co and Ni instead of Fe as catalyst.

REFERENCES

[1] Bernholc, J., Nardelli, M.B., Fattebert, J.-L., Orlikowski, D., Roland, C., Zhao, Q. Mechanical Properties and Electronic Transport in Carbon Nanotubes. In D. Tománek and R.J. Enbody (Eds.), Science and Application of Nanotubes (pp. 195-203). New York: Plenum.

[2] Dresselhaus, M. S., Endo, M., Iijima, S., Carbon Nanotubes, Oxford, Tarrytown, 1996.

[3] Dai, H. Nanotube Growth and Characterization. In M.S. Dresselhaus, G. Dresselhaus, P. Avouris (Eds.), Carbon Nanotubes Synthesis, Structure, Properties and Applications (pp. 29-33). Berlin: Springer.

[4] Iijima, S., Helical Microtubules of Graphitic Carbon. Nature 1991; 254: 56.

[5] Dresselhaus, M.S., Avouris, P. Introduction to Carbon Materials Research. In M.S. Dresselhaus, G. Dresselhaus, P. Avouris (Eds.), Carbon Nanotubes Synthesis, Structure, Properties and Applications (pp. 1-9). Berlin: Springer.

[6] Yu, J., Kalia, R. K. and Vashishta, P., Phonons in Graphitic Tubules. Europhysics Letters 1995; 32: 43.

[7] Iijima, S. and Ichilashi, T., Single-Shell Carbon Nanotubes of 1-nm Diameter. Nature 1993; 363: 603-605.

[8] Bethune, D.S., Kiang, C.H., de Vries, M.S., Gorman, G., Savoy, R., Vazquez, J., Beyers, R., Cobalt-Catalysed Growth of Carbon Nanotubes with Single-Atomic-Layer Walls. Nature 1993; 363: 605-607.

[9] Kiang, C. H., Goddard, W. A., Beyers, R. and Bethune, D. S., Carbon Nanotubes with Single Layer Walls. Carbon 1995; 33: 903-914.

[10] Dresselhaus, M., Dresselhaus, G., Eklund, P., Saito, R., Carbon Nanotubes. Retrieved November 10, 2006 from http://physicsweb.org/articles/world/11/1/9/1

[11] Ayhan, U.B., 2004, Production of Carbon Nanotubes by Chemical Vapor Deposition [Master thesis]: METU, 75 p.

[12] Carbon Nanotubes & Buckyballs. Retrieved February 20, 2009 from http://mrsec.wisc.edu/Edetc/nanoquest/carbon/index.html

[13] Carbon Nanotube. Retrieved September 28, 2006 from en.wikipedia.org

[14] Erkoç, Ş. (2001). Karbon Nanoyapılar. Bilim ve Teknik, 34 (398), 46-51.

[15] Teo, K. B. K., Singh, C., Chhowalla M., Milne, W.,I., Catalytic Synthesis of Carbon Nanotubes and Nanofibers. Encyclopedia of Nanoscience and Nanotechnology 2003; 10: 1-22.

[16] Forró, L., Salvetat, J.-P., Bonard, J.-M., Bacsa, R., Thomson, N.H., Garoj, S., Thien-Nga, L., Gaál, R., Kulik, A., Ruzicka, B., Degiorgi, L., Batchtold, A., Schönenberger, C., Pekker, S., Hernadi, K. Electronic and Mechanical Properties of Carbon Nanotubes. In D. Tománek and R.J. Enbody (Eds.), Science and Application of Nanotubes (pp. 297-320). New York: Plenum.

[17] Ajayan, P.M., Zhou, O.Z. Applications of Carbon Nanotubes. In M.S. Dresselhaus, G. Dresselhaus, P. Avouris (Eds.), Carbon Nanotubes Synthesis, Structure, Properties and Applications (pp. 391-425). Berlin: Springer.

[18] Penza, M., Antolini F. and Antisari, M. V., Carbon Nanotubes as SAW Chemical Sensors Materials. Sensors and Actuators 2004; 100: 47.

[19] Jung, H. Y., Jung, S. M., Suh, J. S., Horizontally Aligned Single-Walled Carbon Nanotube Field Emitters Fabricated on Vertically Aligned Multi-Walled Carbon Nanotube Electrode Arrays, Carbon 2008.

[20] Mamalis, A. G., Vogtländer, L. O. G., Markopoulos, Nanotechnology and Nanostructured Materials: Trends in Carbon Nanotubes. Precision Engineering 2004; 28: 16-30.

[21] Nützenadel, C., Züttel, A., Emmenegger, C., Sudan, P., Schlapback, L. Electromechanical Storage of Hydrogen in Carbon Single Wall Nanotubes. In D. Tománek and R.J. Enbody (Eds.), Science and Application of Nanotubes (pp. 205-213). New York: Plenum.

[22] Endo, M., Strano, M.S., Ajayan, P.M., Potential Applications of Carbon Nanotubes. In A. Jorio, G. Dresselhaus, M.S. Dresselhaus (Eds.), Carbon Nanotubes Advanced Topics in the Synthesis, Structure, Properties and Applications (pp. 13-62). New York: Springer.

[23] Ando, Y., Zhao, X., Sugai, T., Kumar, M., Growing Carbon Nanotubes. Materialstoday 2004; 10: 22-24.

[24] Popov, V., N., Carbon Nanotubes: Properties and Application. Materials Science and Engineering R 2004; 43: 61-102.

[25] Cheap Tubes Inc, Carbon Nanotubes - Production Methods for Carbon Nanotubes Including Arc Discharge, Laser, Chemical Vapor Deposition and Ball Milling. Retrieved November 20, 2006 from http://www.azonano.com/Details.asp?ArticleID=1561

[26] Mauron, P., 2003, Growth Mechanism and Structure of Carbon Nanotubes[Ph.D. thesis]: University of Freiburg, 127 p.

[27] Sampedro-Tejedor, P., Maroto-Valiente, A., Nevskaia, D.M., Múñoz, V., Rodríguez-Ramos, I., Guerrero-Ruíz, A., The Effect of Growth Temperature and Iron Precursor on the Synthesis of High Purity Carbon Nanotubes. Diamond & Related Materials 2007; 16: 542-549.

[28] Kim, Y.A., Hayashi, T., Endo, M., Kaburagi, Y., Tsukada, T., Shan, J., Osato, K., Tsuruoka, S., Synthesis and Structural Characterization of Thin Multi-Walled Carbon Nanotubes with a Partially Facetted Cross Section by a Floating Reactant Method. Carbon 2005; 43: 2243-2250.

[29] Cui, H., Eres, G., Howe, J.Y., Puretkzy, A., Varela, M., Geohegan, D.B., Lowndes, D.H., Growth Behavior of Carbon Nanotubes on Multilayered Metal Catalyst Film in Chemical Vapor Deposition. Chemical Physics Letters 2003; 374: 222-228.

[30] Mauron, Ph., Emmenegger, Ch., Züttel, A., Nützenadel, Ch., Sudan, P., Schlapbach, L., Synthesis of Oriented Nanotube Films by Chemical Vapor Deposition. Carbon 2002; 40: 1339-1344.

[31] Terrado, E., Redrado, M., Muñoz, E., Maser, W.K., Benito, A.M., Martínez M.T., Aligned Carbon Nanotubes Grown on Alumina and Quartz Substrates by a Simple Thermal CVD Process. Diamond & Related Materials 2006; 15: 1059-1063.

[32] Nath, M., Satishkumar, B.C., Govindaraj, A., Vinod, C.P., Rao, C.N.R., Production of Bundles of Aligned Carbon and Carbon-Nitrogen Nanotubes by the Pyrolysis of Precursors on Silica-Supported Iron and Cobalt Catalysts. Chemical Physics Letters 2000; 322: 333-340.

[33] Pan, Z.W., Xie, S.S., Chang, B.H., Sun, L.F., Zhou, W.Y., Wang, G., Direct Growth of Aligned Open Carbon Nanotubes by Chemical Vapor Deposition. Chemical Physics Letters 1999; 299:97-102.

[34] Mohlola, M.S., Coville, N.J., Floating catalyst CVD synthesis of carbon nanotubes from $CpFe(CO)_2X$ (X = Me, I): Poisoning Effects of I. Journal of Organometallic Chemistry 2007; 692: 2965-2970.

[35] Ci, L., Wei, J., Wei, B., Liang, J., Xu, C., Wu, D., Carbon Nanofibers and Single-Walled Carbon Nanotubes Prepared by the Floating Catalyst Method. Carbon 2001; 39: 329-335.

[36] Ci, L., Xie, S., Tang, D., Yan, X., Li, Y., Liu, Z., Zou, X., Zhou, W., Wang, G., Controllable Growth of Single Wall Carbon Nanotubes by Pyrolizing Acetylene on the Floating Iron Catalysts. Chemical Physics Letters 2001; 349: 191-195.

[37] Ci, L., Rao, Z., Zhou, Z., Tang, D., Yan, X., Liang, Y., Liu, D., Yuan, H., Zhou, W., Wang, G., Liu, W., Xie, S., Double Wall Carbon Nanotubes Promoted by Sulfur in a Floating Iron Catalyst CVD System. Chemical Physics Letters 2002; 359: 63-67.

[38] Zhou, Z., Ci, L., Chen, X., Tang, D., Yan, X., Liu, D., Liang, Y., Yuan, H., Zhou, W., Wang, G., Xie, S., Controllable Growth of Double Wall Carbon Nanotubes in a Floating Catalytic System. Carbon 2003; 41: 337.

[39] Hou, H., Schaper, A. K., Weller, F., Greiner, A., Carbon Nanotubes and Spheres Produced by Modified Ferrocene Pyrolysis. Chem. Mater. 2002; 14: 3990-3994.

[40] Hou, H., Schaper, A. K., Jun, Z., Weller, F., Greiner, A., Large-Scale Synthesis of Aligned Carbon Nanotubes Using FeCl3 as Floating Catalyst Precursor. Chem. Mater. 2003; 15:, 580-585.

[41] Vajtai, R., Wei, B., Jung, Y. J., Cao, A., Biswas, S. K., Ramanath, G., Ajayan, P. M., Building and Testing Organized Architectures of Carbon Nanotubes. IEEE TRANSACTIONS ON NANOTECHNOLOGY, vol. 2, no. 4, DECEMBER 2003.

[42] Andrews, R., Jacques, D., Rao, A. M., Derbyshire, F., Qian, D., Fan, X., Dickey, E. C., Chen, J. Continuous Production of Aligned Carbon Nanotubes: A Step Closer to Commercial Realization. Chemical Physics Letters 1999; 303: 467-474.

[43] Mohlala, M. S., Liu, X. Y., Coville, N. J.,Synthesis of Multi-Walled Carbon Nanotubes Catalyzed by Substituted Ferrocenes. Journal of Organometallic Chemistry 2006; 691:4768-4772.

[44] Liu, X.Y., Huang, B.C., Coville, N.J., The Influence of Synthesis Parameters on the Production of Multiwalled Carbon Nanotubes by the Ferrocene Catalyzed Pyrolysis of Toluene. Fullerenes, Nanotubes and Carbon Nanostructures 2002; 10: 339 - 352.

[45] Bai, X., Li, D., Wang Y., Liang J., Effects of Temperature and Catalyst Concentration on the Growth of Aligned Carbon Nanotubes. Tsinghua Science and Technology 2005; 10: 729-735.

[46] Singh, C., Shaffer, M. S. P., Windle, A. H., Production of Controlled Architectures of Aligned Carbon Nanotubes by an Injection Chemical Vapour Deposition Method. Carbon 2003: 41; 359-368.

[47] Bhowmick, R., Clemens, B.C., Cruden, B.A., Parametric Analysis of Chirality Families and Diameter Distributions in Single-Wall Carbon Nanotube Production by the Floating Catalyst Method. Carbon 2008; 46: 907-922.

[48] Sinnott, S.B., Andrews, R., Qian, D., Rao, A.M., Mao, Z., Dickey, E.C., Derbyshire, F., Model of Carbon Nanotube Growth through Chemical Vapor Deposition. Chemical Physics Letters 1999; 315: 25-30.

[49] Endo, H., Kuwana, K., Saito, K., Qian, D., Andrews, R., Grulke, E.A., CFD Prediction of Carbon Nanotube Production Rate in a CVD Reactor. Chemical Physics Letters 2004; 387: 307-311.

[50] Kuwana, K., Endo, H., Saito, K., Qian, D., Andrews, R., Grulke, E.A., Catalyst Deactivation in CVD Synthesis of Carbon Nanotubes. Carbon 2005; 43: 253-260.

[51] Wasel W., Kuwana,K., Saito, K., Chemical and Thermal Structures of a Xylene-based CVD Reactor to Synthesize Carbon Nanotubes. Chemical Physics Letters 2006; 422: 470-474.

[52] Agilent Technologies, The Essential Chromatography and Spectroscopy Catalog. 2007-2008 Edition.

[53] Retrieved April 15, 2009 from http://en.wikipedia.org/wiki/Thermal energy(conductivity) analyzer/detector

[54] Delzeit, L., Nguyen, C.V., Chen, B., Stevens, R., Cassell, A., Han,J., Meyyappan, M., Multiwalled Carbon Nanotubes by Chemical Vapor Deposition Using Multilayered Metal Catalysts. J. Phys. Chem. B 2002; 106: 5629-5635.

[55] Soysal, F., 2009, Investigation of Carbon Nanotube Production by Chemical Vapor Deposition and Vapor Phase Growth Methods [Master thesis]: Ankara University, 222 p.

[56] Becker, A., Hüttinger, K.J., Chemistry and Kinetics of Chemical Vapor Deposition of Pyrocarbon-II Pyrocarbon Deposition from Ethylene, Acetylene and 1,3-Butadiene in the Low Temperature Regime. Carbon 1997; 36: 177-199.

[57] Friedman, N., Bovee, H.H., Miller, S.L., High Temperature Pyrolysis of C1 to C4 Hydrocarbons. J. Org. Chem. 1970; 35: 3230-3232.

[58] Khan, R.U., Bajohr, S., Graf, F., Reimert, R., Modeling of Acetylene Pyrolysis Under Steel Vacuum Carburizing Conditions in a Tubular Flow Reactor. Molecules 2007; 12: 290-296.

[59] Xu, X., Pacey, P.D., Oligomerization and Cyclization Reactions of Acetylene. Phys. Chem. Chem. Phys. 2005; 7: 326-333.

[60] Ogura, H., Pyrolysis of Acetylene Behind Shock Waves. Bulletin of the Chemical Society of Japan 1977; 50: 1044-1050.

[61] Cullis, C.F., Franklin, N.H., The Pyrolysis of Acetylene at Temperatures from 500 to 1000°C. Mathematical and Physical Sciences 1964; 280: 139-152.

[62] Retrieved February 16, 2009 from http://www.nugentec.com/FAQ/Freezing Point Flash Points.htm

[63] Fitch, W.L., Sauter, A.D., Calculation of Relative Electron Impact Total Ionization Cross Sections for Organic Molecules. Anal. Chem. 1983; 55: 832-835.

[64] Sauter, A.D., Downs, J.J., Buchner, J.D., Ringo, N.T., Shaw, D.L., Dulak, J.G., Model for the Estimation of Electron Impact Gas Chromatography/ Mass Spectrometry Response Factors for Quadrupole Mass Spectrometers. Anal. Chem. 1986; 58: 1665-1670.

APPENDIX A

TEMPERATURE PROFILE OF THE FURNACE

Temperature profile of the furnace that was used in CVD experiments was found experimentally. Rod thermocouple was used to measure temperature inside furnace. Temperature was measured along the axis of 40 mm quartz tube. Temperature data was collected along the furnace at different set points and different argon flow rates. Measuring temperature was started at 5 cm from the entrance of 60 cm long furnace. Temperature was measured with 5 cm intervals till 5 cm from the furnace exit.

Temperature profile was first obtained at set point of 500°C without argon flow rate. Temperature was measured from entrance to exit of the furnace. Then, temperature profile was obtained at set point of 500°C with argon flow rate of 1.0 L/min. Temperature was, however, measured from exit to entrance of the furnace. When two temperature profiles were compared, it was seen that there was a difference at the entrance of the furnace. The reason of this difference is that the time for reaching equilibrium while thermocouple is heating, is less than the time for reaching equilibrium while thermocouple is cooling. Hence, rest of the measurements were done from entrance to exit of the furnace to be consistent. Temperature profile of the furnace without argon flow rate is given in Figure A.1.

As it is seen from Figure A.1 furnace temperature is at set point between 15 and 45 cm. At the midpoint of the furnace temperature is approximately 15°C greater than the set point temperature.

In Figure A.2 temperature profiles at different argon flow rates is given for set point of 700°C. According to Figure A.2 flow rate has not a significant effect on temperature profile in the region of velocities we used. At a high flow rate like 4.0 l/min temperature at the entrance of the furnace is slightly lower compared to no flow case and temperature at the exit is slightly

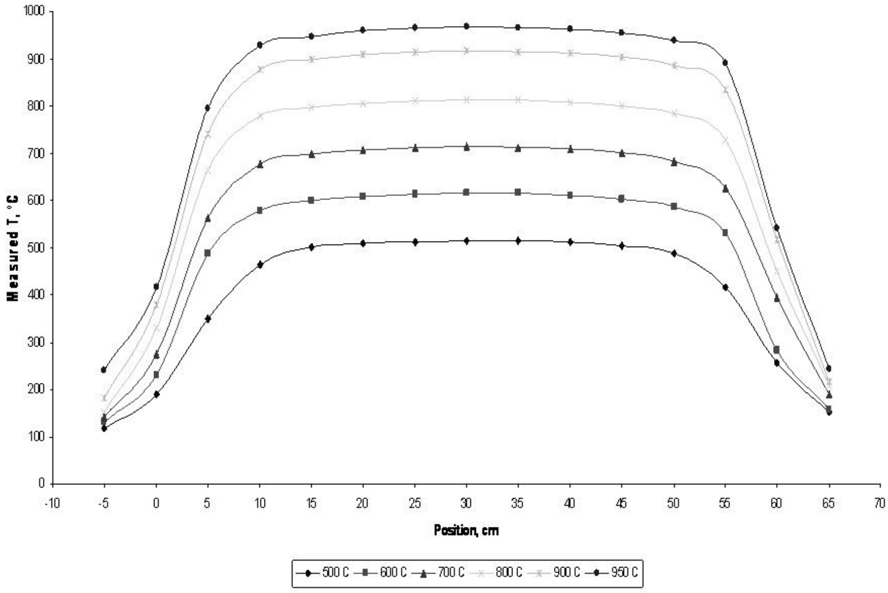

Figure A.1: Temperature Profile of the Furnace without Ar Flow Rate

higher. However, no significant difference occurs in the middle zone.

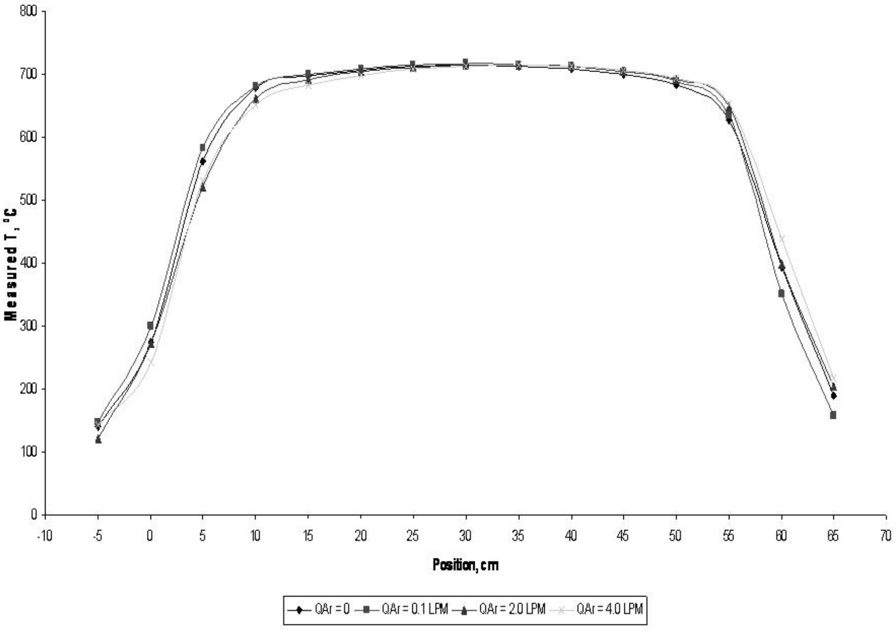

Figure A.2: Temperature Profile of the Furnace at Different Ar Flow Rates at 700°C

APPENDIX B

STUDIES DONE TO COOL PROBE

Probe is used to collect samples from reactor. Samples sucked into the probe have to be quenched so that no further reaction takes place. To do so probe has to be cooled. However, temperature inside probe should not be lower than certain temperature to prevent condensation of samples. For these purposes different fluids were tried.

B.1 COOLING STUDIES WITH DRY AIR

For first trial dry air was used to cool quartz probe, which was previously made. 85 cm long quartz probe was put into furnace. 28 cm of probe was inside the furnace. Thermocouple was inserted into probe to measure the temperature of it. Tip of thermocouple was at the point where probe entered furnace. Furnace was heated to 900°C. N_2 was passing through furnace. Dry air entered probe from inner jacket and exited from outer jacket. Measured temperature data are given in Table B.1.

During the experiments exit temperature of N_2 from furnace was below 30°C. Exit tempera-

Table B.1: Measured Temperatures Using Dry Air At Different Flow Rates-1

Flow Rate of N_2, l/min	Flow Rate of Dry Air, l/min	Measured Temperature, °C
0.7	1.1	345
0.7	2.3	320
0.5	1.1	342
0.5	2.3	334

Table B.2: Measured Temperatures Using Dry Air At Different Flow Rates-2

Flow Rate of N_2, l/min	Flow Rate of Dry Air, l/min	Measured Temperature, °C
0.7	0	377
	0.5	374
	1.1	369
	1.7	373
	2.8	380
	5.7	390
0.5	0	362
	1.1	358
	2.3	347
	2.8	360
	5.7	382

Table B.3: Measured Temperatures Using Dry Air Entering From Outer Jacket

Flow Rate of N_2, l/min	Flow Rate of Dry Air, l/min	Measured Temperature, °C
1.0	0	379
	0.5	391
	1.1	428
	1.7	436
	2.8	478
	5.7	390
	6.4	378

ture of dry air was 25-27°C. When thermocouple was inserted 3 cm into furnace, temperature increased above 500°C.

34 cm of probe was put into furnace and experiments were repeated. Tip of thermocouple was at the point where probe entered furnace. Measured temperature data are given in Table B.2.

Desired results could not be obtained. Inlet of dry air was changed and made to enter the probe from outer jacket. Measured temperature data are given in Table B.3.

When dry air entered from outer jacket, measured temperatures increased. It is logical since air passed inner jacket after it warmed up in the outer jacket.

Even if pressured dry air was directly sent from tube desired cooling was not achieved. It was decided that dry air could not be used for cooling purpose.

B.2 COOLING STUDIES WITH CO_2

CO_2 was used to cool quartz probe instead of dry air. CO_2 was sent while furnace was at room temperature. Thermocouple was inserted into probe to measure the temperature of it. There were no decrease in temperature although gas was passing. It was decided that CO_2 could not be used for cooling purposes either.

B.3 COOLING STUDIES WITH WATER

Water was tried for cooling purpose. Copper rod was used instead of quartz probe since water could crack the probe. Copper rod was composed of two concentric pipes. Water entered from outer jacket. To measure exit temperature of water T connection was made at the exit of the rod. Temperature was measured with taking sample from there. Temperature measurements were done at different furnace temperatures and water flow rates. Results are given in Table B.4. It was seen that desired cooling can be obtained with water.

B.4 COOLING STUDIES WITH ANTIFREEZE-WATER

New probe was made from steel. It was decided to use antifreeze-water mixture (% 50 v/v) to cool steel probe. To circulate mixture inside probe Huber brand circulator was bought. Fluid entered the probe from inner jacket. Thermocouple was attached to end of probe to measure its surface temperature. Temperature of mixture was read from circulator. It was the average temperature of fluid inside bath of circulator. Temperature of fluid coming from probe was obviously greater than that. When furnace reached steady state, 110 cm long probe was put into furnace. 58.5 cm of steel probe was inside furnace. Temperature data was collected against time at different set point temperatures of the furnace. Results are given in Tables B.5, B.6, B.7, B.8, B.9, B.10, B.11, B.12.

Table B.4: Measured Temperatures Using Water At Different Furnace Temperatures and Flow Rates

Flow Rate of Water, l/min	Furnace Temperature, °C	Water Temperature, °C	Flow Rate of Water, l/min	Furnace Temperature, °C	Water Temperature, °C
3.75	26	21	3.75	500	20
3.75	80	22	3.00	502	20
3.75	120	21	2.00	501	21
3.00	133	21	1.43	500	22
2.00	126	21	3.75	600	21
0.50	122	21	3.00	600	20
3.75	240	22	1.76	600	21
3.00	242	23	1.20	600	23
2.50	236	21	0.94	600	24
1.76	229	22	0.75	600	25
0.75	217	21	3.75	700	21
3.75	324	22	2.50	700	21
3.00	318	21	1.88	700	22
2.14	308	20	1.25	700	24
1.67	306	22	0.81	700	28
0.88	307	21	0.61	700	30
3.75	410	19	3.75	799	21
3.00	405	19	3.00	800	22
2.14	400	21	2.00	800	24
1.67	405	21	1.30	800	27
0.86	405	22	0.81	800	30
			0.61	800	34

At set point of 900°C temperature of fluid inside circulator reached 103°C in half an hour. Boiling point of antifreeze-water mixture (% 50 v/v) was 107°C [62]. Since temperature of fluid inside circulator approached boiling point, it was decided to use a fluid with a higher boiling point.

B.5 COOLING STUDIES WITH SHELL THERMIA B

Shell Thermia B that is a heat transfer oil was bought. Boiling point of it is 355°C and it can be safely used up to 320°C. When the furnace reached steady state, 56 cm of steel probe was put inside the furnace. Temperature data was collected against time at different set point temperatures of the furnace. Results are given in Tables B.13, B.14, B.15, B.16, B.17. At

Table B.5: Measured Temperatures Using Antifreeze-Water Mixture (% 50 v/v) At Furnace Set Point of 300°C

Time, min	Temperature of Fluid inside Circulator, °C	Surface Temperature of Probe, °C	Furnace Temperature, °C
0	31.6	33	
2	32.2	35	332
4	32.8	35	328
6	33.4	35	318
8	33.9	35	307
10	34.5	36	296
12	35.0	35	301
14	35.5	36	310
16	36.0	36	307
18	36.4	36	300
20	36.9	37	297
22	37.4	37	306
24	37.8	38	307
26	38.3	38	302
28	38.8	38	296
30	39.2	38	304

Table B.6: Measured Temperatures Using Antifreeze-Water Mixture (% 50 v/v) At Furnace Set Point of 400°C

Time, min	Temperature of Fluid inside Circulator, °C	Surface Temperature of Probe, °C	Furnace Temperature, °C
0	41.0	44	410
8	43.5	44	406
10	44.1	45	398
12	44.6	45	
16	45.8	45	399
18	46.4	44	398
20	46.9	44	405
22	47.5	44	400

Table B.7: Measured Temperatures Using Antifreeze-Water Mixture (% 50 v/v) At Furnace Set Point of 500°C

Time, min	Temperature of Fluid inside Circulator, °C	Surface Temperature of Probe, °C	Furnace Temperature, °C
0	48.0	45	500
2	48.7	49	497
4	49.4	50	505
6	50.2	50	496
8	51.0	49	502
10	51.7	50	501
12	52.4	51	498

Table B.8: Measured Temperatures Using Antifreeze-Water Mixture (% 50 v/v) At Furnace Set Point of 600°C

Time, min	Temperature of Fluid inside Circulator, °C	Surface Temperature of Probe, °C	Furnace Temperature, °C
0	52.9		600
2	54.1		603
4	55.2		599
6	56.3	58	601
8	57.4	58	600
10	58.5	60	600
12	59.5	59	600
14	60.6	60	600

Table B.9: Measured Temperatures Using Antifreeze-Water Mixture (% 50 v/v) At Furnace Set Point of 700°C

Time, min	Temperature of Fluid inside Circulator, °C	Surface Temperature of Probe, °C	Furnace Temperature, °C
0	53.5		695
2	55.2	60	701
4	56.9	60	700
6	58.6	62	700
8	60.2		700
10	61.8	64	700
12	63.3	63	700
14	64.9	64	700
16	66.4	65	700
18	67.9	66	
20	69.5	68	
22	70.9	68	
24	72.3	69	
26	73.8	70	
28	75.1	70	

Table B.10: Measured Temperatures Using Antifreeze-Water Mixture (% 50 v/v) At Furnace Set Point of 800°C

Time, min	Temperature of Fluid inside Circulator, °C	Surface Temperature of Probe, °C	Furnace Temperature, °C
0	71.6	74	800
1	72.7	75	800
2	73.8	75	800
4	76.0	76	
6	78.2	76	
8	80.5	77	
10	82.3	76	
12	84.4	77	
14	86.4	79	
16	88.3	79	
18	90.2	80	
20	92.0	81	
22	93.7	82	
24	95.5	82	
26	97.2	83	
28	98.8	82	
30	100.4	84	

Table B.11: Measured Temperatures Using Antifreeze-Water Mixture (% 50 v/v) At Furnace Set Point of 900°C

Time, min	Temperature of Fluid inside Circulator, °C	Surface Temperature of Probe, °C	Furnace Temperature, °C
0	38.2	52	874
1	39.5	61	871
2	41.2	62	866
3	42.9	62	862
4	44.7	61	859
5	46.3	61	856
6	47.9	63	854
7	49.5	64	852
8	51.1	64	851
9	52.6	63	850
10	54.2	64	849
11	55.7	62	848
12	60.2	64	847
14	63.1	65	847
16	66.0	65	846
18	68.8	66	847
20	71.5	67	847
24	74.2	68	847
26	76.9	68	848
27	78.2	69	848
28	79.5	70	848
29	80.8	70	848
30	82.1	70	849

Table B.12: Measured Temperatures Using Antifreeze-Water Mixture (% 50 v/v) At Furnace Set Point of 900°C -II

Time, min	Temperature of Fluid inside Circulator, °C	Surface Temperature of Probe, °C	Furnace Temperature, °C
0	63.5	60	885
1	64.8	68	875
2	66.5	69	869
3	68.0	69	865
4	69.6	69	862
5	71.2	69	860
6	72.6	68	858
7	74.1	67	856
8	75.5	68	855
11	79.7	65	853
12	81.1	67	852
13	82.4	67	852
14	83.7	69	852
15	85.0	70	852
16	86.3	68	852
17	87.5	68	852
18	88.8	67	852
19	90.0	70	852
20	91.2	70	852
21	92.4	71	852
22	93.6	70	852
23	94.8	69	853
24	95.9	69	853
25	97.1	70	853
26	98.2	71	853
27	99.3	71	853
28	100.4	71	854
29	101.5	71	854
30	102.6	71	854

Table B.13: Measured Temperatures Using Shell Thermia B At Furnace Set Point of 300°C

Time, min	Temperature of Fluid inside Circulator, °C	Furnace Temperature, °C
0	36.2	334
2	36.6	325
4	37.1	313
6	37.6	302
8	38.0	296
10	38.5	306
14	39.5	305
16	40.1	299
18	40.7	300
20	41.3	307
22	42.0	305
24	42.5	299
26	43.1	298

Table B.14: Measured Temperatures Using Shell Thermia B At Furnace Set Point of 400°C

Time, min	Temperature of Fluid inside Circulator, °C	Furnace Temperature, °C
0	45.9	410
2	46.2	397
6	46.8	407
8	47.3	400
10	47.9	397

set point of 700°C it was observed that plastic used to hold probe started to melt towards the end of the experiment. Entrance of oil was changed and it entered from outer jacket. To cool oil in circulator copper coil was made and put into bath. Water was passing through coil and cooling oil. It was seen that desired cooling was achieved using Shell Thermia B.

Table B.15: Measured Temperatures Using Shell Thermia B At Furnace Set Point of 600°C

Time, min	Temperature of Fluid inside Circulator, °C	Furnace Temperature, °C
0	51.3	596
2	51.4	601
4	51.7	600
6	52.7	600
8	54.2	601
10	55.8	600
12	57.5	600
14	59.1	600
16	60.8	600
18	62.4	600
43	78.7	600

Table B.16: Measured Temperatures Using Shell Thermia B At Furnace Set Point of 700°C

Time, min	Temperature of Fluid inside Circulator, °C	Furnace Temperature, °C
0	73.5	696
2	73.2	698
3	72.9	701
4	72.6	701
5	72.9	700
6	73.6	700
7	74.5	700
8	75.5	
9	76.5	
10	77.5	
12	79.5	
14	81.5	
16	83.4	
18	85.3	
20	87.1	
22	88.9	
24	90.7	
26	92.4	
28	94.1	
30	95.7	
35	99.5	
40	103.1	
50	110.3	

Table B.17: Measured Temperatures Using Shell Thermia B At Furnace Set Point of 800°C

Time, min	Temperature of Fluid inside Circulator, °C	Furnace Temperature, °C
0	21.6	790
1	21.6	785
2	21.5	785
3	22.5	785
4	25.4	786
5	27.7	787
6	29.5	787
7	31.0	788
8	32.4	789
9	33.6	790
10	34.8	791
11	35.8	792
12	36.8	793
13	37.7	794
14	38.5	795
15	39.3	796
16	40.1	797
18	41.4	799
20	42.5	800
22	43.5	800
24	44.3	800
26	45.1	800
27	45.4	800
28	45.8	800
29	46.1	800
30	46.4	800
35	47.3	800
40	48.0	800
50	48.2	800
52	48.2	800

APPENDIX C

STUDIES DONE WITH SAMPLE LOOPS

Experiments were done with sample loops. It was controlled whether samples can be taken to loops using designed probe. Loops were investigated at different conditions. Moreover, reproducibility of analysis done with loops were controlled by doing experiments with same conditions at different times.

C.1 CONTROL OF SYSTEM WORKING PROPERLY

Samples were taken into sample loops while probe was inside reactor. 0.5 l/min C_2H_2 passed through reactor while reactor was at room temperature. Pressure inside reactor was atmospheric. After 15 minutes was waited to reach steady state, loops were started to fill with samples. Loops were filled with samples at 170 Torr and room temperature. After that loops were analyzed one by one. Two major peaks were detected according to TCD. To identify these two peaks analysis were done at MS. One of them was acetylene, as expected, and other was acetone. Acetone was coming from acetylene tank since acetylene was stored in dissolved acetone. Areas obtained with TCD analysis are given in Figure C.1. Since loops 6 and 12 were analyzed with MS, they did not have areas. Acetylene and acetone areas of loop 1 are greater than that of other loops. After filling loops was finished, position of 6 port valve was changed. Gas between 6 port valve and multiposition valve was sent to analyze. For this reason volume of first sample was greater than volume of other loops. Since loop 1 was first sent to analyze, its area was greater. When areas of other loops were compared with each other, no significant difference was detected. According to TCD analysis of all loops including loop 1, 91% of total area belonged to acetylene and rest was acetone. Taking samples with probe and analyzing them were successfully achieved.

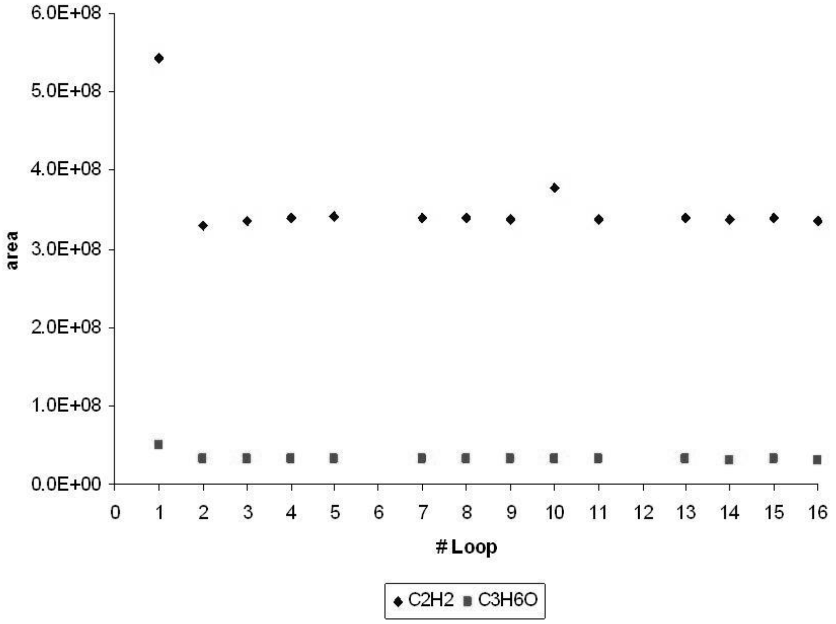

Figure C.1: Areas Obtained With TCD During 0.5 l/min C_2H_2 Passing Through Reactor

C.2 INVESTIGATION OF BEHAVIOR OF LOOPS AT DIFFERENT CONCENTRATIONS

Samples at different acetylene concentrations were taken into sample loops while probe was inside reactor. While 1.0 l/min argon passed through reactor at room temperature, loops were filled with three different acetylene flow rates (0.25, 0.10 and 0.05 l/min). Loops were filled with samples at 170 Torr and room temperature. First 5 loops were filled with 1.0 l/min Ar + 0.1 l/min C_2H_2, second 5 loops were filled with 1.0 l/min Ar + 0.25 l/min C_2H_2 and third 5 loops were filled with 1.0 l/min Ar + 0.05 l/min C_2H_2. After that loops were analyzed with TCD. Areas obtained with TCD analysis are given in Figure C.2. As it is seen in Figure C.2, different areas are obtained for different concentrations. Except loop 6, loops were consistent with each other. During the filling of loop 6 less amount of sample should be stored due to some experimental error and area was less.

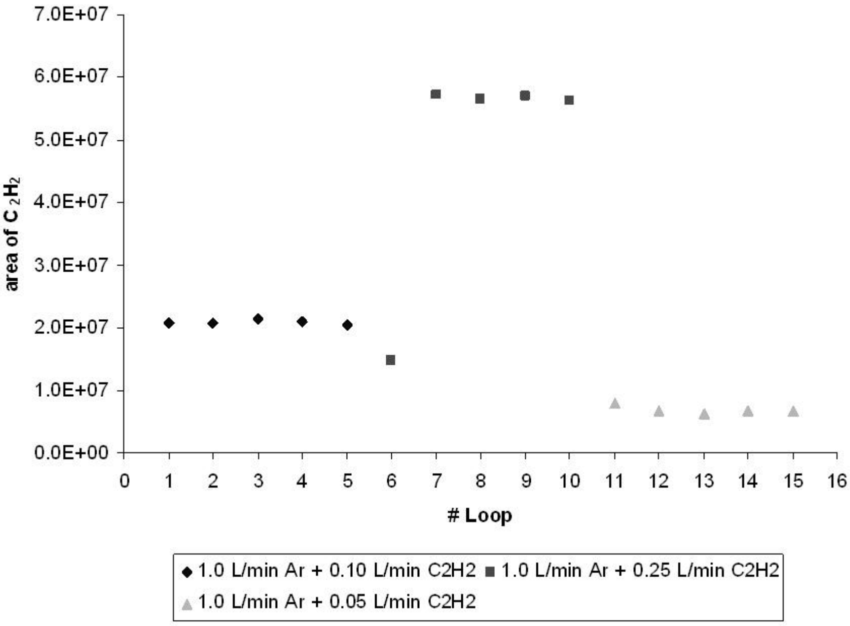

Figure C.2: Areas Obtained With TCD At Different C_2H_2 Concentrations

C.3 EFFECTS OF FILLING TIME OF LOOPS

Effect of filling time was investigated. 0.75 l/min Ar + 0.5 l/min C_2H_2 + 0.05 l/min H_2 passed through reactor while reactor was at room temperature. Loops were filled with samples at 170 Torr and 100°C. Filling time of loops are given in Table C.1. After loop 16 was filled, loop 1 was filled 1 minute more, then it was sent to analyze. Areas obtained with TCD analysis are given in Figure C.3. According to experiments it was determined that filling time did not affect amount of sample in loops.

C.4 ADSORPTION CONTROL IN LOOPS

It was controlled whether samples adsorbed in loops in time. 0.75 l/min Ar + 0.5 l/min C_2H_2 + 0.05 l/min H_2 passed through reactor while reactor was at room temperature. Loops were filled with samples at 170 Torr and 100°C. After 15 minutes were waited to reach steady state,

Table C.1: Filling Time of Each Loop

# Loop	Filling Time, min	# Loop	Filling Time, min
1	5 + 1	9	8
2	1	10	9
3	2	11	10
4	3	12	11
5	4	13	12
6	5	14	13
7	6	15	14
8	7	16	15

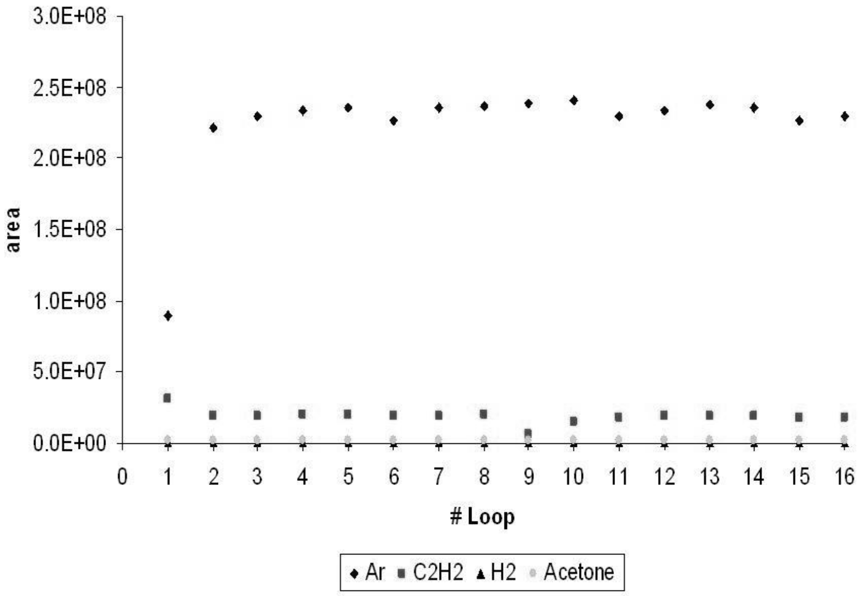

Figure C.3: Areas Obtained With TCD At Same Conditions With Different Filling Time loops were started to fill with samples. 5 more minutes were waited so that loop 1 and lines reached steady state. Other loops were filled for 1 minute since we proofed that filling time has no effect. After loop 16 was filled, loop 1 was filled 1 minute more, then it was sent to analyze. Samples were analyzed with TCD in 40 minutes intervals. Areas obtained with TCD analysis are given in Figure C.4. According to experiments it was determined that samples did not adsorb in loops in time. Areas obtained after 9 hours were closed to areas obtained at the beginning.

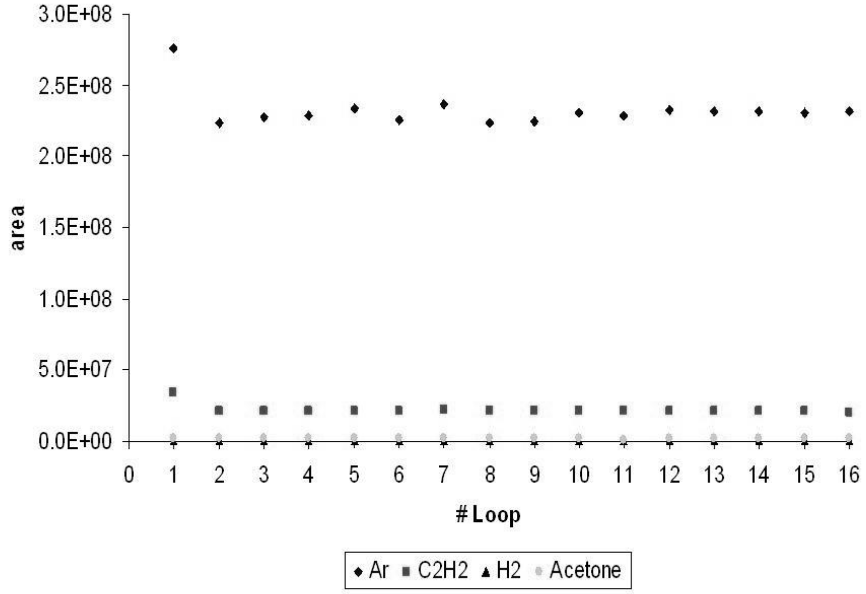

Figure C.4: Areas Obtained With TCD At Same Conditions With 40 Minutes Time Interval

Then, loops were controlled with products of acetylene pyrolysis. Acetylene pyrolysis was carried on at 800°C and 500 Torr. 0.5 l/min argon and 0.1 l/min acetylene passed through reactor. Loops were filled with samples at 150°C and 300 Torr. After 5 minutes were waited to reach steady state, loops were started to fill with samples. 5 more minutes were waited to fill loop 1. Other loops were filled for 1 minute. After loop 16 was filled, loop 1 was filled 1 minute more and sent to analyze. Samples were analyzed at GC/MS. Argon and acetylene were analyzed at TCD, benzene and hydrocarbons greater than benzene were analyzed at MS. Areas obtained are given in Figures C.5, C.6 and C.7. Although loop 8 was analyzed one day later than loop 2, there was no significant change. It was decided that products of acetylene pyrolysis did not adsorb in loops in time.

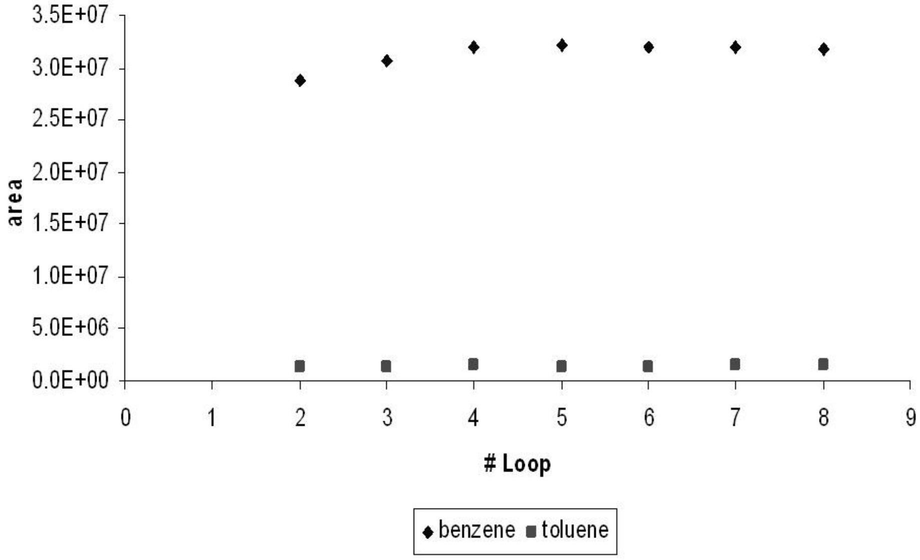

Figure C.5: Areas Obtained For Benzene and Toluene

C.5 REPRODUCIBILITY EXPERIMENTS WITH LOOPS

Reproducibility of filling loops at same conditions was controlled repeating experiments at different times. 0.75 l/min Ar + 0.5 l/min C_2H_2 + 0.05 l/min H_2 passed through reactor while reactor was at room temperature. Loops were filled with samples at 170 Torr and 100°C. After that loops were analyzed with TCD. This experiment was repeated 3 times at different days. Comparisons of areas of argon, acetylene, hydrogen and acetone are given in Figures C.8, C.9, C.10 and C.11, respectively. Areas of C_2H_2, Ar and C_3H_6O were closed to each other. There were differences for few of the areas due to experimental error. Areas of H_2 had differences even for the same experiment. Since there was no such problem for other chemicals, differences in areas of H_2 were not taken into account. It was concluded that loops

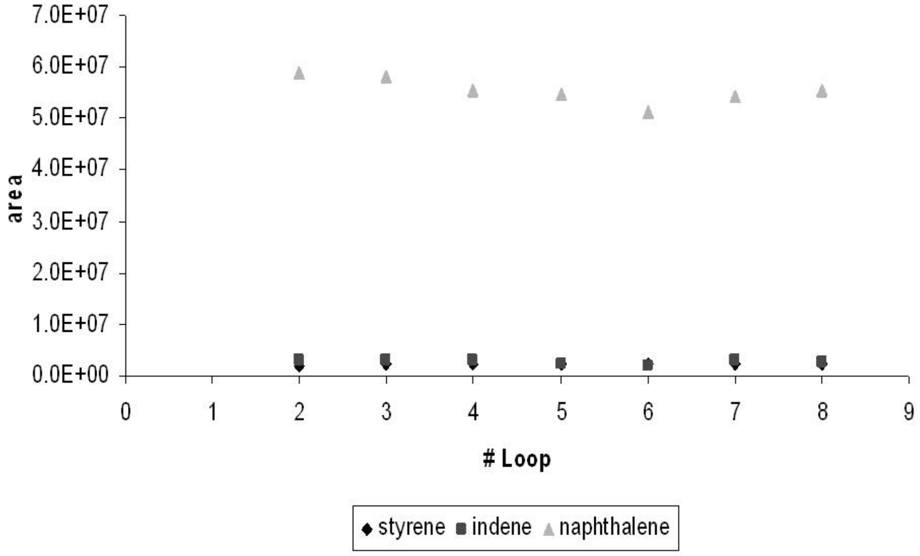

Figure C.6: Areas Obtained For Styrene, Indene and Naphthalene

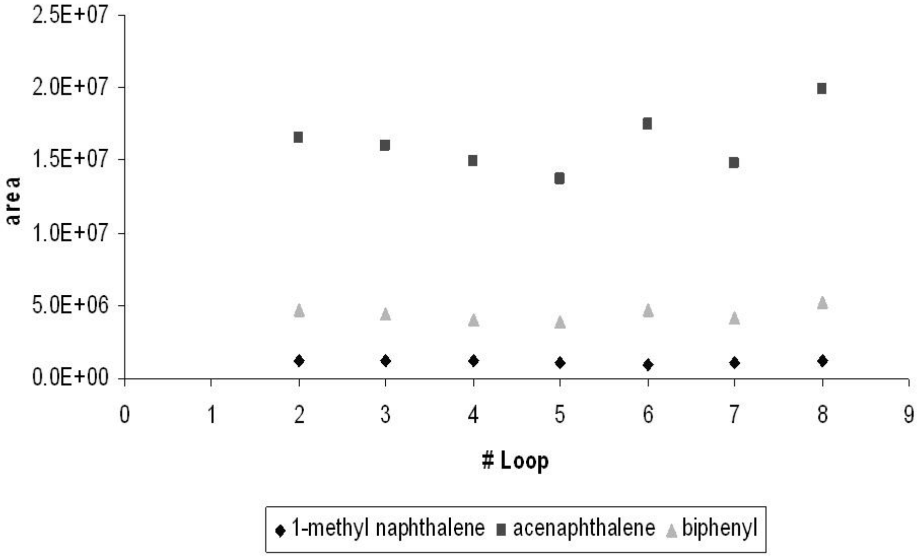

Figure C.7: Areas Obtained For 1-Methyl Naphthalene, Acenaphthalene and Biphenyl can be filled and analyzed in a reproducible manner.

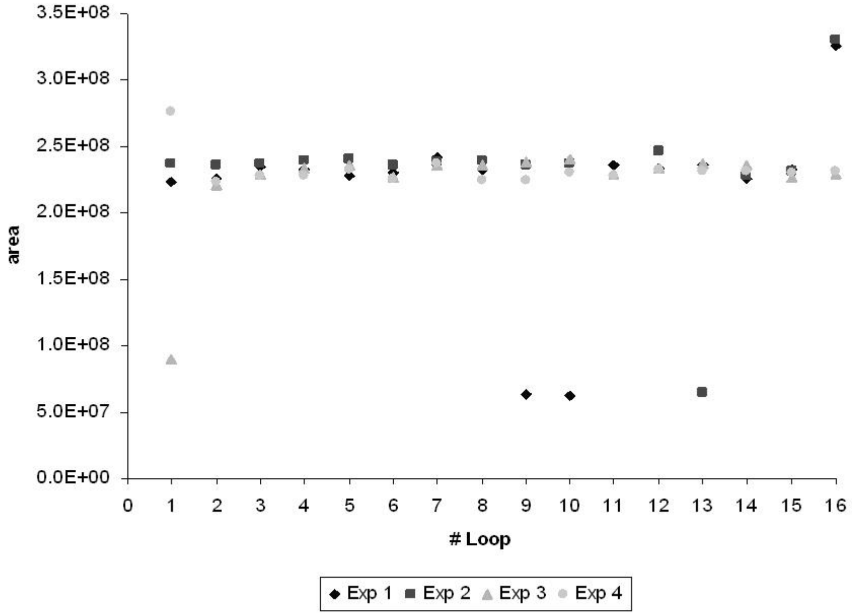

Figure C.8: Areas of Argon Obtained With TCD At Same Conditions But Different Times

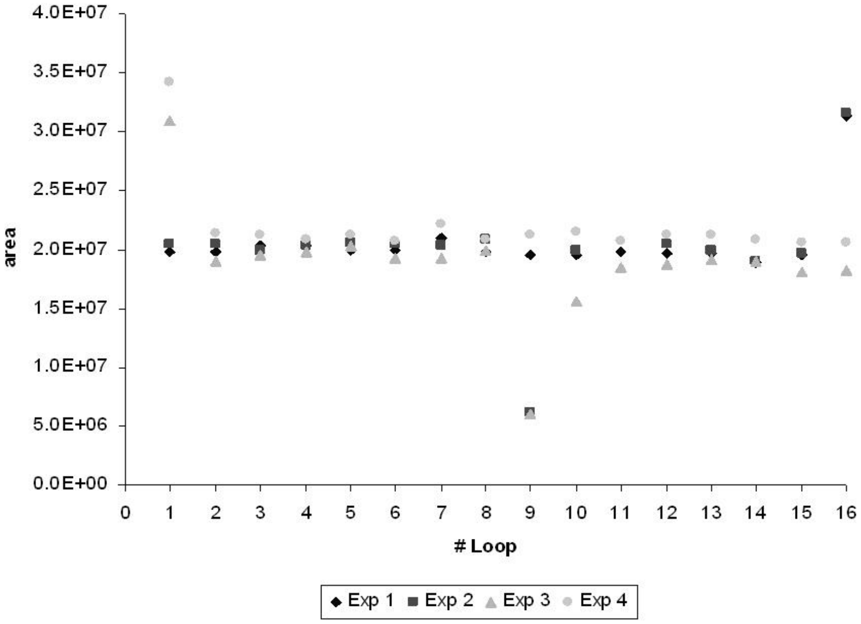

Figure C.9: Areas of Acetylene Obtained With TCD At Same Conditions But Different Times

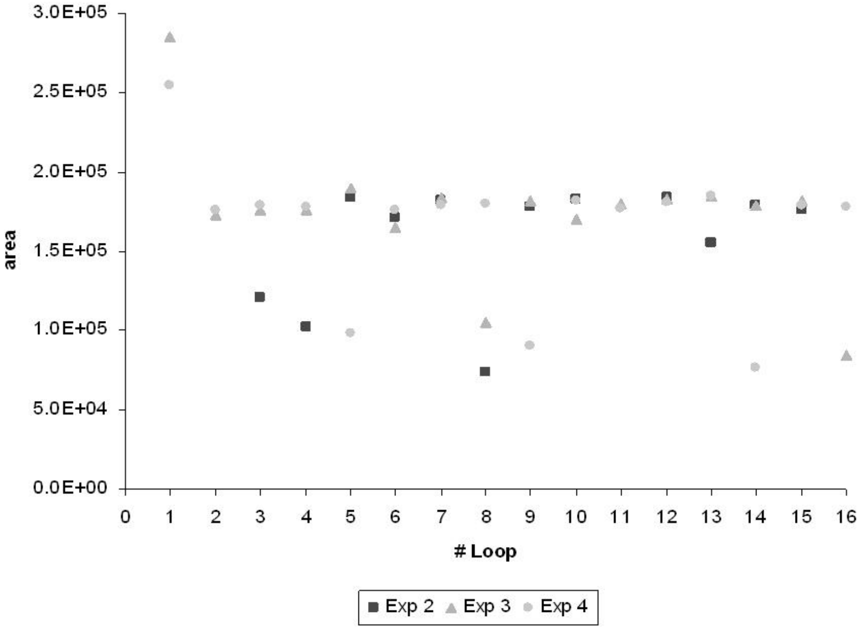

Figure C.10: Areas of Hydrogen Obtained With TCD At Same Conditions But Different Times

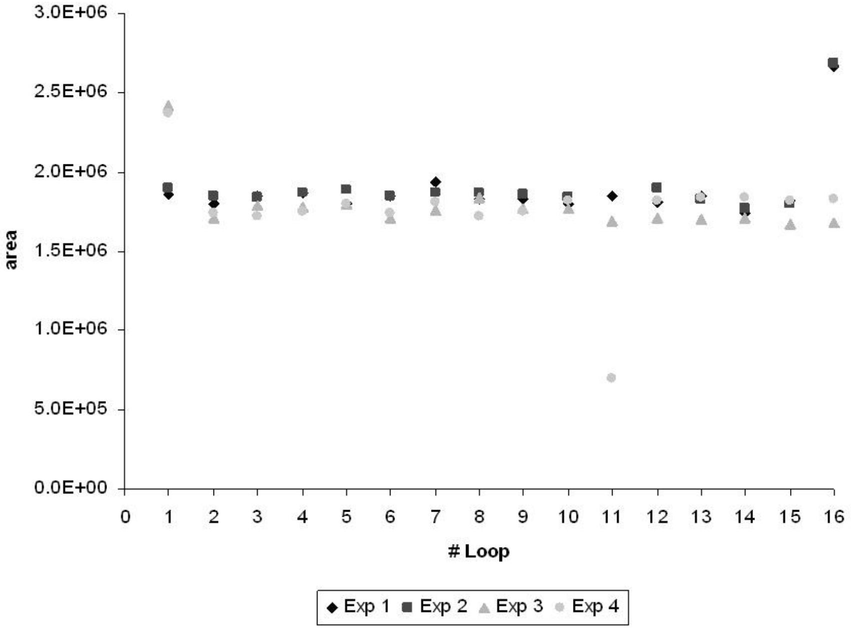

Figure C.11: Areas of Acetone Obtained With TCD At Same Conditions But Different Times

APPENDIX D

SAMPLE CHROMATOGRAM AND SPECTRUM OF EXPERIMENTS

Type of detector used and time interval of analyzed chemicals were given in Table D.1. Characteristic peaks of chemicals that were analyzed at MS were used. Characteristic peaks of chemicals were given in Table D.2.

Table D.1: Time Intervals and Detectors Used of Chemicals Analyzed

Name	Detector	Time Interval	Name	Detector	Time Interval
Argon	TCD	7.35-9.80	Indene	MS	18.08-18.86
Acetylene	TCD	11.61-12.55	Naphthalene	MS	19.40-20.52
Benzene	MS	8.48-12.04	1-Methyl Naphthalene	MS	20.50-22.00
Toluene	MS	12.65-14.74	Acenaphthalene	MS	21.81-23.37
Styrene	MS	15.44-16.78	Biphenyl	MS	21.32-23.57

Sample chromatogram of TCD belonged to argon and acetylene was given in Figure D.1. In chromatogram there were other peaks not belonged to argon and acetylene. Those peaks were most probably belonged to products of acetylene pyrolysis such as diacetylene and vinylacetylene. However, time interval of those chemicals could not be detected since pure samples of them were not available. So, analysis of them could not be done. Sample spectrum of MS and sample spectrum with characteristic peaks were given in Figures D.2 and D.3.

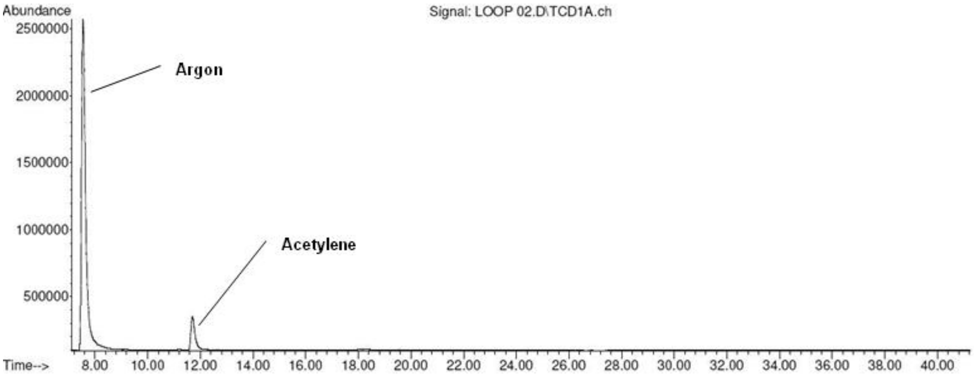

Figure D.1: Sample Chromatogram of TCD

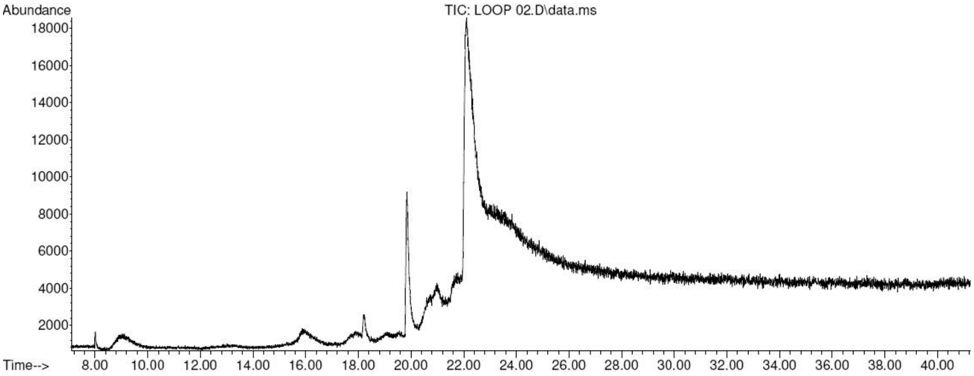

Figure D.2: Sample Spectrum of MS

Table D.2: Characteristic Peaks of Chemicals Analyzed at MS

Name	Characteristic Peak	Name	Characteristic Peak
Benzene	78	Naphthalene	128
Toluene	91	1-Methyl Naphthalene	142
Styrene	104	Acenaphthalene	152
Indene	116	Biphenyl	154

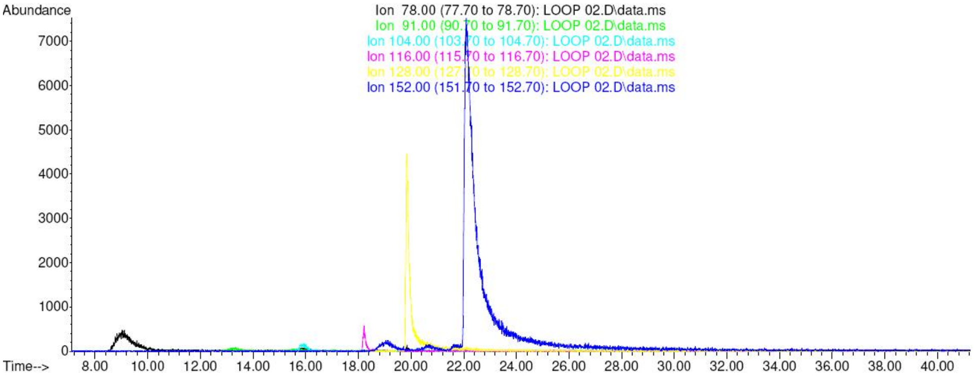

Figure D.3: Sample Spectrum of MS with Characteristic Peaks

APPENDIX E

CALIBRATIONS

E.1 CALIBRATION OF ACETONE

Acetone came as an impurity from acetylene tank that was used in experiments. To determine the amount of acetone in acetylene calibration of acetone was done. Known amount of acetone-toluene samples were injected to GC/MS with syringe. Amount of acetone and toluene in injected samples were given in Table E.1.

Table E.1: Volume Ratios of Acetone and Toluene in Samples

Sample	$x_{Acetone}$	$x_{Toluene}$	V_{Total}
1	0.9	0.1	10 ml
2	0.5	0.5	10 ml
3	0.1	0.9	10 ml
4	0.3	0.7	10 ml

0.1 μl was injected from prepared samples. Acetone was analyzed at TCD and toluene was analyzed at MS with prepared program. 5 injections were done for each sample. Measured acetone areas and average of them for each injection were given in Table E.2.

After that mole of acetone in each sample was calculated. To calculate mole of acetone equation E.1 was used.

$$n_i = \frac{x_i V \rho_i}{MW_i} \tag{E.1}$$

In equation E.1 x_i represents ratio of substance i in mixture, V represents injected volume (μl),

Table E.2: Measured Acetone Areas and Average of Them for Each Injection

Sample	Injection No.	Area of Acetone	Average Area of Acetone
1	1	413918357	399096860
	2	418082750	
	3	336479057	
	4	358962823	
	5	468041315	
2	1	195934115	182218613
	2	200692339	
	3	178908459	
	4	150871403	
	5	184686750	
3	1	19032887	17598739
	2	19856950	
	3	18140050	
	4	12796458	
	5	18167349	
4	1	114408695	94166078
	2	92087844	
	3	98512497	
	4	42293195	
	5	123528159	

ρ_i represents density of substance i (g/μl), MW$_i$ represents molecular weight of substance i (g/mole) and n$_i$ represents mole of substance i (mole). Density of acetone is 0.79 kg/l and molecular weight of acetone is 58.08 g/mole. Calculated moles of acetone and areas corresponding them were given in Table E.3.

Table E.3: Calculated Moles and Average of Measured Areas of Acetone in Samples

Mole of Acetone	Average Area of Acetone
$1.23x10^{-6}$	399096860
$6.81x10^{-7}$	182218613
$1.36x10^{-7}$	17598739
$4.09x10^{-7}$	94166078

Calibration curve was drawn according to these data and given in Figure E.1. Equality between measured area and corresponding mole of acetone was found from calibration curve.

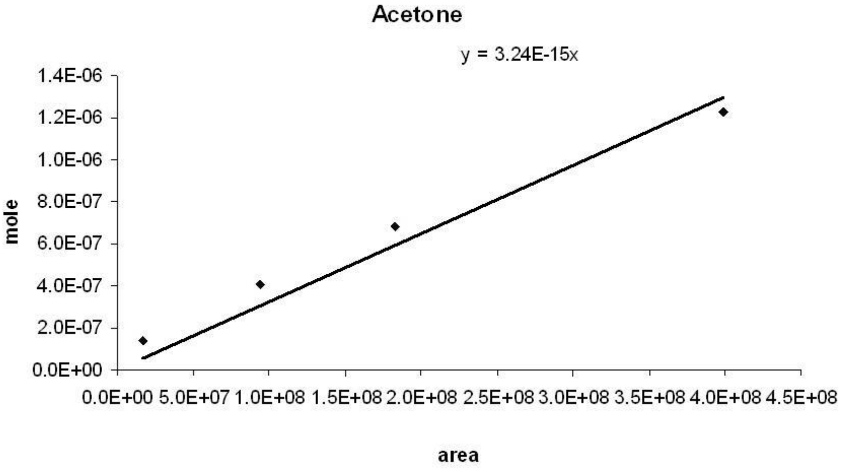

Figure E.1: Calibration Curve of Acetone

$$n_{Acetone} = (3.24x10^{-15})x\ \text{area}_{Acetone} \tag{E.2}$$

E.2 CALIBRATION OF ARGON AND ACETYLENE

To obtain calibration curves of argon and acetylene known amount of argon, acetylene and hydrogen was fed to the reactor. Loops were filled with probe. Then, analysis were done at TCD. Gas flow rates and average measured areas were given in Table E.4.

Area of hydrogen was only measured for sample 1. Area of acetone was not measured for sample 3, 4 and 5.

First of all amount of acetone that came from acetylene tank as an impurity was calculated. Mole of acetone at sample 1 was found using average area and equality E.1.

$$n_{Acetone} = (3.24\text{x}10^{-15})(1783539) = 5.779\text{x}10^{-9} \text{ mole}$$

Total mole in one loop was calculated using ideal gas law.

$$P = 172.7 \text{ Torr}$$

$$T = 100^{\circ}\text{C}$$

$$V = 0.5 \text{ ml}$$

$$R = 0.08314 \text{ bar}\cdot\text{L}\cdot\text{K}^{-1}\cdot\text{mole}^{-1}$$

Table E.4: Gas Flow Rates and Average Measured Areas of Argon, Acetylene, Hydrogen and Acetone

Sample	Ar, l/min	C_2H_2, l/min	H_2, l/min	Average Area			
				Argon	Acetylene	Hydrogen	Acetone
1	0.75	0.1	0.05	232612983	19545633	162450	1783539
2	1	0.1	0.05	316379606	20094792	-	2149675
3	1	0.1	0	352720140	20973242	-	-
4	1	0.25	0	312286097	48310313	-	-
5	1	0.05	0	363477653	6892848	-	-
6	0	0.5	0	-	340641628	-	31953405

Table E.5: Calculated Moles and Average of Measured Areas of Argon and Acetylene in Samples

Mole of Argon	Average Area of Argon	Mole of Acetylene	Average Area of Acetylene
$3.094\text{x}10^{-6}$	232612983	$4.067\text{x}10^{-7}$	19545633
$4.041\text{x}10^{-6}$	316379606	$3.984\text{x}10^{-7}$	20094792
$4.224\text{x}10^{-6}$	352720140	$4.165\text{x}10^{-7}$	20973242
$3.717\text{x}10^{-6}$	312286097	$9.163\text{x}10^{-7}$	48310313
$4.425\text{x}10^{-6}$	363477653	$2.182\text{x}10^{-7}$	6892848
		$4.582\text{x}10^{-6}$	340641628

$$P{\cdot}V = n{\cdot}R{\cdot}T$$

$$(172.7 \text{ Torr} \cdot 1.333224\text{x}10^{-3} \text{ bar/ Torr})(0.5 \text{ ml} \cdot 10^{-3} \text{ l/ ml})$$
$$= n{\cdot}(0.08314 \text{ bar}{\cdot}\text{L}{\cdot}\text{K}^{-1}{\cdot}\text{mole}^{-1})(100 + 273\text{K})$$

$$n_{total} = 3.712 \text{ x}10^{-6} \text{ mole}$$

Ratio of acetone in acetylene tank was calculated using equality E.3.

$$(x_{Acetone} \cdot \frac{Q_{C2H2}}{Q_{Ar} + Q_{C2H2} + Q_{H2}}){\cdot}n_{total} = n_{Acetone} \tag{E.3}$$

$$(x_{Acetone} \cdot \frac{0.1\text{l/min}}{0.75\text{l/min} + 0.1\text{l/min} + 0.05\text{l/min}}){\cdot}3.712\text{x}10^{-6} = 5.779\text{x}10^{-9}$$

$$x_{Acetone} = 0.014$$

After finding ratio of acetone, mole of others were calculated. Calculated moles and areas corresponding them were given in Table E.5.

Calibration curves of argon and acetylene were drawn according to these data and given in Figures E.2 and E.3. Equality between measured area and corresponding mole of argon and acetylene were found from calibration curves.

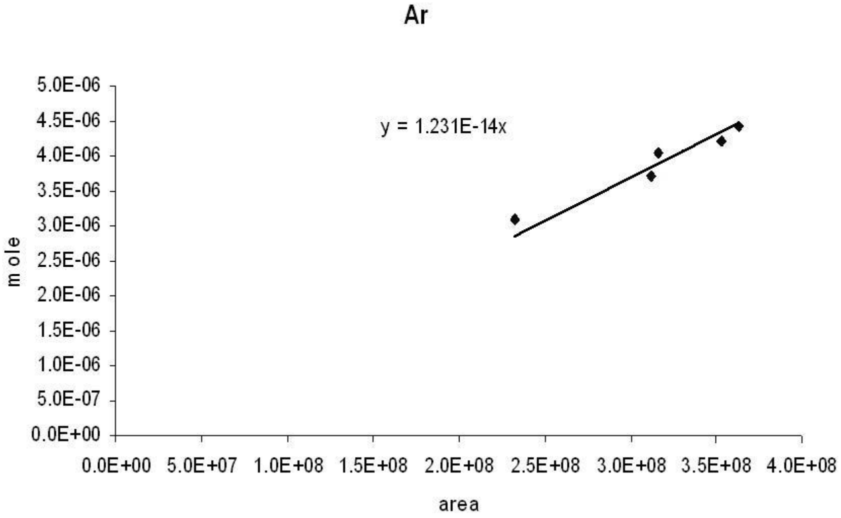

Figure E.2: Calibration Curve of Argon

$$n_{Argon} = (1.231\text{x}10^{-14})\text{x area}_{Argon} \tag{E.4}$$

$$n_{Acetylene} = (1.363\text{x}10^{-14})\text{x area}_{Acetylene} \tag{E.5}$$

E.3 CALIBRATION OF BENZENE AND TOLUENE

Known amount of benzene-toluene samples were injected to GC/MS with syringe. Amount of benzene and toluene in injected samples were given in Table E.6.

0.1 μl was injected from prepared samples. Benzene and toluene was analyzed at MS. Injection was repeated for 3 times for each sample. Measured areas of benzene and toluene and average of them for each injection were given in Table E.7.

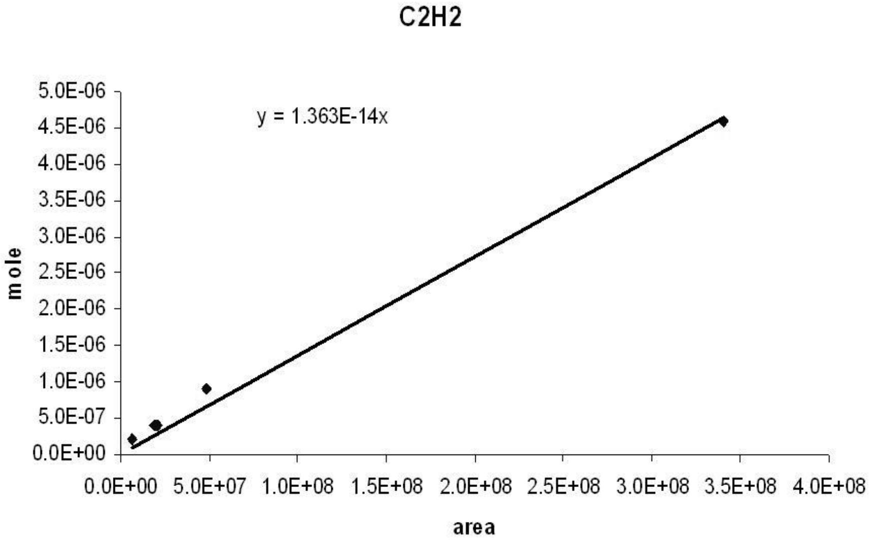

Figure E.3: Calibration Curve of Acetylene

Table E.6: Volume Ratios of Benzene and Toluene in Samples

Sample	$x_{Benzene}$	$x_{Toluene}$	V_{Total}
1	0.9	0.1	10 ml
2	0.5	0.5	10 ml
3	0.1	0.9	10 ml
4	0.3	0.7	10 ml

Table E.7: Measured Areas of Benzene and Toluene and Average of Them for Each Injection

Sample	Injection No.	Area of Benzene	Average Area of Benzene	Area of Toluene	Average Area of Toluene
1	1	2023029304	2113657694	619136787	688822180
	2	2193086221		736030736	
	3	2124857557		711299017	
2	1	1716020100	1640442620	2106532845	2150248626
	2	1646259132		2249081375	
	3	1559048627		2095131657	
3	1	593033931	595872225	2796267090	2660548652
	2	543921687		2537546663	
	3	650661058		2647832204	
4	1	1205226295	1247635937	2293680911	2447332177
	2	1328051275		2591431838	
	3	1209630240		2456883783	

Table E.8: Calculated Moles and Average of Measured Areas of Benzene and Toluene in Samples

Mole of Benzene	Average Area of Benzene	Mole of Toluene	Average Area of Toluene
$1.02\text{x}10^{-6}$	2113657694	$9.46\text{x}10^{-8}$	688822180
$5.64\text{x}10^{-7}$	1640442620	$4.73\text{x}10^{-7}$	2150248626
$1.13\text{x}10^{-7}$	595872225	$8.51\text{x}10^{-7}$	2660548652
$3.38\text{x}10^{-7}$	1247635937	$6.62\text{x}10^{-7}$	2447332177

After that mole of benzene and toluene in each sample was calculated. To calculate moles equation E.1 was used.

Density of benzene is 0.88 kg/l and molecular weight of benzene is 78 g/mole. Density of toluene is 0.87 kg/l and molecular weight of toluene is 92 g/mole. Calculated moles of benzene and toluene and areas corresponding them were given in Table E.8.

Calibration curves of benzene and toluene were drawn according to these data and given in Figures E.4 and E.5. Equality between measured area and corresponding mole of benzene and toluene were found from calibration curves.

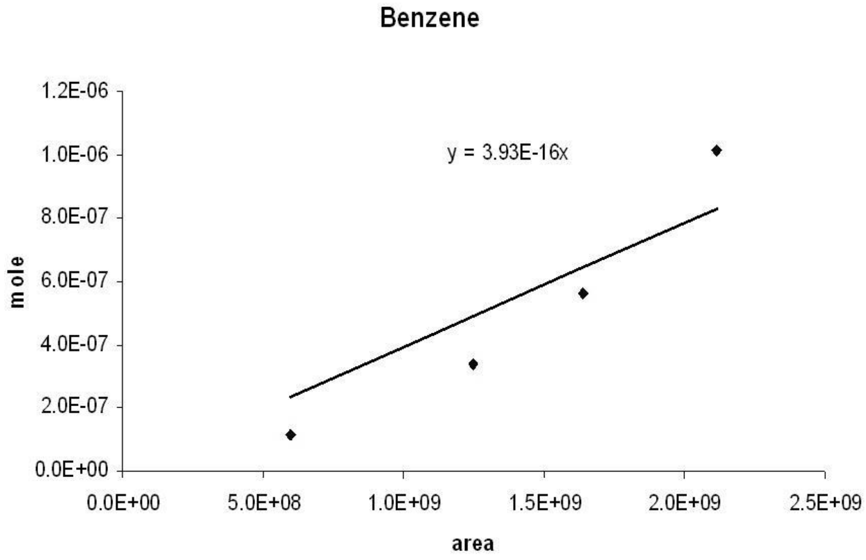

Figure E.4: Calibration Curve of Benzene

$$n_{Benzene} = (3.93\text{x}10^{-16})\text{x area}_{Benzene} \tag{E.6}$$

$$n_{Toluene} = (2.73\text{x}10^{-16})\text{x area}_{Toluene} \tag{E.7}$$

E.4 CALIBRATION OF REST OF THE CHEMICALS

Chemicals that pure samples could not be found were calibrated according to method in Fitch et al. [63, 64]. For calibration of chemicals that pure samples could not be found equation E.8 was used.

$$N_i = (N_R{\cdot}MW_R{\cdot}\frac{Q_R}{A_R})(\frac{1}{MW_i{\cdot}Q_i})A_i \tag{E.8}$$

In equation E.8 N was referred to number of moles, MW was referred to molecular weight, Q

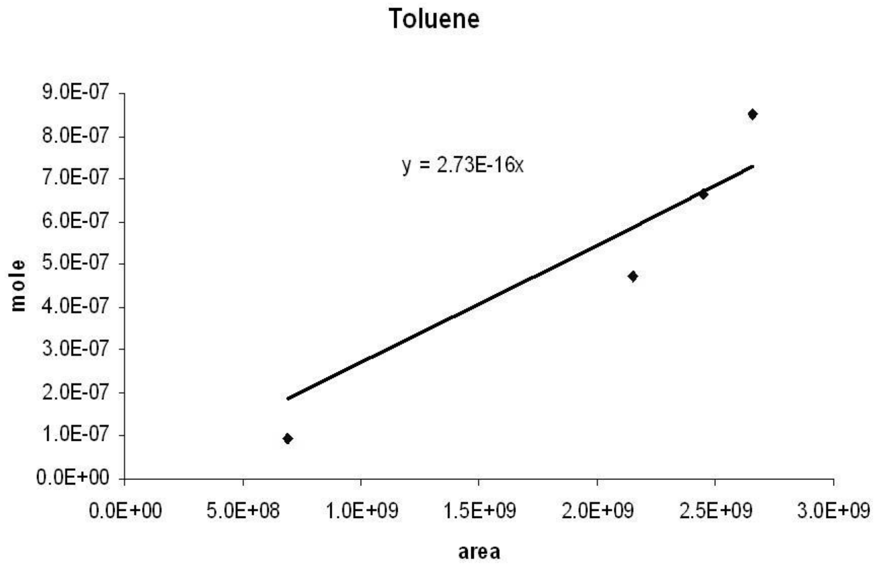

Figure E.5: Calibration Curve of Toluene

was referred to ionization cross section, A was referred to area measured in MS. i was referred to chemical whose mole was calculated, R was referred to reference chemical whose calibration was previously done. In our calculation benzene was chosen as a reference chemical. To calculate ionization cross section equation E.9 [63] was used.

$$Q = 0.082 + \sum_{i=1}^{8} a_i \cdot n_i \tag{E.9}$$

In this equation a_i and n_i are the coefficient and number of each of the eight atom types, H, C, N, O, F, Cl, Br and I. Coefficients were taken from reference [63]. For carbon a_i is equal to 1.43 and for hydrogen a_i is equal to 0.73. Ionization cross sections of chemicals whose calibrations were done and that of benzene, reference chemical, were calculated using equation E.9 and given in table E.9.

Table E.9: Calculated Ionization Cross Sections of Chemicals

Chemical	MW	Formula	Q
Benzene	78	C_6H_6	13.042
Styrene	104	C_8H_8	17.362
Indene	116	C_9H_8	18.792
Naphthalene	128	$C_{10}H_8$	20.222
1-Methyl Naphthlane	142	$C_{11}H_{10}$	23.112
Acenaphthalene	152	$C_{12}H_8$	23.082
Biphenyl	154	$C_{12}H_{10}$	24.542

APPENDIX F

CALCULATIONS

F.1 CALCULATION OF SPACE TIME

Space times were calculated for points where samples were taken. To calculate space time equation F.1 was used.

$$\tau = \frac{V}{\dot{Q}} = \frac{(\frac{\pi \text{ x } D^2}{4}) \text{ x } L}{\dot{Q}_{total}} \tag{F.1}$$

In equation F.1 D is diameter of quartz tube (cm), L is distance from entrance (cm), $\dot{Q}_{total}$ is total gas flow rate (cm^3/s) and π is space time (s). In our experiments quartz tube with 36 mm inner diameter was used.

In acetylene pyrolysis experiments total gas flow rate was 1725 ml/min. In acetylene pyrolysis with addition of hydrogen experiments and carbon nanotube production experiments total gas flow rate was 2025 ml/min.

Calculated space time at each point for both flow rates were given in Table F.1.

F.2 CALCULATION OF MOLE PERCENTAGE

Mole percentages in experiments were calculated using moles of chemicals. Since pressure of loop was fluctuated in each case, total mole was calculated using ideal gas law for each loop. Then, ratio of moles of chemical to total mole at that point was found.

Table F.1: Space Times at Each Point for Total Gas Flow Rate of 1725 ml/min and 2025 ml/min

Distance from entrance, cm	Space time, s	
	$\dot{Q}_{total}$=1725 ml/min	$\dot{Q}_{total}$=2025 ml/min
0	0.0	0.0
2	0.7	0.6
4	1.4	1.2
6	2.1	1.8
8	2.8	2.4
10	3.5	3.0
12	4.2	3.6
14	5.0	4.2
16	5.7	4.8
18	6.4	5.4
20	7.1	6.0
22	7.8	6.6
24	8.5	7.2
26	9.2	7.8
28	9.9	8.4

$$x_i\% = \frac{n_i}{n_{total}} \text{ x } 100\%$$

F.3 CALCULATION OF RATIO OF UNCONVERTED ACETYLENE AND PRODUCED BENZENE AND TOLUENE

If reaction had not been taken place inside reactor, how much acetylene should be in loops would have been calculated. It was calculated from moles of argon at that point since initial ratio of acetylene to argon was known.

$$n_{C2H2,initial} = n_{Ar} \text{ x } \frac{v_{C2H2}}{v_{Ar}} = n_{Ar} \text{ x } \frac{0.225 \text{ l/min}}{1.5 \text{ l/min}}$$

After that ratios of moles of acetylene, benzene and toluene to moles of acetylene in case of no reaction were calculated.

$$\text{unconverted } C_2H_2 \text{ \%} = \frac{n_{C2H2}}{n_{C2H2,initial}} \text{ x } 100\%$$

$$\text{produced } C_6H_6 \text{ \%} = \frac{n_{C6H6}}{n_{C2H2,initial}} \text{ x } 100\%$$

$$\text{produced } C_7H_8 \text{ \%} = \frac{n_{C7H8}}{n_{C2H2,initial}} \text{ x } 100\%$$

APPENDIX G

CONTROL OF TIME THAT CATALYST CARRIED ON ITS ACTIVITY

In CVD experiments, catalyst can be hold active for a limited time. To determine how long catalyst carried on its activity, experiment was done. During CNT production experiment samples were taken with probe from same position and then they were analyzed by GC/MS. All the experimental methods and the parameters were identical with the carbon nanotube production experiments except moving probe. Probe was 26 cm behind the entrance of the furnace. All samples were taken from that point with 5 minutes interval. Total time of the experiment was 75 minutes. Products of experiment were send to SEM analysis. SEM images were given in Figure G.1. According to SEM analysis, CNTs were successfully produced.

Mole percentages of chemicals whose calibration were done were plotted against time and given in Figures G.2, G.3, G.4, G.5, G.6, G.7, G.8, G.9, G.10 and G.11.

Moles of acetylene also did not change in 75 minutes time interval. As it was seen from Figures G.4 and G.5, there was no significant change in moles of benzene and toluene.

There was a little decrease in amounts of styrene after 65 minutes. In first 60 minutes, amounts of indene fluctuated but then decreased. Amounts of naphthalene increased after first 5 minutes and remained constant till 50^{th} minutes. Then, amounts of naphthalene also decreased little. Behavior of 1-methyl naphthalene was similar to naphthalene. Amounts of biphenyl remained constant from 20^{th} minutes to 50^{th} minutes. Then, biphenyl started to decrease.

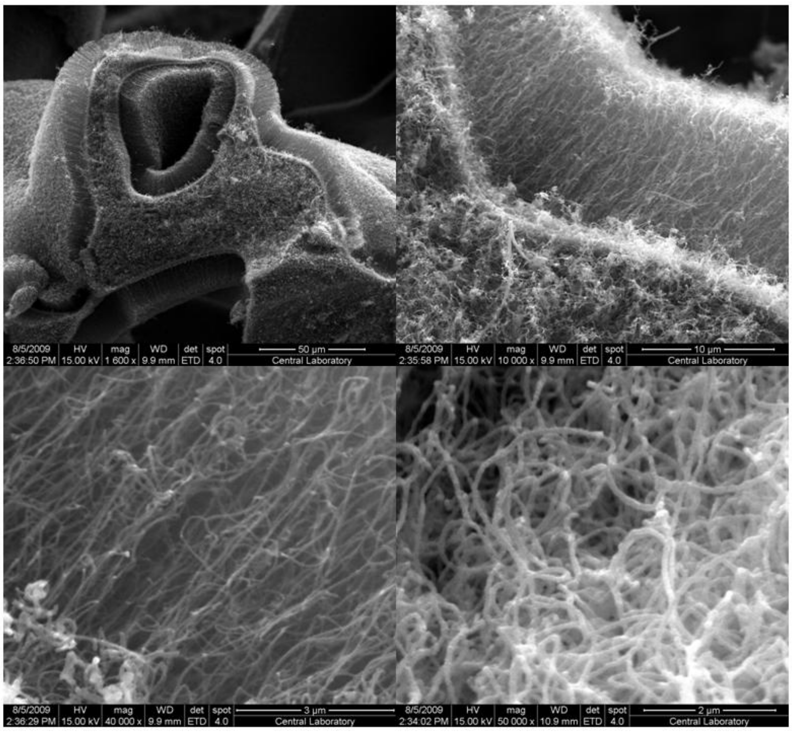

Figure G.1: SEM Images of Experiment

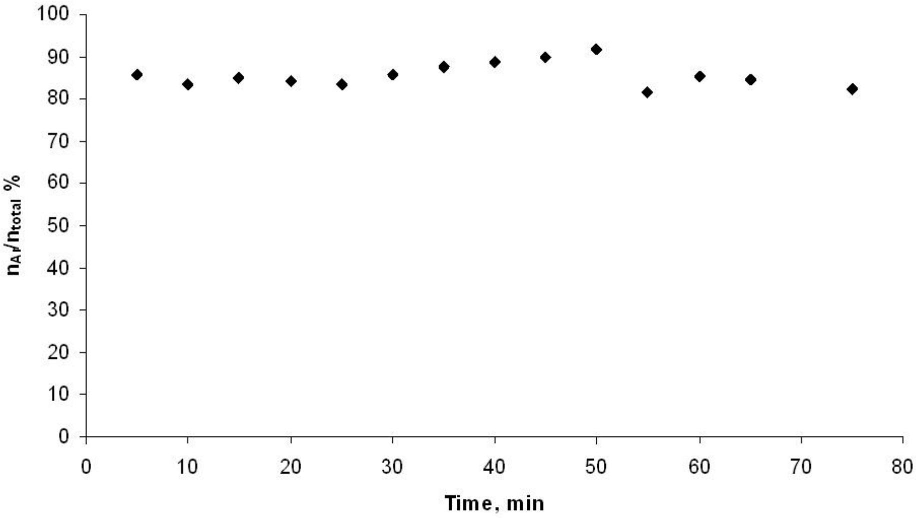

Figure G.2: Mole Percentages of Argon with Time

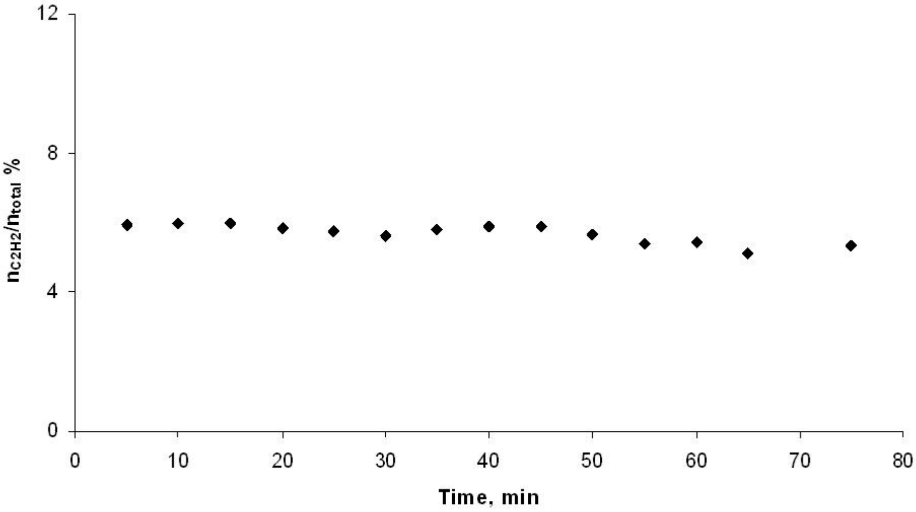

Figure G.3: Mole Percentages of Acetylene with Time

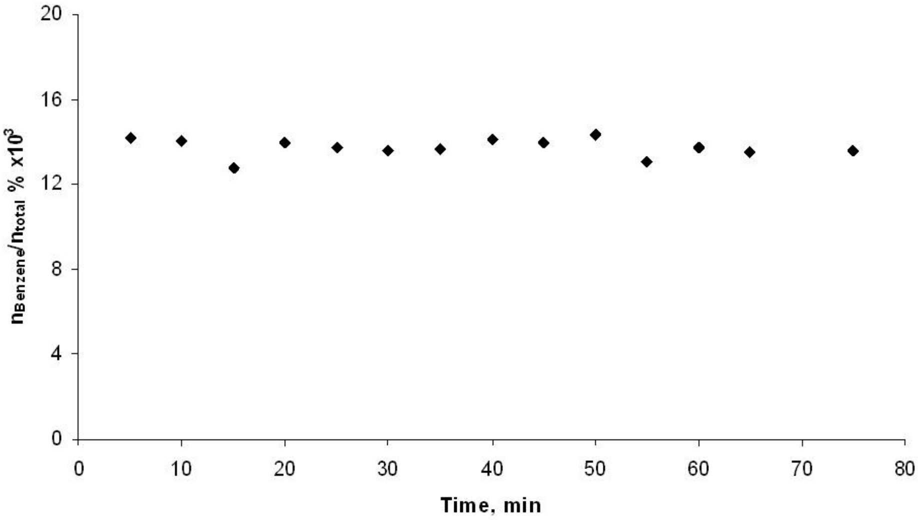

Figure G.4: Mole Percentages of Benzene with Time

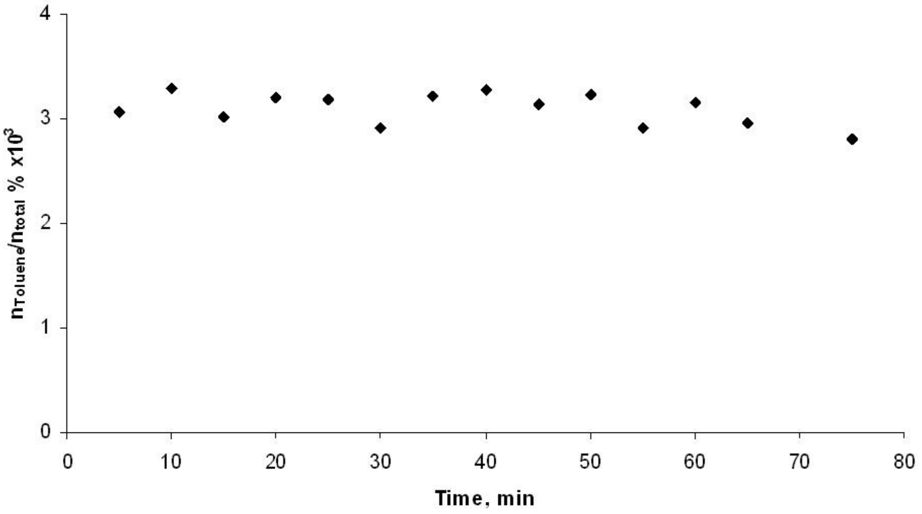

Figure G.5: Mole Percentages of Toluene with Time

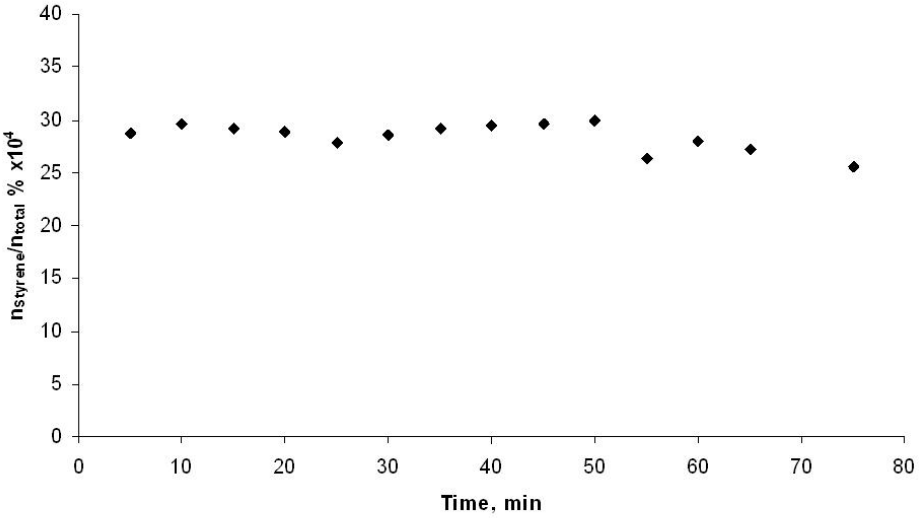

Figure G.6: Mole Percentages of Styrene with Time

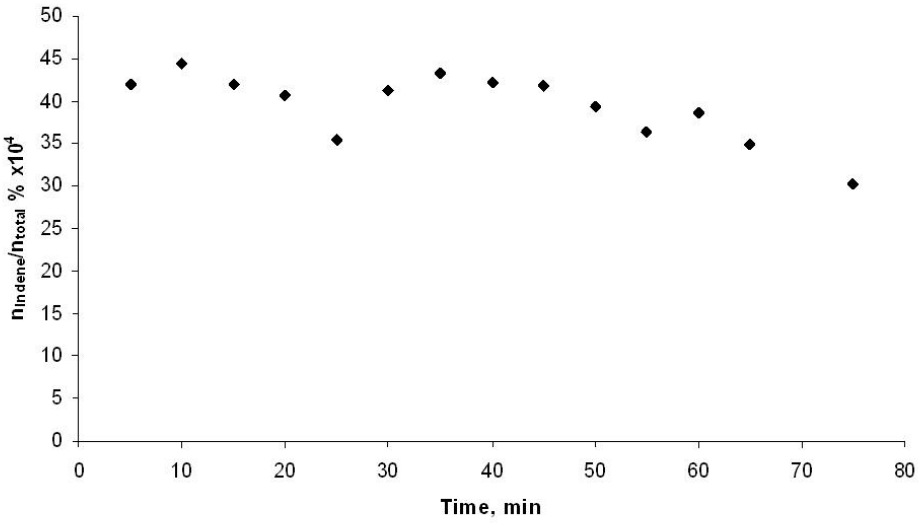

Figure G.7: Mole Percentages of Indene with Time

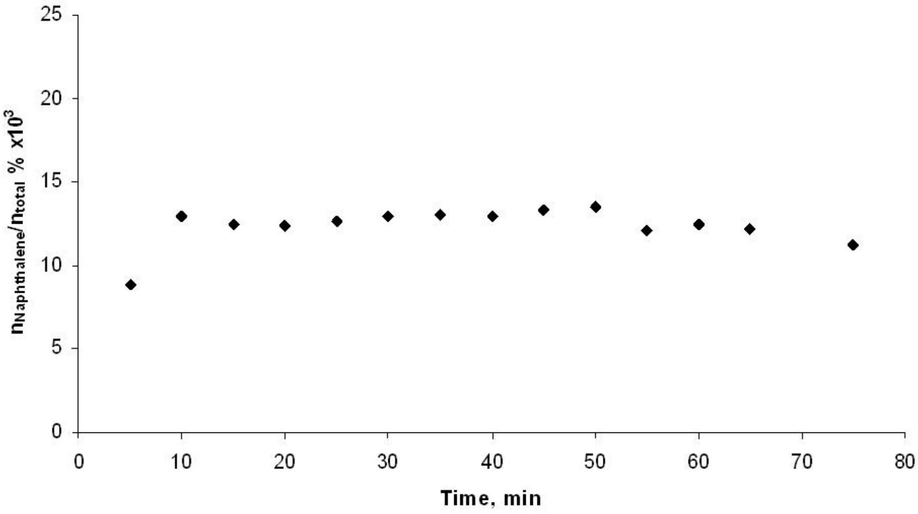

Figure G.8: Mole Percentages of Naphthalene with Time

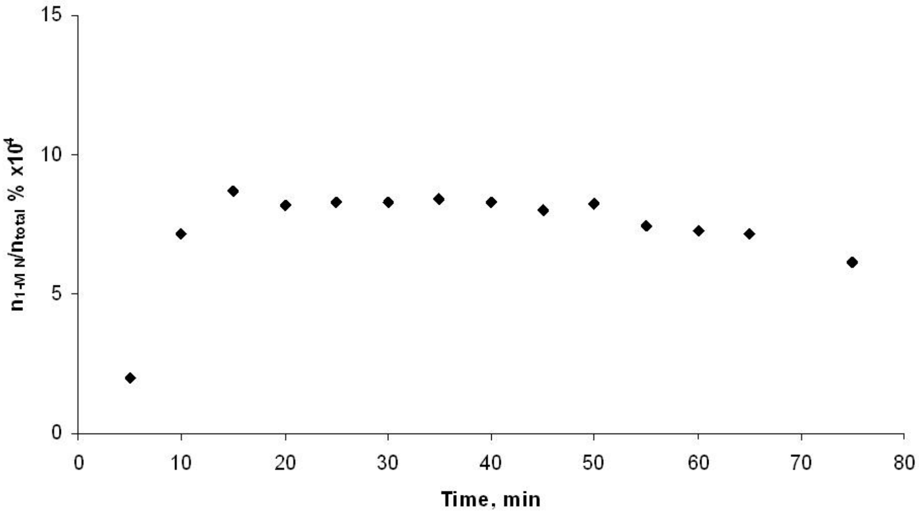

Figure G.9: Mole Percentages of 1-Methyl Naphthalene with Time

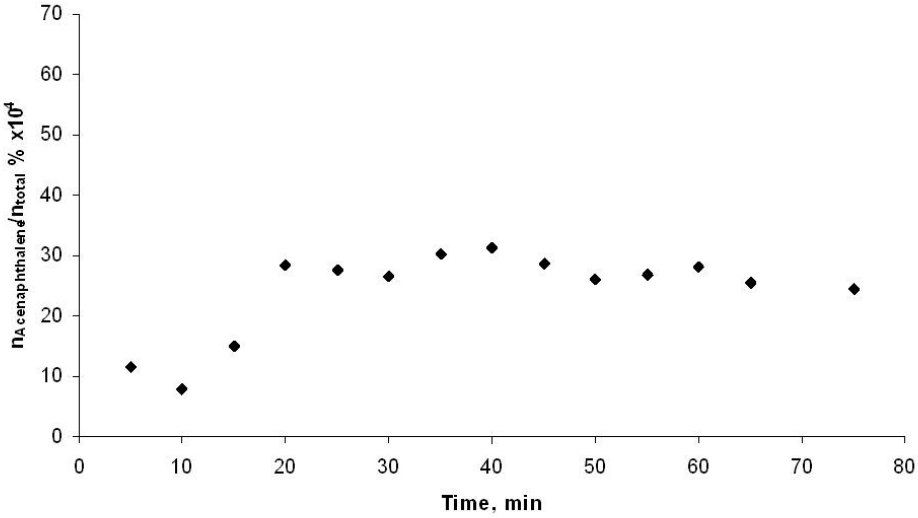

Figure G.10: Mole Percentages of Acenaphthalene with Time

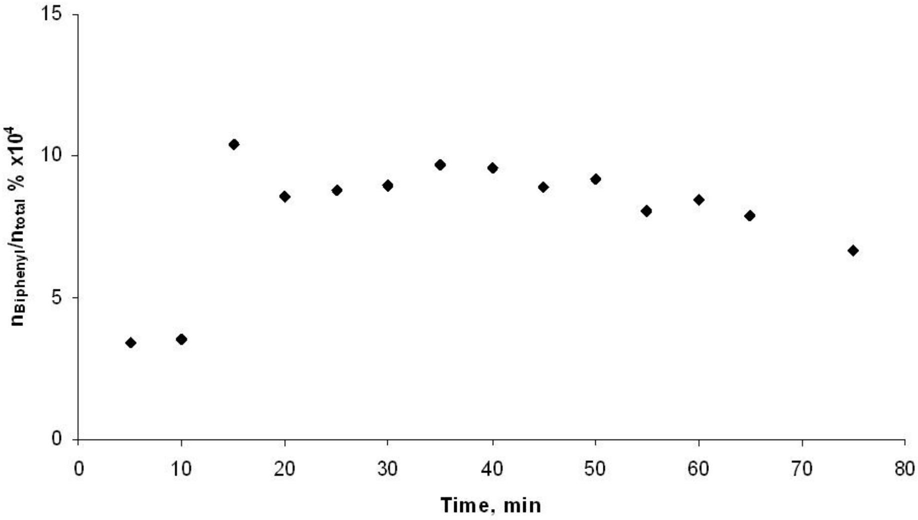

Figure G.11: Mole Percentages of Biphenyl with Time